WATER REQUIREMENTS OF A SOUTHERN ALBERTA RIPARIAN COTTONWOOD ECOSYSTEM

TRINA ORCHARD
Bachelor of Science, University of Calgary, 2012

A Thesis
Submitted to the School of Graduate Studies
of the University of Lethbridge
in Partial Fulfilment of the
Requirements for the Degree

MASTER OF SCIENCE

Department of Biological Sciences
University of Lethbridge
LETHBRIDGE, ALBERTA, CANADA

WATER REQUIREMENTS OF A SOUTHERN ALBERTA RIPARIAN COTTONWOOD ECOSYSTEM

TRINA ORCHARD

Date of Defence: July 15, 2015

Dr. Lawrence B. Flanagan Supervisor	Professor	Ph.D
Dr. Craig Coburn Thesis Examination Committee Member	Associate Professor	Ph.D
Dr. Stewart Rood Thesis Examination Committee Member	Professor	Ph.D
Dr. Theresa Burg Chair, Thesis Examination Committee	Associate Professor	Ph.D

Abstract

The eddy covariance (EC) method was used to determine the amount of water used for evapotranspiration (ET) over the 2014 growing season by a Southern Alberta riparian cottonwood ecosystem in Lethbridge, AB, Canada. Isotopic measurements of deuterium content in water were used to determine what portion of the water supplying evapotranspiration came from the each of the two cottonwood woodland water sources: the Oldman River and seasonal precipitation.

Isotopic analysis of the woodland water sources identified the Oldman River as the sole source of water for the resident cottonwood trees. Based on EC measurements, 465 mm of water was used during the 2014 growing season by the cottonwood woodland. An estimated woodland area of 1.7×10^5 m^2 was used to determine the approximate volume of water used by the woodland over the 2014 growing season to be 7.9×10^4 m^3.

Acknowledgments

I would like to offer my gratitude to Dr. Lawrence B. Flanagan for providing me with the opportunity to pursue graduate studies. I also offer my gratitude to my committee, Dr. Craig Coburn and Dr. Stewart Rood, for taking this journey with me. This research was made possible by grant funds obtained from a variety of sources. The eddy covariance and other meteorological equipment was purchased using grants from the Natural Sciences and Engineering Research Council of Canada to L.B. Flanagan. My student salary stipend and the materials & supplies costs for the research was paid from the "Functional Flows: a practical strategy for healthy rivers" project grant from Alberta Innovates - Energy and Environment Solutions to S.B. Rood (PI), L.B. Flanagan and other U of L researchers. The aluminum tower, used to support the eddy covariance and other meteorological instruments above the tree canopy, was purchased using funds awarded to S.B. Rood from Conocco-Phillips Canada for the Functional Flows project.

Thank you to Dr. David Pearce for allowing me to use your groundwater wells and for your kindness and patience as you showed me the ropes. A special thank you is offered to Linda Wever and residents of the biology storeroom for providing equipment, a wonderful environment in which to perform my assistantships, and a place where I could find emotional support. Thank you to Joanne Golden for welcoming me into the greenhouses and for firmly believing I could keep all the plants alive. Lastly, to my friends and family, your unshakable faith in me keeps me moving forward. Without your kindness, love, and support I never would have made it so far. Thank you.

Table of Contents

List of Tables

List of Figures

List of Symbols and Abbreviations

α_w	Woody-to-total leaf area ratio
α	Parameterized coefficient describing the response of leaf conductance to incident photosynthetically active radiation
AWESB	Alberta Water and Environmental Sciences Building
c_p	Specific heat of air (MJ kg^{-1} °C^{-1})
Δ	Change in saturation vapour pressure (kPa °C^{-1})
DBH	Diameter at breast height
δ	Isotopic abundance (‰)
δ^2H	Isotopic abundance of deuterium (‰)
e_a	Actual vapour pressure of air (kPa)
e_s	Saturated vapour pressure of air (kPa)
EC	Eddy covariance
ET	Evapotranspiration
$f(Q)$	Function of photosynthetic photon flux density (mmol m^{-2} s^{-1})
G	Soil heat flux (W m^{-2})
g_a	Boundary layer conductance (mol m^{-2} s^{-1})
g_c	Canopy conductance (mol m^{-2} s^{-1})
g_{max}	Maximum surface conductance (mmol m^{-2} s^{-1})
g_s	Surface conductance (mmol m^{-2} s^{-1})
γ_E	Needle-to-shoot area ratio
GEP	Gross Ecosystem Productivity (µmol m^{-2} day^{-1})
GPP	Gross Primary Productivity (µmol m^{-2} day^{-1})
H	Sensible heat flux (W m^{-2})
HSNC	Helen Schuler Nature Centre
κ_D	Parameterized coefficient describing the response of leaf conductance to vapour pressure deficit
λ	Psychrometric constant (kPa °C^{-1})
L_e	Effective LAI (m^2 m^{-2})
LAI	Leaf area index (m^2 m^{-2})
λE	Latent heat flux (W m^{-2})
NEE	Net Ecosystem Exchange (µmol m^{-2} day^{-1})
NEP	Net Ecosystem Productivity (µmol m^{-2} day^{-1})
NR	Net radiation (W m^{-2})
Ω_E	Clumping index
$\theta_v(\tau)$	Volumetric water content (m^3 m^{-3})
OMRB	Oldman River Basin
P	Air pressure (kPa)
ρ_a	Dry air density (mol m^{-3})
PAR	Photosynthetically active radiation (µmol m^{-2} s^{-1})

PM equation	Penman-Monteith equation
PPFD	Photosynthetic photon flux density (μmol m^{-2} s^{-1})
Q	Photosynthetic photon flux density (μmol m^{-2} s^{-1})
R_{sample}	Measured $^2H/H$ ratio
$R_{standard}$	Known $^2H/H$ of a sample standard
τ	Pulse period (μ s)
T	Air temperature (°C)
TER	Total Ecosystem Respiration (μmol m^{-2} day^{-1})
TRAC	Tracing Radiation and Architecture in Canopies system
u	Wind speed (m s^{-1})
u^*	Friction velocity (m s^{-1})
VPD	Vapour pressure deficit (kPa)
W	Woody surface area (m^2 m^{-2})
WUE	Water-use efficiency (mmol mol^{-1})

1. INTRODUCTION

1.1 The Oldman River Basin

Water resources in Southern Alberta, Canada are under high demand (Rock and Mayer 2007). The extensive irrigation systems required to support agriculture, as well as continued population and economic growth have put strain on the limited water supply in this semi-arid region (Rock and Mayer 2007). Much of the water that supplies this agricultural community comes from the Oldman River Basin (OMRB) which is the largest watershed in southern Alberta (Rock and Mayer 2007).

At the heart of the OMRB is the Oldman River which flows through several municipalities in southern Alberta including Fort Macleod, Lethbridge, and Taber before joining with the Bow River to form the South Saskatchewan River (Oldman Watershed Council 2007). With 87% of its surface water allocated to agriculture the OMRB remains one of three southern basins closed to new water allocations (Water Matters Society of Alberta 2012).

In addition to the intense agricultural, commercial, and municipal use, the Oldman River also supplies water for local riparian cottonwood woodlands (Oldman Watershed Council 2007, Rock and Mayer 2007). With the high demand for river resources there is concern over whether the riparian woodlands will be able to survive with increased dewatering over time. Drought induced decline in cottonwood populations as the result of river dewatering for agriculture has already been observed in southern Alberta along the St. Mary River (Rood et al. 1995). Accounting for the seasonal water requirements of the riparian cottonwood

woodlands along the Oldman River when allocating river resources may help prevent further drought induced reductions in the population of southern Alberta cottonwoods.

1.2 Riparian woodlands

1.2.1 The importance of riparian systems

Riparian corridors are ecosystems which reside on the shores of streams and lakes (Naiman and Decamps 1997). They are areas of intense biological activity in semi-arid regions and provide valuable habitat for local plant and animal species (Naiman and Decamps 1997, Scott et al. 2004). Their potential access to shallow groundwater is the basis for their high productivity and biodiversity compared to the surrounding semi-arid regions (Scott et al. 2004).

Covering less than 2% of available land area, riparian ecosystems provide habitat for one third of plant species in western North America, making their continued existence an important environmental issue (Poff et al. 2011). These systems are composed of species well adapted to disturbance caused by high river flows, due in part to being located along floodplains which experience long periods of seasonal flooding (Naiman and Decamps 1997).

Riparian ecosystems are invaluable to their environments because of their ability to filter out sediment and pesticides, influence light penetration and air and water temperatures (Poff et al. 2011). In semi-arid environments of North America, the riparian tree species are almost exclusively cottonwoods (*Populus* spp.) (Rood

et al. 2003a). Known to be colonizers of fallow riparian sites they provide wildlife habitat, contribute to the stabilization of stream banks, and provide woody debris and litter to aquatic habitats (Rood et al. 2003a, Poff et al. 2011). However, precipitation input in semi-arid regions is not enough to provide a continuous source of water for woody vegetation (Rood et al. 2003a). Thus, the cottonwood riparian systems are dependent on sufficient river flows to supply local groundwater to maintain the stability of the ecosystem (Rood et al. 2003a).

1.2.2 Threats to riparian survival

The primary threats to riparian ecosystems in western North America are caused by human activity. For example, tree harvesting, clearing for agriculture, and the expansion of human settlements all have detrimental impacts on cottonwood riparian woodlands (Rood et al. 2003a). Grazing by livestock has been suggested to be the largest threat to the survival of western riparian ecosystems (Poff et al. 2011). Grazing causes compaction of the soil, removal of vegetation, and changes to fluvial systems that can be detrimental to cottonwood germination sites (Poff et al. 2011). As cattle are drawn to riparian sites for shade or water they ultimately move through regions of newly established seedlings (Samuelson and Rood 2004). This creates a pattern of grazing and crushing of the young trees, reducing overall cottonwood recruitment (Samuelson and Rood 2004).

Due to their reliance on riverine inputs to groundwater, altered flow patterns in rivers and streams due to human built dams are a major threat to all

riparian systems (Poff et al. 2011). Altered flow patterns, reductions in sediment deposition downstream, as well as fragmentation of the river corridor impact the natural systems downstream from the dam (Bradley and Smith 1986, Braatne et al. 2008). Decline of riparian cottonwood tree populations downstream from dams or intensive irrigation centres is a common occurrence (Rood et al. 2003a). The reduction in base flows caused by damming and irrigation prevents newly established cottonwood seedlings from maintaining contact with the water table which is needed in order to survive periods of drought (Poff et al. 2011). In severe cases of dewatering due to irrigation, mortality of entire cottonwood riparian woodlands is known to occur (Rood et al. 2003a). Cottonwood mortality as the result of dewatering has been observed along Big Lost River, Idaho, as well as locally in Southern Alberta along the St. Mary River (Rood et al. 1995, Rood et al. 2003a).

By virtue of their dependence on river water and the increasing use of freshwater by human populations, cottonwood riparian systems are in need of river management practices (Clipperton et al. 2003, Rood et al. 2003a). Such practices would ensure that river flows are sufficient to sustain their adjacent terrestrial ecosystems while still providing enough fresh water for human use (Rood et al. 2003a).

1.2.3 Riparian cottonwoods

Cottonwood species vary by climate and geographic region, but their dependence on natural riverine processes is a unifying factor between them (Junk et al. 1989, Benjankar et al. 2014). Precipitation and temperature are the largest controls on the species distribution of cottonwood trees (Rood et al. 2003a). Typically, *Populus deltoides* and *Populus fremontii* occur in warmer, semi-arid regions and the rivers they are associated with tend to lose water when travelling downstream (Rood et al. 2003a, Pearce et al. 2006). Conversely, *Populus balsamifera* and *Populus trichocarpa* are typically present in cooler, wetter climes where rivers tend to gain water when travelling downstream (Rood et al. 2003a, Pearce et al. 2006). *Populus angustifolia* is a species that lies between the two species groupings noted above in terms of climate preferences (Rood et al. 2003a).

In semi-arid regions cottonwoods are phreatophytic, maintaining contact with the groundwater table through the capillary fringe, a saturated zone where water is drawn in to soil pores via capillary flow as a result of surface tension (Rood et al. 2011, Haberer et al. 2015). Soil composition determines the breadth of the capillary fringe which can range in size from 5 to 130 cm above the groundwater table (Mahoney and Rood 1998). Cottonwood trees use the high water table present in river valleys to avoid water stress (Pearce et al. 2006). With their high transpiration rates and poor water use efficiency, cottonwoods trees are intolerant to water stress brought on by drought (Pearce et al. 2006). Drought response in cottonwoods can include stomatal closure, reduced transpiration and photosynthesis, reduced growth in shoots, root growth altered by a search for

moisture, as well as the death of larger branches and portions of the crown (Rood et al. 2003a).

Recruitment is dependent both on seasonal seedling dispersal and clonal regeneration, although seedling dispersal is the primary means of cottonwood recruitment (Mahoney and Rood 1998, Rood et al. 1998). Cottonwoods are adapted so that seedling dispersal is correlated with the time of year during which seasonal flooding is likely to occur (Lytle and Merritt 2004). Moderate flood events occurring less than 10 years apart are necessary for successful seedling establishment (Mahoney and Rood 1998). After spring peak flows, point bars are fully saturated with water and free of competing colonizing plant species allowing cottonwood seedlings to establish (Lytle and Merritt 2004). Via transport by wind or water, seedlings are quick to take root and can reach densities of 4000 seedlings m^{-2}, however a large portion of seedlings ultimately die as a result of drought stress (Mahoney and Rood 1998, Rood et al. 1998).

Survival of cottonwood seedlings on point bars is dependent on the rate of groundwater decline (Benjankar et al. 2014). The rate of river stage decline directly controls the rate at which the groundwater table declines in riparian regions (Lytle and Merritt 2004). Seedling mortality occurs if the groundwater table declines faster than the rate of cottonwood seedling root growth (Benjankar et al. 2014). This process of seedling growth on point bars, exposed by the natural meandering of the river, creates a cottonwood forest with bands of growth (Rood et al. 1998, Lytle and Merritt 2004). The youngest cottonwood trees are found near the river

and tree age progresses to older growth when moving inland (Rood et al. 1998, Lytle and Merritt 2004).

Seedling roots grow on average 60 to 100 cm in their initial year, relying on contact with the capillary fringe as the water table declines (Mahoney and Rood 1998). The recruitment box model as described by Mahoney and Rood (1998) gives a successful recruitment band for cottonwood seedlings as being between 0.6 to 2 m above the groundwater table by late summer. This carries the caveat that if groundwater table decline is greater than 2.5 cm per day then seedlings will be unable to match root growth with the rapidly falling water table (Mahoney and Rood 1998). Where seedlings successfully establish in this 0.6 to 2 m range is dependent on how quickly the river stage declines as well as the cottonwood species being considered (Mahoney and Rood 1998).

1.2.4 Cottonwood water usage

Dependence on river water is not a requirement for a riparian ecosystem (Dawson and Ehleringer 1991). A mature, mixed oak and maple woodland (*Quercus* sp.*, Acer* spp.) in the Wasatch mountains of Utah, USA was found to have little to no reliance in the adjacent stream water (Dawson and Ehleringer 1991). The mature trees instead used roots deep in the soil profile to draw water from zones below the surface water in the stream channel (Dawson and Ehleringer 1991).

For the majority riparian systems however, studies have shown that they most often rely on stream flow supplying the groundwater in the region (Stromberg et al. 1996, Naiman and Decamps 1997, Rood et al. 2003a, Lamontagne et al. 2005, O'Grady et al. 2006). In the absence of sufficient river water input these ecosystems will struggle to survive, exhibiting signs of tree drought stress or suffer complete tree mortality (Stromberg et al. 1996). This has been shown to be particularly true for cottonwood riparian systems (Rood et al. 2003a). In some areas, a series of ramping and decreasing flows generated by dams over the growing season have been met with success for increasing cottonwood recruitment and decreasing stand mortality (Rood et al. 2003b, Rood et al. 2005).

In addition to understanding the level of increasing or decreasing flows beneficial to recruitment and growth throughout the season, it is also desirable to understand the precise amount of water that is used by cottonwood riparian systems during photosynthetic gas exchange. In semi-arid regions, precipitation input is often the greatest limiting factor on ecosystem productivity (Lázaro et al. 2001, O'Connor et al. 2001, Heisler-White et al. 2008, Flanagan and Adkinson 2011). In southern Alberta, irrigation for agriculture consumes the majority of growing season river flows (Water Matters Society of Alberta 2012). Due to these limitations on available water, understanding the total amount of precipitation versus river water that is needed by local cottonwood riparian woodlands would allow for precise allocations of river water to be distributed to protect these vital ecosystems in semi-arid regions. The methods used in this study will allow for the

quantification of water used by trees in a southern Alberta cottonwood riparian system on a daily, weekly, monthly, or seasonal basis.

The study site used in this project is a southern Alberta cottonwood riparian system located in the Helen Schuler Nature Centre (HSNC), Lethbridge Alberta, Canada. It is a largely open canopy woodland and part of a unique region due to the presence of three separate species of cottonwood (*P. deltoides, P. angustifolia, P. balsamifera*), all existing near the extent of their natural range and hybridizing on site (Pearce et al. 2006, Rood et al. 2013).

1.3 Evapotranspiration

The focus of this study is evapotranspiration (ET) measured as water flux from the canopy. Evapotranspiration consists of evaporation from soil and leaf surfaces as well as transpiration of water released from the open pores on leaves (stomata) during photosynthetic gas exchange (Ayer 1949). While it is driven by a variety of environmental controls, ET is most strongly related to incident solar radiation, soil water availability, and local atmospheric moisture content represented as vapour pressure deficit (VPD) (Penman 1948, Teuling et al. 2009, Wang and Dickinson 2012). Evapotranspiration is also affected by air temperature, wind speed, and other parameters that influence the magnitude of stomatal conductance and its control of ET (Penman 1948, Ponton et al. 2006, Tabari 2011).

The May to October seasonal evapotranspiration in a southern Alberta grassland eddy covariance site, located just outside the city of Lethbridge, is

strongly controlled by precipitation (Flanagan and Adkinson 2011). It ranges from 188 mm in a dry year with only 90 mm of precipitation to 456 mm in an extremely wet year with 521 mm of precipitation (Flanagan and Adkinson 2011). In forested semi-arid ecosystems cumulative seasonal evapotranspiration has been found to range between 375 mm and 744 mm for varying stand densities within a velvet mesquite (*Prosopis velutina*) riparian system in southern Arizona (Scott et al. 2000, Scott et al. 2004). Seasonal evapotranspiration of 405 mm was found for a trembling aspen forest (*Populus tremuloides*) in northern Saskatchewan and 1271 mm for a cottonwood/willow (*Populus fremontii, Salix gooddingii,* and *Baccaris glutinosa*) forest in southern Arizona (Scott et al. 2000, Scott et al. 2004, Zha et al. 2010). These values provide a starting range for what kinds of water usages may be expected at the study site.

1.4 Objectives

The ecosystem present at the Helen Schuler Nature Centre is vulnerable to the same threats present against semi-arid riparian woodlands around the globe. Dewatering of the Oldman River for agricultural, municipal, and industrial use has the potential to cause cottonwood mortality. Understanding the precise water requirements of the HSNC cottonwood woodland during the growing season will increase our understanding of the needs of this ecosystem and others similar to it, as well as provide policy makers with an additional tool to use when allocating the demand for river resources. The methods used in this study will result in the parameterization of an empirical model of cottonwood stomatal conductance to

water vapour which can be used with measurements of meteorological variables and the Penman-Monteith equation of evapotranspiration to calculate water usage of local cottonwood woodlands over time per unit of woodland area (Methods, section 2.5). This can be used as a tool to determine water usage of local cottonwood woodlands over a larger region than the bounds of the Helen Schuler Nature Centre. The objective of determining cumulative water use for the HSNC cottonwood woodland is presented as two component parts.

1) The first objective is to determine the amount of water used by the cottonwood woodland for evapotranspiration over the 2014 growing season. This will be accomplished using the eddy covariance method which will continuously measure the water flux from the woodland throughout the growing season as a product of vertical wind speed and scalar gas (H_2O) concentrations (Baldocchi 2003).
2) The second objective is to determine the portion of water used in evapotranspiration that is supplied by the Oldman River versus summer precipitation. This will be accomplished by analyzing the isotopic composition of tree stem water, ground water, the Oldman River, as well as that of summer precipitation.

1.5 Eddy Covariance measurement method

The eddy covariance (EC) method is a micrometeorological technique for measuring fluxes of water, carbon dioxide, and other trace gases (Swinbank 1951, Wilson et al. 2001, Burba and Anderson 2010). Atmospheric turbulence,

represented as vertical wind speed, drives the transport of gases from the canopy to the instrumentation where the gas concentrations of incoming air parcels can be measured (Aubinet et al. 2012). The EC method determines fluxes from the canopy as the product of vertical wind speed and scalar fluctuations in the gas of interest such as H_2O or CO_2 (Wever et al. 2002). The size of the collection region, known as the flux footprint, can range from a few meters to hundreds of meters depending on instrument height, wind speed, and roughness of the canopy (Burba and Anderson 2010). The technique can be applied over exceedingly short or long time scales of minutes to years, or even decades (Wofsy et al. 1993, Baldocchi 2003).

Eddy covariance is a relatively recent practice dating back to the late 1960's (Baumgartner 1969, Denmead 1969, Baldocchi 2003). EC became the measurement tool of choice for carbon budgets and ET studies in the early 1990's as technology improved (Wofsy et al. 1993). However, despite the numerous EC studies performed across the globe, riparian systems are still largely underrepresented in the literature (Baldocchi 2003). This is due to the fact that riparian systems are often located in river valleys with complex geographical features, such as large cliffs or steep inclines. These features make EC difficult to perform as they disturb the uniform air currents on which the method relies (Baldocchi 2003).

In an ideal ecosystem for eddy covariance, the canopy would be uniform and the terrrain would be flat (Burba and Anderson 2010). These assumptions which are made in the practice of EC methodology can be violated in complex ecosystems,

such as the woodland in the HSNC (Burba and Anderson 2010). The HSNC cottonwood canopy is often sparse, and lies in a river valley. Raised grassland coulees are located immediately to the east of the riparian corridor. The effectiveness of the EC method in this region will be determined by the relative closure of the energy balance between incoming and outgoing energy measured at the site.

Local EC measurements can be applied to larger, similar regions using empirical modelling which relies on data collection of environmental variables, EC measurements, and application of general mathematical relationships between ET and environmental conditions (Wever et al. 2002). The environmental variables required consist mostly of meteorological measurements, such as vapour pressure deficit, incoming photosynthetically active radiation, and air temperature. When the relationship between these variables and measured evapotranspiration is known, a model can be parameterized for the observed cottonwood system and applied to other similar systems using meteorological and supplemental measurements from the new location. Applying this method to similar systems would allow for a prediction of water requirements for cottonwood riparian systems throughout much larger regions than just the observed study site.

1.6 Stable isotopes for partitioning water sources

To determine cumulative use of river water for photosynthetic gas exchange by the HSNC woodland, the water used by the cottonwood trees must be separated

into its source components. In the HSNC semi-arid riparian ecosystem these sources are the Oldman River and local precipitation. The isotopic signature of each source can be determined using the ratio of the hydrogen stable isotope deuterium (^{2}H) relative to the more abundant hydrogen isotope protium (^{1}H). The abundance of deuterium relative to protium can be affected by natural processes throughout the year (Dansgaard 1964, Rock and Mayer 2007). In rivers, the abundance of deuterium is altered through isotopic fractionation from evaporation causing a progressive increase in the $\delta^{2}H$ throughout the growing season (Rock and Mayer 2007). Whereas, seasonal variation of deuterium in precipitation is the result of seasonal temperature changes, progressive changes in the isotopic content of cloud water sources as the growing season progresses, and the "amount effect" where increases in deuterium are observed as the amount of monthly precipitation decreases (Dansgaard 1964, Kendall et al. 2004).

Water is not fractionated when taken up by plant roots and transported into stems for use in photosynthetic gas exchange (Flanagan and Ehleringer 1991). As a result, stem water is isotopically the same as the soil water available to the plant (Flanagan and Ehleringer 1991). By comparing the isotopic composition of cottonwood stem water to that of the Oldman River and summer precipitation, the relative contribution of each to seasonal cottonwood transpiration can be determined.

2. MATERIALS AND METHODS

2.1 Study site details

The cottonwood woodland used in this study is located in the Helen Schuler Nature Centre (HSNC), Lethbridge AB, Canada on the East side of the Oldman River (49° 42' 08.58" N, 112° 51' 41.79" W). The HSNC woodland is primarily bordered by grassland coulees to the east and the Oldman River to the west (Figure 2.1). Groundwater in the HSNC flows northwards driven by the directional flow of the Oldman River (Figure 2.2). Mean daily temperatures are 18°C and -6°C for July and January respectively based on a 30-year average (1981 – 2010) (Government of Canada 2010). Lethbridge is classified as a semi-arid region with mean annual precipitation of 380 mm with an average of 273 mm falling in the months May to October (Government of Canada 2010).

The woodland at the HSNC had a mixture of grasses, shrubs, and forbs in the understory in addition to the cottonwood trees which contributed to the total leaf area of the site. The cottonwood canopy was mostly made up of plains cottonwood (*Populus deltoides*) with narrow-leaf cottonwood (*Populus angustifolia*) and possibly some balsam poplar (*Populus balsamifera*) spread throughout (Rood et al. 2013). Hybridization was present among these three species. The cottonwood canopy in the HSNC had a mean height of 18 ± 5 m with a mean tree diameter of 36 ± 15 cm based on diameter at breast height (DBH) and clinometer measurements of 60 cottonwood trees spaced throughout the HSNC.

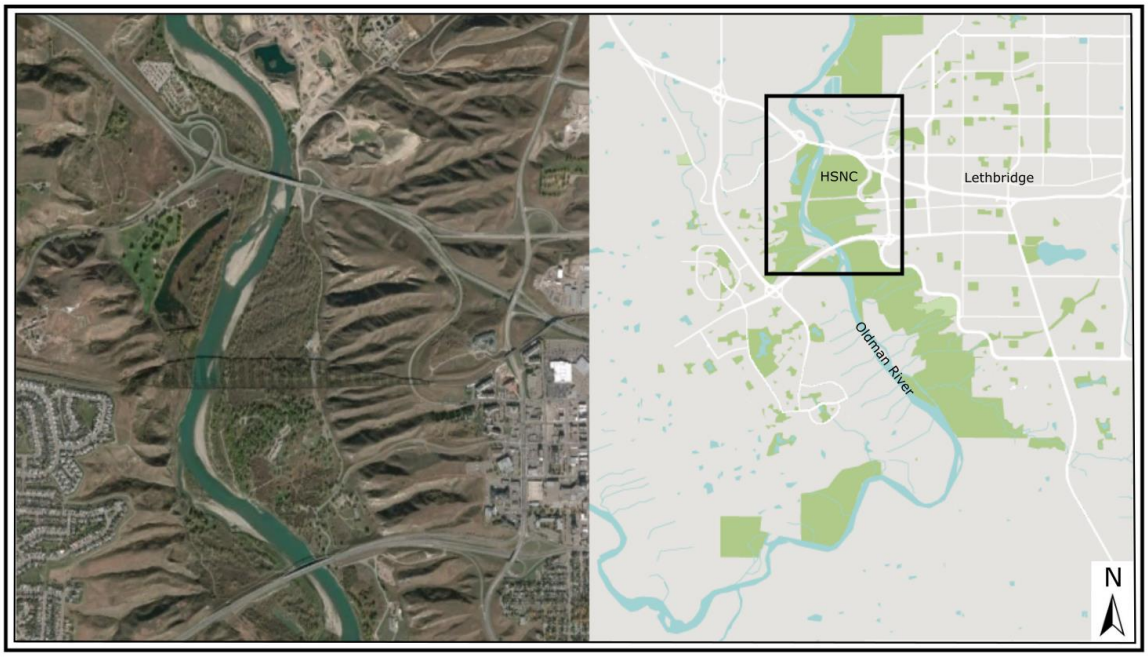

Figure 2.1: Location of the HSNC cottonwood woodland study site relative to the City of Lethbridge in southern Alberta (Google Earth: Digital Globe 2015).

Figure 2.2: Map of hydrological flow in the HSNC and corresponding directional flow of the Oldman River (Google Earth: Digital Globe 2015).

2.2 Experimental set-up

The eddy covariance technique was used to measure latent heat, H_2O, CO_2, and sensible heat fluxes in the woodland from April 30th to October 14th, 2014. Instrumentation was located near the eastern edge of the woodland on a telescoping aluminum tower and powered using a system of solar panels and automotive batteries (Figure 2.3).

The top of the tower housed a three-dimensional sonic anemometer (CSAT3, Campbell Scientific Inc., Logan UT, USA) and an infrared gas analyzer (LI-7200, LI-COR Biosciences, Lincoln NE, USA) mounted at 22 m above ground. These measured the three components of wind velocity as well as the density of water vapour and CO_2, respectively. A photosynthetically active radiation (PAR) sensor (LI-190 Quantum Sensor, LI-COR Biosciences, Lincoln NE, USA) and a net-radiometer (NR-Lite, Kipp and Zonen, Delft, Holland) were also located at the top of the tower.

Three soil heat flux plates (HFT3, Campbell Scientific Inc., Logan UT, USA) were located approximately 1 metre to the west of the tower at 5 cm depth. A temperature and relative humidity probe (HC2S3, Campbell Scientific Inc., Logan UT, USA) was affixed to a nearby scaffold at 1 m above ground. All measurements were recorded on a data logger (CR23X, Campbell Scientific Inc., Logan UT, USA) and associated multiplexer (AM416, Campbell Scientific Inc., Logan UT, USA).

Due to the amount of disturbance in the shallow soil layers caused by the installation of the tower, an additional data logger (CR23X, Campbell Scientific

Inc., Logan UT, USA) was placed approximately 60 m to the west of the tower and equipped with soil moisture, temperature and heat flux probes in the shallow soil layers. Four soil heat flux plates (HFT3, Campbell Scientific Inc., Logan UT, USA) were placed at 5 cm depth. Four water content reflectometers (CS616, Campbell Scientific Inc., Logan UT, USA) were placed in the 0 to 15 cm range and four soil temperature probes (107, Campbell Scientific Inc., Logan UT, USA) were placed at 7.5 cm depth. Soil moisture measurements were calibrated as noted in the Appendix (section 7.5).

A plastic collection jar attached inside a modified tipping bucket rain gauge was used to collect precipitation. The rain gauge housing served as protection from the wind as well as a screen from solar radiation to prevent evaporation from the collection jar. The precipitation collection device was located on the roof of the Alberta Water and Environmental Sciences Building (AWESB) in West Lethbridge, Alberta.

Figure 2.3: Helen Schuler Nature Centre (HSNC) cottonwood woodland in Lethbridge AB, Canada. Locations of the main flux tower and second auxiliary data logger are shown. (Image credit: Gordon Logie, personal communication, March 2015.)

Figure 2.4: Primary HSNC measurement compound and the flux tower. Water vapour fluxes were measured at the top of the tower at a height of 22 m, 4 meters above the cottonwood canopy when the tower was extended. Systems were powered using solar panels and automotive batteries.

2.3 Ecosystem leaf area index

2.3.1 Understory vegetation harvesting

The one-sided leaf area per unit ground area (leaf area index, LAI, $m^2\ m^{-2}$) of the low lying plant matter at the HSNC was measured using a harvesting method. Every two weeks all vegetation within a 20 x 50 cm frame was clipped down to the soil and the total green leaf area measured. Four sampling points (1 m^2 quadrats) were placed in separate locations throughout the HSNC. The spatial sampling was included as a way to capture the variability observed in understory vegetation throughout the site (Figure 2.5). For each harvest during the growing season a new 20 x 50 cm portion of each 1 m^2 quadrat was clipped so that areas which were previously harvested would not be sampled again.

Samples from each quadrat were individually sorted to remove any dead matter and the remaining living green biomass was weighed. The LAI of the dry green biomass for each quadrat was measured in triplicate using the LI-3100C Leaf Area Meter (LI-COR Biosciences, Lincoln NE, USA). This was done for the first half of the season until peak biomass was observed. After which a regression between dry green biomass and measured LAI was used to calculate LAI until the conclusion of the growing season (Equation 2.1: n=16, R^2=0.96).

$$LAI = 0.004 \cdot biomass + 0.14 \qquad (2.1)$$

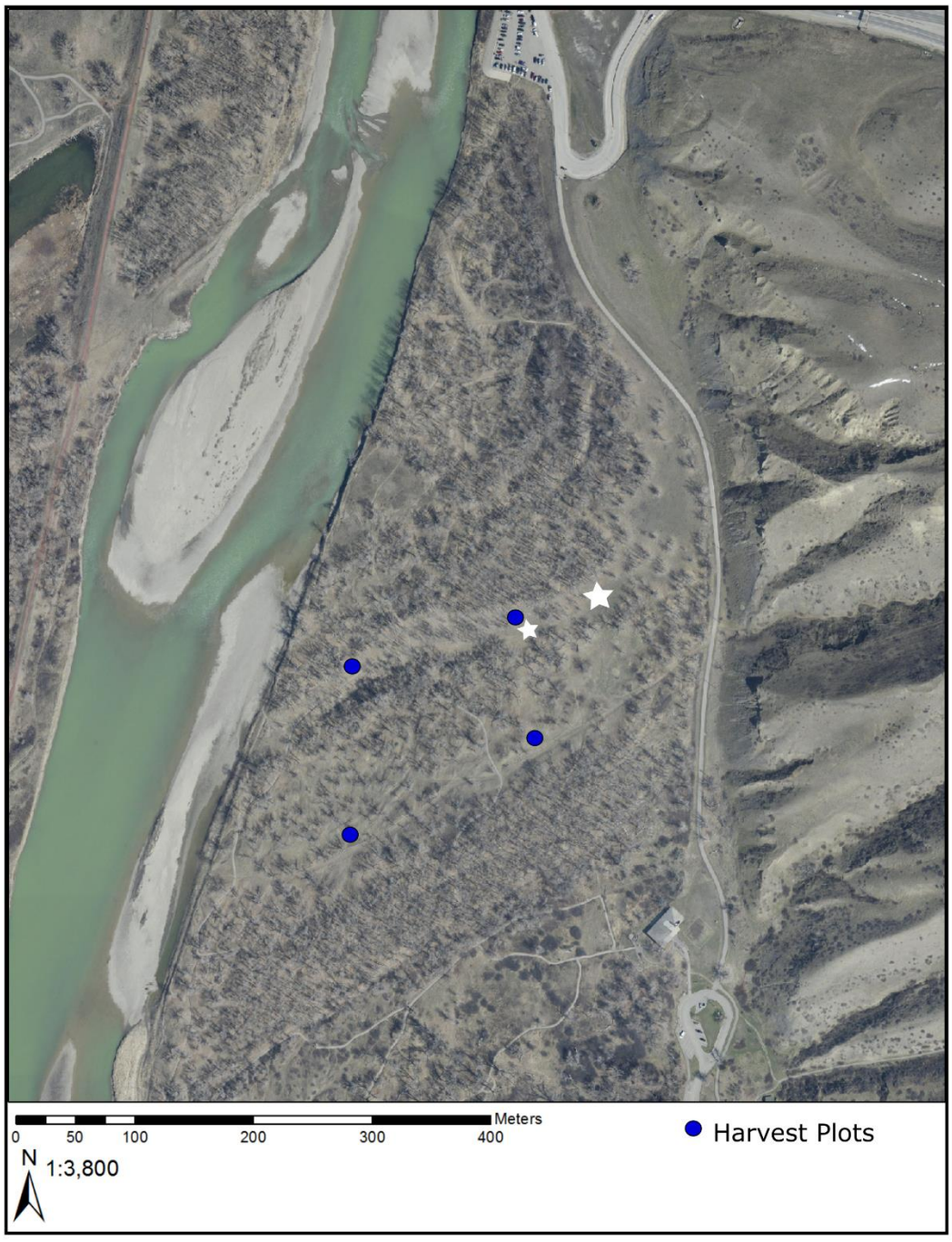

Figure 2.5: Aerial view of the cottonwood woodland in the HSNC. White stars show the locations of the flux tower and auxiliary data logger. Blue markers show the relative location of the four, 1 m^2 quadrats used to collect low-lying biomass throughout the growing season (Image credit: Gordon Logie, personal communication, March 2015).

2.3.2 Optical LAI measurements

LAI was estimated for the cottonwood canopy using the LAI-2000 (LI-COR Biosciences, Lincoln NE, USA) and the Tracing Radiation and Architecture in Canopies (TRAC) optical sampling instruments. Two LAI-2000 instruments were employed to measure the LAI of the canopy. One LAI-2000 was placed on a tripod in a large open region of the cottonwood woodland. It was used to collect measurements of incoming radiation with no interference from the cottonwood canopy. The second LAI-2000 was carried through the woodland along pre-determined transects to measure incoming radiation below the tree canopy. The Tracing Radiation and Architecture in Canopies (TRAC) (Leblanc et al. 2002) was used to measure the canopy clumping index throughout the cottonwood woodland along pre-determined transects. The clumping index was used to correct the results obtained from the LAI-2000 which does not account for within branch canopy clumping (Chen 1996). Optical measurements were made every two weeks throughout the 2014 growing season.

The LAI-2000 requires that no direct light be present on the canopy during measurements (LI-COR Biosciences 1992). To accommodate this, all measurements with the LAI-2000 were made shortly before dawn or just after sunset when only diffuse light was present. TRAC measurements were made as close to the ideal measurement time as possible, when the sun was at a zenith angle of approximately 60 degrees (Leblanc et al. 2002). For the HSNC this typically corresponded to late-morning or mid-afternoon. Care was taken to ensure the LAI-2000 and TRAC measurements were taken under clear skies to reduce the chance

of error introduced by variable sky conditions (LI-COR Biosciences 1992, Leblanc et al. 2002). For each bi-weekly measurement period, LAI-2000 measurements were taken at 72 separate measurement points. Points were spread over 5 transects spaced throughout the site with an average of 14 measurement points per transect. Transects were aligned along a North-West axis and all measurements were taken with the operator facing North-West (Figure 2.6). Measurements were completed using the field methodology outlined in the LAI-2000 operating manual (LI-COR Biosciences 1992).

Figure 2.6: Aerial view of the cottonwood woodland in the HSNC. White stars show the locations of the flux tower and auxiliary data logger. Blue markers show the location of the 72 LAI-2000 measurement points arranged over 5 transects used to measure LAI every two weeks from April to October, 2014. (Image Credit: Gordon Logie, personal communication, March 2015.)

The NW orientation of the LAI transects was intended to satisfy the requirement of the TRAC which ideally has the operator walking in a direction that is perpendicular to the transitory path of the sun (Leblanc et al. 2002). However, it was found that during the height of the season it was impractical to follow the previously defined LAI-2000 transects using the TRAC. The dense vegetation present in the understory at the HSNC made the steady walking pace required for the TRAC impossible. As a result, TRAC measurements were performed along a different set of 5 transects on a two-week basis from July to September (Figure 2.7). The TRAC transects made use of the abundant walking paths and deer trails present in the HSNC. Care was taken to follow as closely as possible to the NW orientation of the LAI-2000 transects.

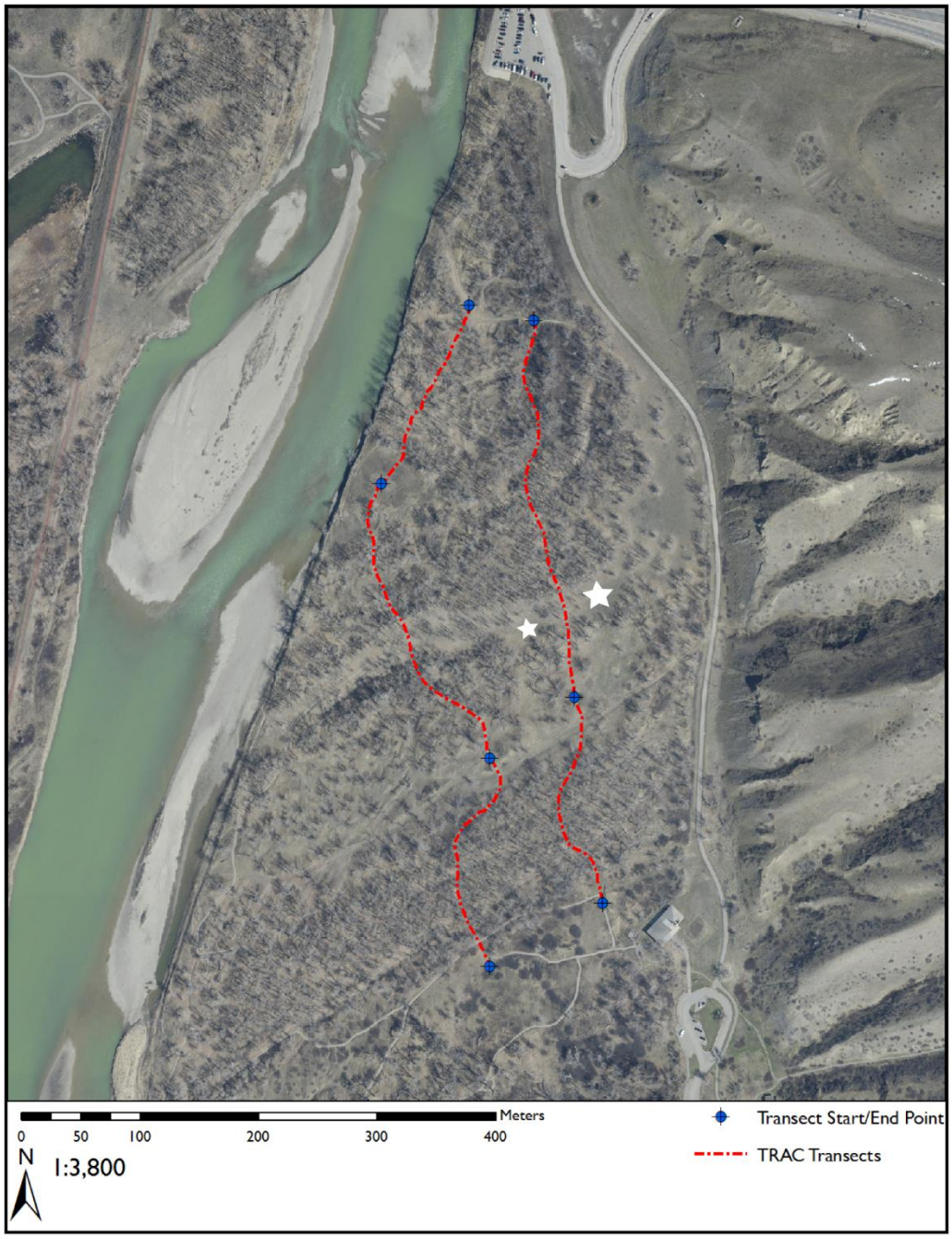

Figure 2.7: Aerial view of the cottonwood woodland in the HSNC. White stars show the locations of the flux tower and auxiliary data logger. Line markers show the location of the TRAC measurement paths arranged over 5 transects used to measure the clumping index on a two-week basis from July to September. Blue markers show the start/end points of each transect (Image Credit: Gordon Logie, personal communication, March 2015).

LAI-2000 measurements were corrected for within-branch clumping using the average clumping index obtained with TRAC measurements according to the method in Chen et al. (2006).

$$LAI = \frac{(1 - \alpha_w) \cdot L_e \cdot \gamma_E}{\Omega_E} \qquad (2.2)$$

L_e is the effective LAI as measured by the LAI-2000 ($m^2\ m^{-2}$). Gamma (γ_E) is the leaf-to-shoot area ratio, where γ_E is 1 for broadleaf deciduous trees. Omega (Ω_E) is the clumping index as measured using the TRAC. Alpha (α_w) is the woody-to-total leaf area ratio and is determined using the method described in Serbin et al. (2013).

$$\alpha_w = \frac{W}{L_e \left(\frac{\gamma_E}{\Omega_E}\right)} \qquad (2.3)$$

W is the woody surface area ($m^2\ m^{-2}$) measured with the LAI-2000 after leaf senescence had occurred. When correcting LAI values, the seasonal average clumping index was used.

2.3.3 Litter-trap collection

Collection of fallen leaves (litter) during leaf senescence allowed for the determination of woodland LAI at a time when LAI was at its highest. These results were used to confirm the validity of LAI measurements made using the optical instruments throughout the season.

A total of 19 laundry baskets, with drainage holes drilled through the base, were placed at regular intervals throughout the cottonwood woodland to collect leaf litter. A large collection region within the HSNC was used to give a broad sampling distribution of the variety of terrain, foliage density, and species diversity (Nasahara et al. 2008). All litter-trap locations corresponded to optical LAI measurement points (Figure 2.8).

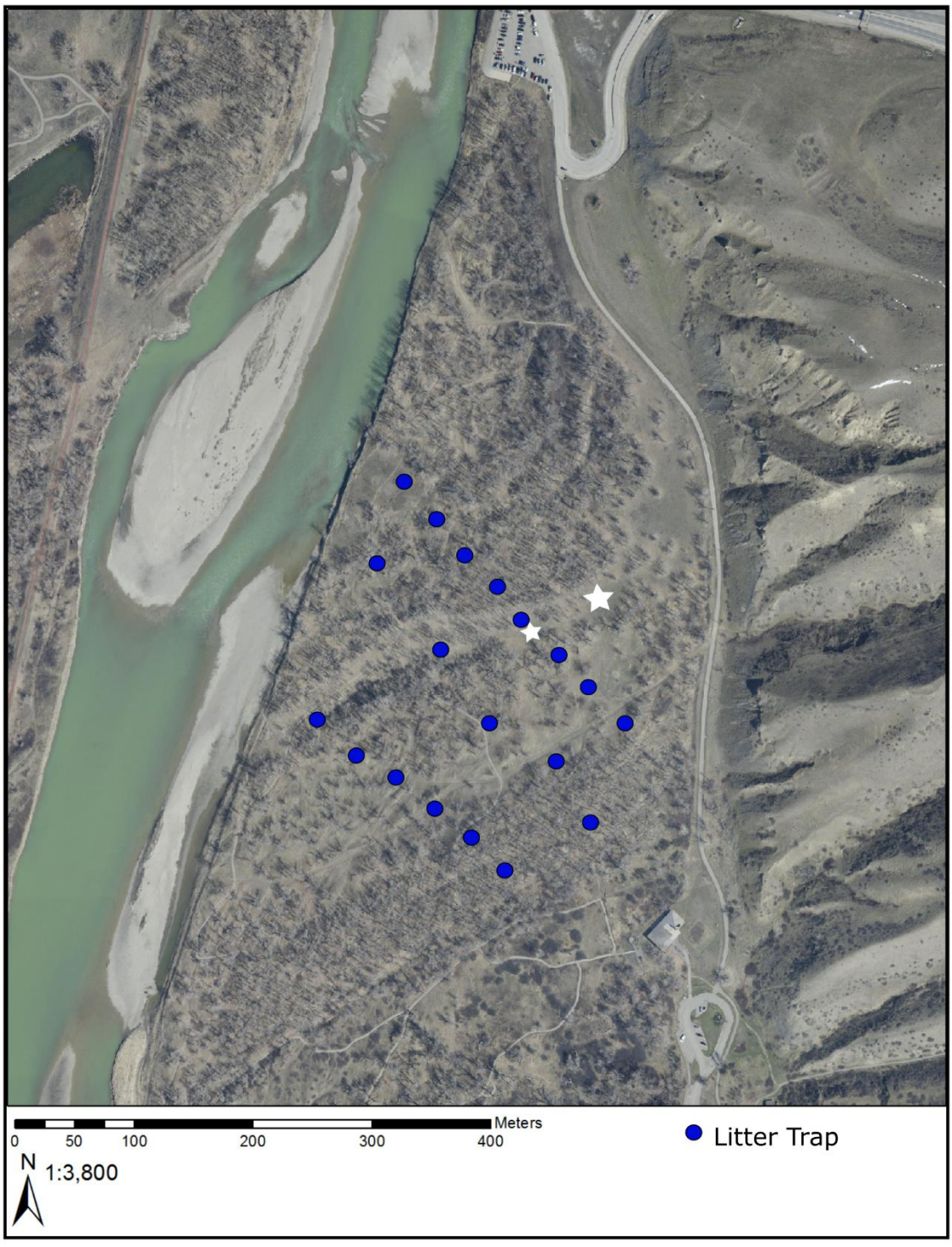

Figure 2.8: Aerial view of the cottonwood woodland in the HSNC. White stars show the locations of the flux tower and auxiliary data logger. Blue markers show the location of litter trap collection points. Baskets were installed in September 2014 and collected on a two week basis until the conclusion of the season. (Base image credit: Gordon Logie, personal communication, March 2015.)

Two sizes of basket traps were employed, with collection areas of 0.195 m^2 and 0.213 m^2 respectively. Litter was collected at two week intervals starting in mid-September and continuing until late October when leaves had fully senesced. Collected litter from each trap was sorted into three categories: broad-leaf cottonwood (*P. deltoides, P. balsamifera*), narrow-leaf cottonwood (*P. angustifolia*), and understory shrub leaves (shrub sp.). Hybrids were grouped into either cottonwood category based on similarity of leaf shape.

A small collection of leaves was made in September, independent of the litter trap collection. This collection was used to measure the average leaf area per unit dry mass for the three leaf categories used in the litter trap collection. The LAI of collected litter was calculated as the product of the average leaf area per unit mass for each leaf type and the dry weight of the collected litter (divided by the basket collection area) (Table 2.1).

Table 2.1: The average leaf area per unit of dry biomass for three categories of leaf: broad-leaf cottonwood, narrow-leaf cottonwood, and shrub sp.

Classification:	**Average leaf area per unit mass: ($cm^2 \cdot g^{-1}$)**
Broad-leaf	107.9
Narrow-leaf	117.8
Shrub sp.	118.0

2.3.4 Calculation of functional LAI

A daily estimate of LAI was calculated using the CO_2 flux recorded with the eddy covariance (EC) method. Net ecosystem productivity (NEP) is the CO_2 flux measured using eddy covariance and is equal to the carbon uptake through photosynthesis minus total ecosystem respiration through heterotrophic and autotrophic respiration (Woodwell and Whittaker 1968, Flanagan et al. 2013). Written as: NEP = GEP - TER, where GEP is gross ecosystem productivity and TER is total ecosystem respiration (Woodwell and Whittaker 1968, Flanagan et al. 2013).

The amount of photosynthesis occurring is dependent on the presence of photosynthesizing surfaces, such as leaves. As a result, GEP can be used to determine functional leaf area. Functional LAI is a measure of leaf area index based on the total carbon uptake through photosynthesis (GEP) occurring in the leaves. This is in contrast to the optically measured LAI which represents only the physical area of the leaves. The measured NEP at the HSNC was partitioned into its respective components of GEP and TER (Lawrence B. Flanagan, personal communication, 2015). The values for GEP were normalized and a curve was fitted. This fitted curve was then multiplied by the optically measured peak LAI of 1.8 m^2 m^{-2} which then provided an estimate of functional LAI at the HSNC over the span of the growing season (Lawrence B. Flanagan, personal communication, 2015).

2.4 Eddy covariance data screening and preliminary analysis

2.4.1 Eddy covariance data screening

Available ET data was limited during the 2014 growing season due to flooding in late June when instrumentation was removed and due to a gas analyzer malfunction in August. To compensate for this, the data screening process was structured in such a way to minimize the removal of remaining data. This was done by testing four levels of data screening to determine the best parameters for removing inaccurate values while still retaining the largest possible amount of accurate data for analysis (Table 2.2). Factors considered for screening were precipitation events (including time periods a minimum of two hours after rain events), times with inadequate turbulence ($u^* < 0.33$), and times when the wind was coming from the east (45° < wind direction < 135°). The most ideal screening procedure was determined to be the one which provided the best fit between modelled ET and measured ET (Appendix, section 7.4).

Lack of adequate turbulence was considered to occur when turbulent flow was below the friction velocity (u^*) threshold ($u^* < 0.33$, Appendix, section 7.2). Eddy covariance requires turbulent flow to accurately measure fluxes (Baldocchi 2003). For precipitation screening, two levels of screening were tested to determine the best filtering method to use (Table 2.2). Precipitation filtering included the rain event ($p > 1$ mm) as well as the evaporative period afterwards (2 or 24 hours) when the canopy was wet. Lastly, ET fluxes measured during eastern originating winds may not have been representative of cottonwood transpiration at the HSNC. The eddy covariance method assumes that the measured canopy is flat (Baldocchi

2003). This assumption was violated at the HSNC when the primary wind direction was originating from the east where the raised grassland coulees were located. Additionally, the coulees did not have any trees and were not a part of the cottonwood woodland. Wind direction screening removed any measured values where the primary wind direction was originating in the east, defined as the wind direction range, 45° to 135° from North.

Table 2.2: A comparison table showing the four levels of data screening performed to test which provided the best modelled ET versus measured ET. Levels included removing all data below a u^* threshold of 0.33 m s^{-1}, removing all data from eastern originating winds, and removing data during time periods with precipitation events greater than 1 mm (and a minimum of 2 hours afterwards).

Filtering Level	**Turbulence Threshold $u^* > 0.33$ ms^{-1}**	**Eastern Wind Direction (135°>x>45°)**	**Precipitation $p > 1$ mm and 24 hr after**	**Precipitation $p > 1$ mm and 2 hr after**
Full Filtering	x	x	x	
No u^* Filter		x	x	
Reduced Filter		x		x
No Filtering				

For each level of filtering, the change in the linear regression slope between measured ET and modelled ET was minimal (Appendix, section 7.4). As a consequence, the reduced filtering method (Table 2.2) provided a slight advantage over the other levels of filtering.

Screened ET data and HSNC meteorological measurements were bin-averaged according to time of day to smooth daily fluctuations for effective modelling. Bin-averaging by time of day was performed by taking all values from a variable of interest in a date range and averaging together all values recorded at a specific time. The result was a data set which has one value for each of the 48 half-hour time slots in a day. This process was repeated for each measured variable required for modelling. To continue with modelling, a subset of the bin-averaged data was used consisting of daylight hours when photosynthesis and transpiration were occurring, defined as 6:30 to 19:00 hours.

2.4.2 Calculations of water-use efficiency

The water-use efficiency (WUE) of the HSNC cottonwood woodland was calculated for June, July, and August of the 2014 growing season. It was used as a check on leaf conductance to water vapour as the canopy aged. WUE is defined as the ratio of carbon assimilation during photosynthesis to water loss through transpiration (Osmond et al. 1982, Ponton et al. 2006, Yu et al. 2008) as expressed in Equation 2.4.

$$WUE = \frac{GEP}{ET} \quad (2.4)$$

Where GEP is carbon assimilation given by gross ecosystem photosynthesis (μmol m^{-2} day^{-1}) and ET is water flux as evapotranspiration (mmol m^{-2} day^{-1}). Any days with rain events ($p \geq 2$ mm) were removed from calculations of monthly average WUE.

2.4.3 Calculation of HSNC energy balance closure

A test of EC flux data quality was performed by checking the energy balance closure. The energy balance closure determines the amount of total energy exchange measured by the EC instrumentation at the HSNC. The energy balance equation accounts for all energy input and output of an ecosystem and is given by NR = G + H + λE (Penman 1948, Wever et al. 2002). Where NR is the net radiation, G is the soil heat flux, H is the sensible heat flux, and λE is the latent heat flux. A geometric mean regression between NR – G and H + λE determines closure. The energy balance closure check was performed for July at the height of the growing season when LAI and ET were at their peak values.

2.5 Eddy covariance data modelling

ET data were unavailable during times when they were filtered out (Methods, section 2.4.1) as well as for two extended periods where the EC instrumentation was not fully functioning. The first extended period of data loss was from June 17th (day 168) to July 2nd (day 183) due to flooding at the HSNC during which much of the instrumentation was removed to prevent water damage. A second extended period of data loss was due to a malfunction of the gas analyzer from July 28th (day 209) to August 22nd (day 234) where no water vapour densities were being measured.

2.5.1 Eddy covariance data modelling procedure

The Penman-Monteith (PM) equation was used to calculate evapotranspiration using known drivers of ET. For this research it was used to provide a calculation of evapotranspiration during times when measured values were unavailable.

The PM equation is given in Equation 2.5 (Monteith 1965).

$$E = \frac{\Delta(NR - G) + \lambda\gamma g_a \left(\frac{e_s - e_a}{P}\right)}{\lambda\left[\Delta + \gamma\left(1 + \frac{g_a}{g_c}\right)\right]} \qquad (2.5)$$

Where *NR* is the net radiation (W m^{-2}), *G* is soil heat flux (W m^{-2}), *P* is atmospheric pressure (kPa), e_s is the saturation vapour pressure of air at air temperature (kPa), e_a is the measured vapour pressure of air (kPa). g_c is the canopy conductance to water vapour (mol m^{-2} s^{-1}).

Boundary layer conductance to water vapour (g_a, mol m^{-2} s^{-1}) is a function of wind speed (u) and friction velocity (u^*) and calculated as shown in Equation 2.6 (Wever et al. 2002).

$$\frac{1}{g_a} = \frac{u}{(u^*)^2} + 6.2(u^*)^{-0.67} \qquad (2.6)$$

Δ is the change in saturation vapour pressure (e_s) with change in temperature (kPa °C^{-1}) and is given by Equation 2.7 (Allen et al. 1998).

$$\Delta = \frac{4098 \cdot e_s}{(T + 237.3)^2} \qquad (2.7)$$

Where *T* is the temperature of air (°C) and e_s is the saturation vapour pressure of air (kPa).

γ is the psychrometric constant (kPa °C^{-1}) and is given by Equation 2.8 (Ventura et al. 1999).

$$\gamma = \frac{c_p \cdot P}{0.622 \cdot \lambda} \qquad (2.8)$$

Where c_p is the specific heat of air which is equal to 0.001 MJ kg^{-1} °C^{-1}. P is the atmospheric pressure, and λ is the latent heat of vapourization (MJ kg^{-1}) calculated as given in Equation 2.9 (Henderson-Sellers 1984).

$$\lambda = 2.501 - 0.002361 \cdot T \qquad (2.9)$$

Where T is the temperature of air (°C). For calculating γ, λ remains in units of (MJ kg^{-1}) as given by Equation 2.9. However, for use in the PM equation λ is converted to units of J mol^{-1}.

$$\lambda\ (MJ\ kg^{-1}) = \lambda \cdot \frac{10^6 J}{MJ} \cdot 0.018\ \text{kg mol}^{-1} \qquad (2.10)$$

Where 0.018 kg mol^{-1} is the molecular weight of water.

With the suite of measurements made at the HSNC flux tower, all variables in the PM equation were available to use either through direct measurement or indirect calculation, with the exception of canopy conductance (g_c). To determine canopy conductance the PM equation was inverted, solving for canopy conductance (g_c) at times when ET was known (Equation 2.11).

$$g_c = g_a \left[\frac{\Delta(NR - G) + \lambda\gamma g_a \left(\frac{e_s - e_a}{P}\right)}{\lambda\gamma E} - \frac{\Delta}{\gamma} - 1 \right]^{-1} \qquad (2.11)$$

Where all variables are those as given following Equation 2.5. After using the inverted PM equation, all calculated canopy conductance values were divided by the LAI to scale down to leaf-level conductance (g_s, mmol m^{-2} s^{-1}) for use in modelling.

A Jarvis-type model was used to calculate leaf-level conductance (g_s) as a function of VPD and PPFD (Jarvis 1976, Wever et al. 2002). The model was parameterized using times when g_s, VPD, and PPFD were known.

$$g_s = g_{max} \cdot f(Q) \tag{2.12}$$

Where g_{max} (mmol m^{-2} s^{-1}) is a maximum value of leaf-level conductance as a function of VPD (hPa) (Wever et al. 2002). g_{max} is parameterized with the coefficient κ_D.

$$g_{max} = \frac{1}{\kappa_D (VPD)^{0.5}} \tag{2.13}$$

f(Q) is a function of photosynthetic photon flux density (PPFD, Q, μmol m^{-2} s^{-1}) and describes the response of leaf-level conductance to incident photosynthetically active radiation (Wever et al. 2002). *f(Q)* ranges between 0 and 1 is parameterized using the coefficient α.

$$f(Q) = \left(\frac{Q\alpha}{[1 + (Q^2\alpha^2/{g_{max}}^2)]^{0.5}}\right)\left(\frac{1}{g_{max}}\right) \qquad (2.14)$$

The SYSTAT10.2 software package was used to apply a non-linear least-squares regression to estimate values for α and κ_D using the Gauss-Newton method.

2.5.2 Determination of best model fit

The model fitting procedure described in section 2.5.1 was performed for three time periods during the growing season: early June, all of July, and late August. This was done to determine which time period provided the best fit between modelled values of ET and measured ET throughout the growing season. A complete seasonal data set was created which estimated ET on a half-hourly basis using the PM equation with modelled values of canopy conductance. Within this modelled dataset, daily LAI was estimated as a fitted function of gross ecosystem productivity (GEP) (Methods, section 2.3.4).

These modelled values of half-hourly ET were compared with measured 30-minute averages of ET for key periods during the growing season: July during peak LAI, early June before the loss of data to flooding, and late August after the gas analyzer outage was repaired. Modelled to measured evapotranspiration comparisons were made both for the 30-minute values, as well as for the same values bin-averaged according to time of day.

Comparing how well the modelled ET fit with the measured ET throughout the growing season was the deciding factor in which month was the most ideal from which to parameterize a seasonal model. The best fit was defined by the height of the slope and the closeness of the intercept to zero for linear regressions between measured and modelled ET for both the raw 30-minute averages and for the same values bin-averaged by time of day.

2.5.3 Cumulative water usage

To determine the cumulative water use by the HSNC cottonwood woodland over the span of the growing season, a gap-filled evapotranspiration dataset was created for the period from May 1st (day 121) to October 12th (day 286). Measured ET values were screened for inaccurate values using the reduced filtering method (Table 2.2). The screened ET dataset was gap-filled using calculated ET values from the PM equation and the parameterized conductance model with most accurate fit. Using final gap-filled ET dataset daily, weekly, and monthly sums of ET were calculated.

2.6 Cottonwood water sample collection and isotopic analysis

2.6.1 Water sample collection

Water samples were collected from three sources during the 2014 growing season: the Oldman River, HSNC groundwater, and Lethbridge precipitation.

River water and groundwater samples were collected every two weeks throughout the 2014 growing season and precipitation was collected weekly.

River water samples were collected below the surface in the centre of the Oldman River. This was achieved by lowering a weighted collection vessel from a pedestrian overpass near the southern end of the HSNC. Groundwater was collected from three existing groundwater wells made from 1 inch diameter vertical pipes which penetrated the saturated groundwater zone beneath the surface. The groundwater wells were located near the flux tower, in a gully near the geographical centre of the HSNC woodland, and at the woodland edge on the southern end of the HSNC a few meters from the Oldman River. Before each collection, any standing water in the wells was discarded to eliminate possible fractionation effects caused by evaporation. Collected river and groundwater samples were filtered for debris and sediment using a Buchner funnel connected to a vacuum pump and 1.1 μm filter papers (Whatman International Ltd, Maidstone England). Precipitation samples were collected from the roof of the Alberta Water and Environmental Sciences Building (AWESB) at the University of Lethbridge.

2.6.2 Stem sample collection

Clippings of cottonwood stems were taken from trees throughout the HSNC every two weeks from June 4th (day 155) to October 2nd (day 275). For most sample dates 6 replicates were collected, each originating from a separate tree. Only 4

replicates were collected on June 4th (day 155) and August 25th (day 237) due to difficulty peeling away bark in a timely fashion. Care was taken to select a large variety of cottonwood trees while ensuring no tree was sampled more than once throughout the growing season.

For each sample, a 5 cm long segment (n=2, roughly 1 cm in diameter) of a living branch on a healthy tree was clipped. All bark and green photosynthesizing layers were peeled off. Collected stem samples were sealed in glass vials using Parafilm and stored in a freezer to prevent evaporation prior to cryogenic water extraction.

2.6.3 Cryogenic water extraction and isotopic analysis

To determine the isotopic content of the water present in collected stem samples, the water had to be drawn out from the stems and bottled. This was done using cryogenic vacuum extraction following the method outlined in Ehleringer et al. (2000). Each stem sample was extracted for 90 minutes to remove all moisture (West et al. 2006).

All water samples collected from the Helen Schuler Nature Centre (HSNC) were analyzed for their δ^2H values. δ represents the deviation in isotopic abundance of deuterium (^2H) from a standard of known isotopic composition, written in parts per thousand (Harmon 1961).

$$\delta^2 H(‰) = \left(\frac{R_{Sample}}{R_{Standard}} - 1\right) \cdot 1000 \qquad (2.15)$$

Where R_{Sample} is the measured $^2H/H$ ratio and $R_{Standard}$ is the $^2H/H$ ratio of a known standard. All samples were analyzed at the University of Calgary Isotope Science Laboratory, AB Canada using a laser isotope analyzer (DLT-100 v.2, LosGatosResearch Inc., Mountain View CA, USA) with a liquid auto-sampler (CTC LC PAL, LEAP Technologies, Carrboro NC, USA) and laboratory water standards calibrated against international reference materials. Tests for precision and accuracy of the stable isotope measurements are included in the Appendix (section 7.6).

3. RESULTS

3.1 Seasonal variation of environmental variables

3.1.1 Temperature, precipitation, and Oldman River levels for 2014 and long-term average

The May to October 2014 growing season in the Helen Schuler Nature Centre (HSNC) was a wet year with above average precipitation, receiving a total of 370 mm compared to the 30-year average of 273 ± 33 mm (1981 - 2010) (Government of Canada 2010). A large fraction (49 %) of the precipitation was received in June, with an input of 180 mm compared to the 82 mm of the 30-year normal (Figure 3.1) (Government of Canada 2010). The other months in the 2014 growing season did not have substantially higher or lower than average precipitation. The wet growing season of 2014 contributed to above average peak flows in the Oldman River (Figure 3.2). Discharge reached a maximum of 572 $m^3\ s^{-1}$ relative to 319 $m^3\ s^{-1}$, as given by the historical average (1911 – 2012) (Water Survey of Canada 2014). The above average peak flows in the Oldman River led to flooding throughout the HSNC from June 17th (day 168) to July 2nd (day 183).

The 2014 daily average temperature was higher than the 30-year average for the months of July (20.2 compared to 18.2 ± 1.6 °C) and October (10.1 relative to 6.6 ± 1.7 °C). The remaining months showed no difference relative to the 30-year normal as shown in Figure 3.1 (Government of Canada 2010).

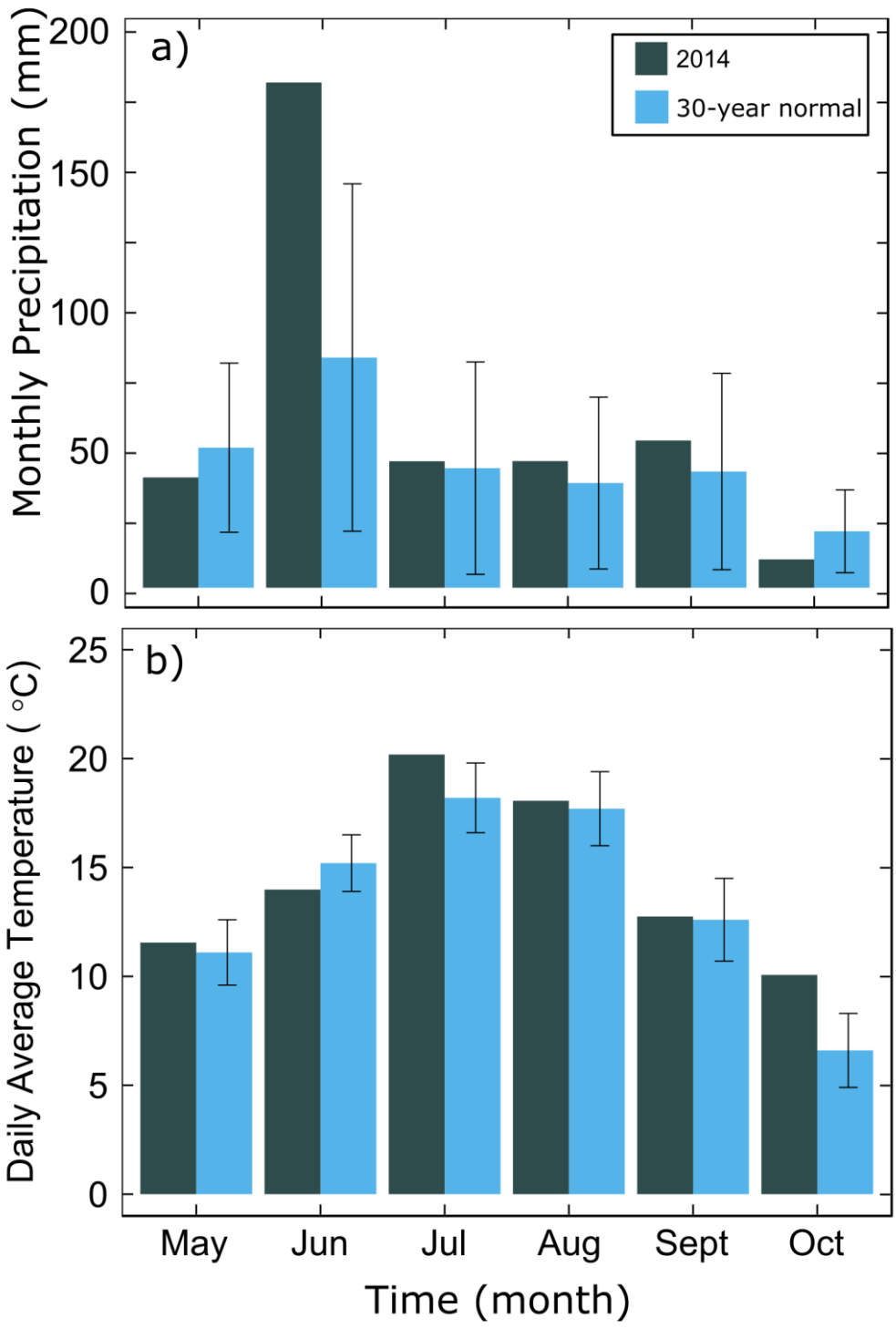

Figure 3.1: Major 2014 environmental conditions (temperature and precipitation) relative to the long-term 30-year average (± SD) from 1981 – 2010 (Government of Canada 2010).

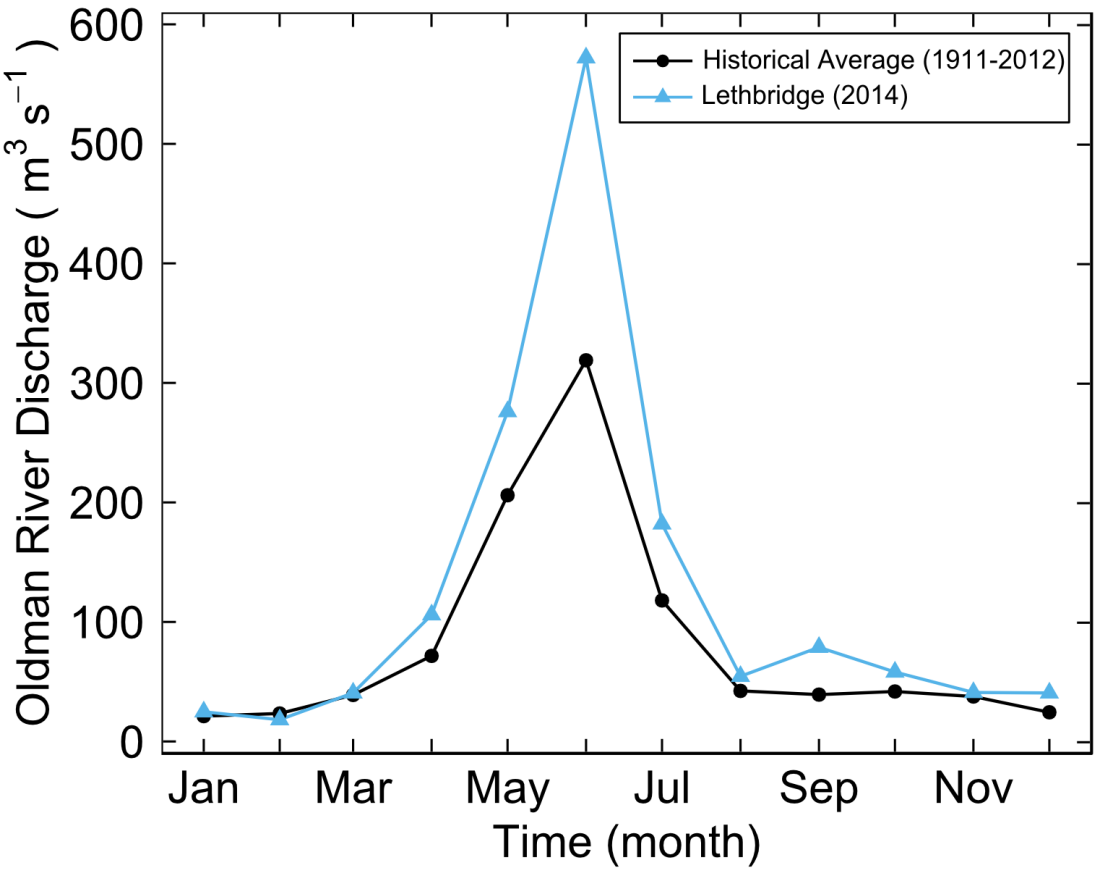

Figure 3.2: Monthly Oldman River discharge for 2014 relative to the historical average (1911 - 2012). Data given as recorded by the Water Survey of Canada at station no. 05AD007 (Water Survey of Canada 2014).

3.1.2 Seasonal variation in environmental drivers of ET

Estimating evapotranspiration (ET) using the Penman-Monteith (PM) equation and the empirical model for stomatal conductance relied on measurements of major environmental conditions for the 2014 growing season (Figure 3.3). In 2014, air temperature reached its maximum daily average at the peak of the growing season in July. Highest and lowest temperatures of the growing season were 34 °C and -7 °C respectively. A similar seasonal trend was observed for net radiation which peaked early in July at approximately 600 W m^{-2}, this dropped to approximately 300 W m^{-2} by the conclusion of the growing season.

Maximum daily vapour pressure deficit showed a gradual increase and decline over the season but had large variation in daily values, ranging from close to zero to approximately 4 kPa. For the shallow surface layers (0 – 15 cm) in the HSNC, the soil water content increased directly in relation to precipitation input. Soil water content was at a maximum of 0.27 m^3 m^{-3} near the start of May (day 124) and at its lowest at the conclusion of the season, 0.17 m^3 m^{-3} (day 289). The saturated period during the HSNC flooding was not captured due to the removal of instrumentation. Average wind speed for the HSNC was 1.7 ± 0.7 m s^{-1} with a maximum daily wind speed of 5.2 m s^{-1}. The 2014 May to October HSNC groundwater table had an average depth of 2.15 ± 0.80 m below ground relative to ground level at the EC tower compound (David Pearce, personal communication, 2015). This reached a maximum of 2.07 m above ground on June 20th (day 171) during the extensive HSNC flooding and a minimum of 2.88 m below ground at the conclusion of the season on October 21st (day 294).

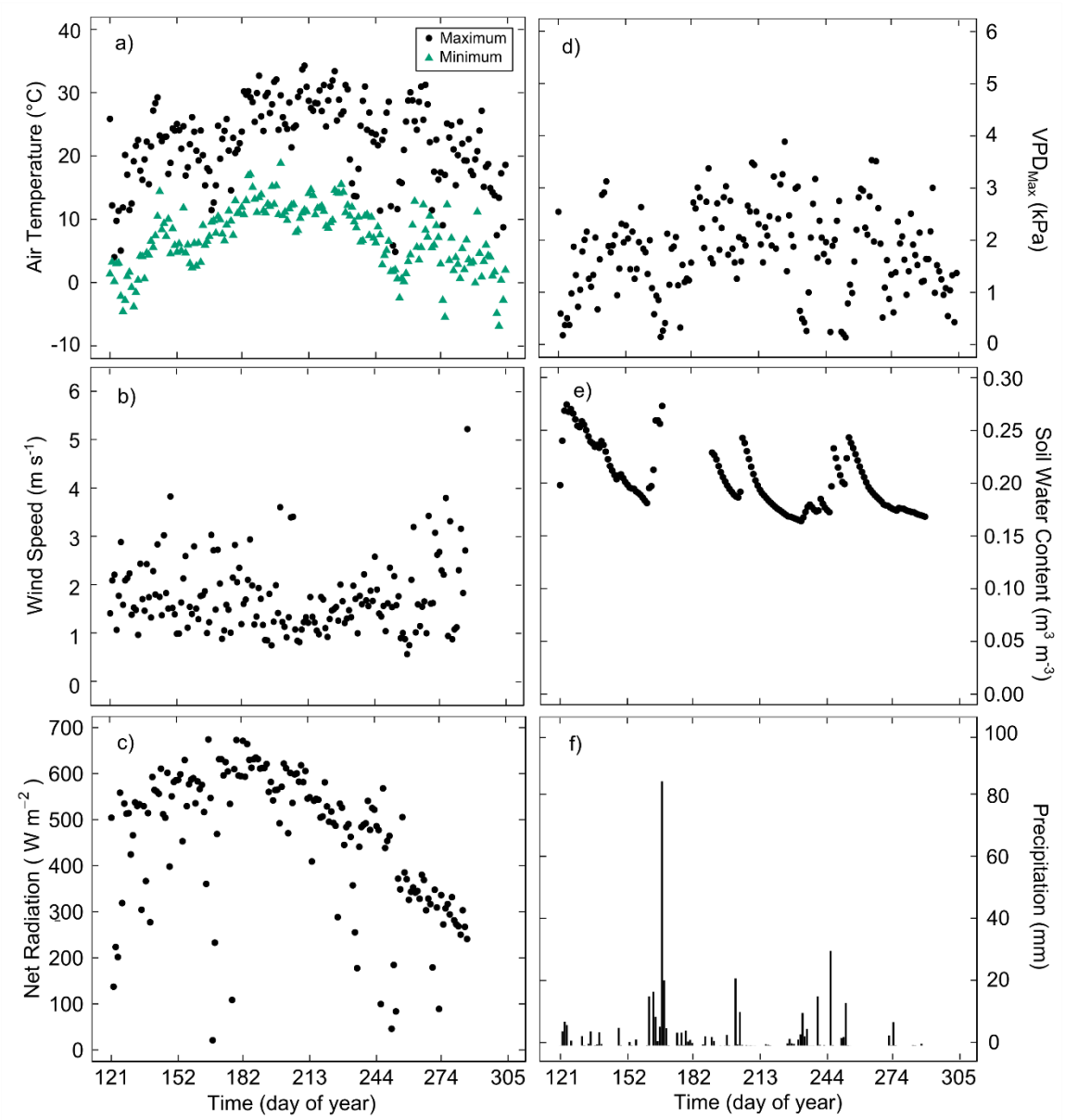

Figure 3.3: Seasonal variation in daily maximum and minimum air temperature, daily average wind speed, daily maximum net radiation, maximum daily vapour pressure deficit, daily average soil moisture content, and daily total precipitation.

3.2 Seasonal variation in ecosystem leaf area index

3.2.1 Understory herbaceous vegetation and optical cottonwood canopy LAI

Total understory leaf area index (LAI) varied strongly among the four harvest locations throughout the HSNC. The north-west and south-west sampling areas had higher peak average LAI compared to the north-east and south-east plots (Figure 3.4). The understory LAI reached a mean peak of 0.9 ±0.2 $m^2 m^{-2}$ between July 10th (day 191) and August 25th (day 237), 2014.

The cottonwood canopy was at peak leaf area roughly between July 11th (day 192) and August 26th (day 238) before a decline was observed with the optical measurement methods. LAI for this peak period was found to be 0.9 ± 0.1 $m^2 m^{-2}$ (Figure 3.5). The cumulative LAI of the HSNC was 1.8 ± 0.2 $m^2 m^{-2}$ with the understory and canopy each contributing to approximately 50 ‰ of the total leaf area. Measurements made with the LAI-2000 underestimated LAI by an average of 0.1 $m^2 m^{-2}$ at the height of the growing season. This underestimation was corrected using the average HSNC clumping index of 0.93 as measured by the TRAC. The clumping corrected values were then corrected for the woody-to-total leaf area ratio which reduced total LAI by an average of 0.3 $m^2 m^{-2}$ compared to the clumping corrected LAI.

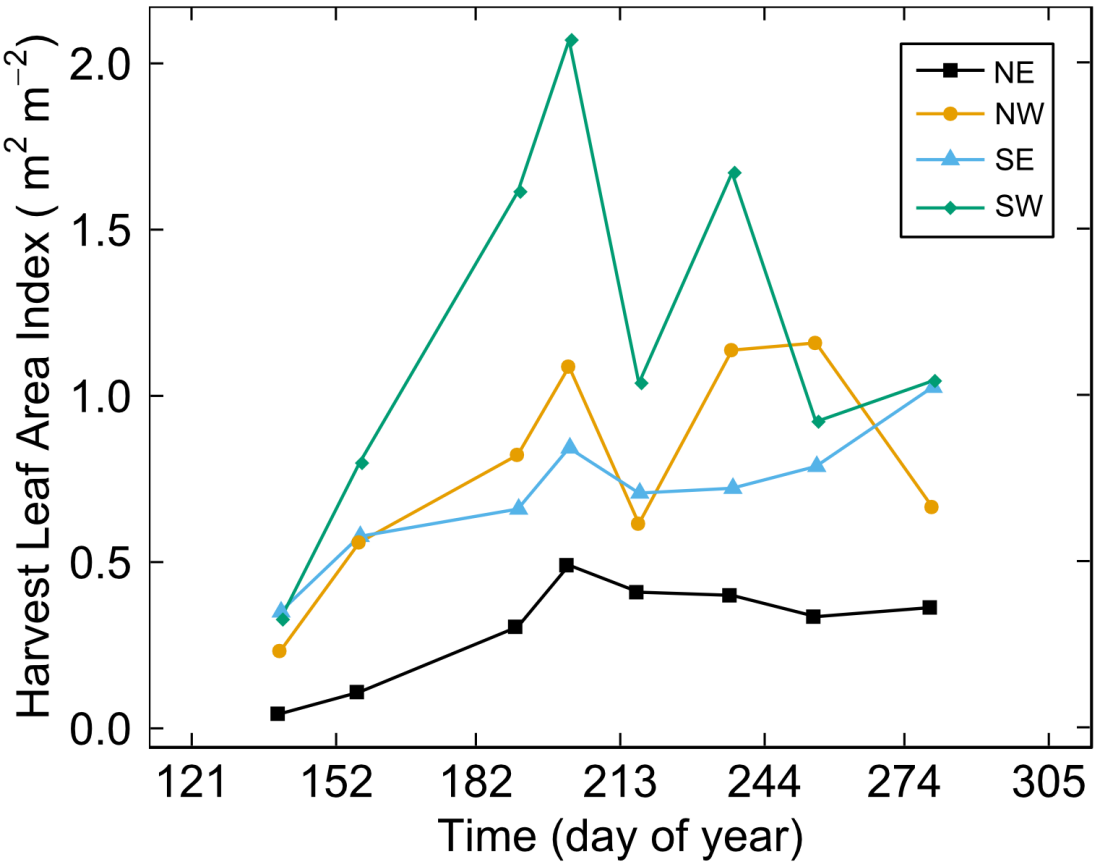

Figure 3.4: Variation in LAI among the four harvest plots at the HSNC.

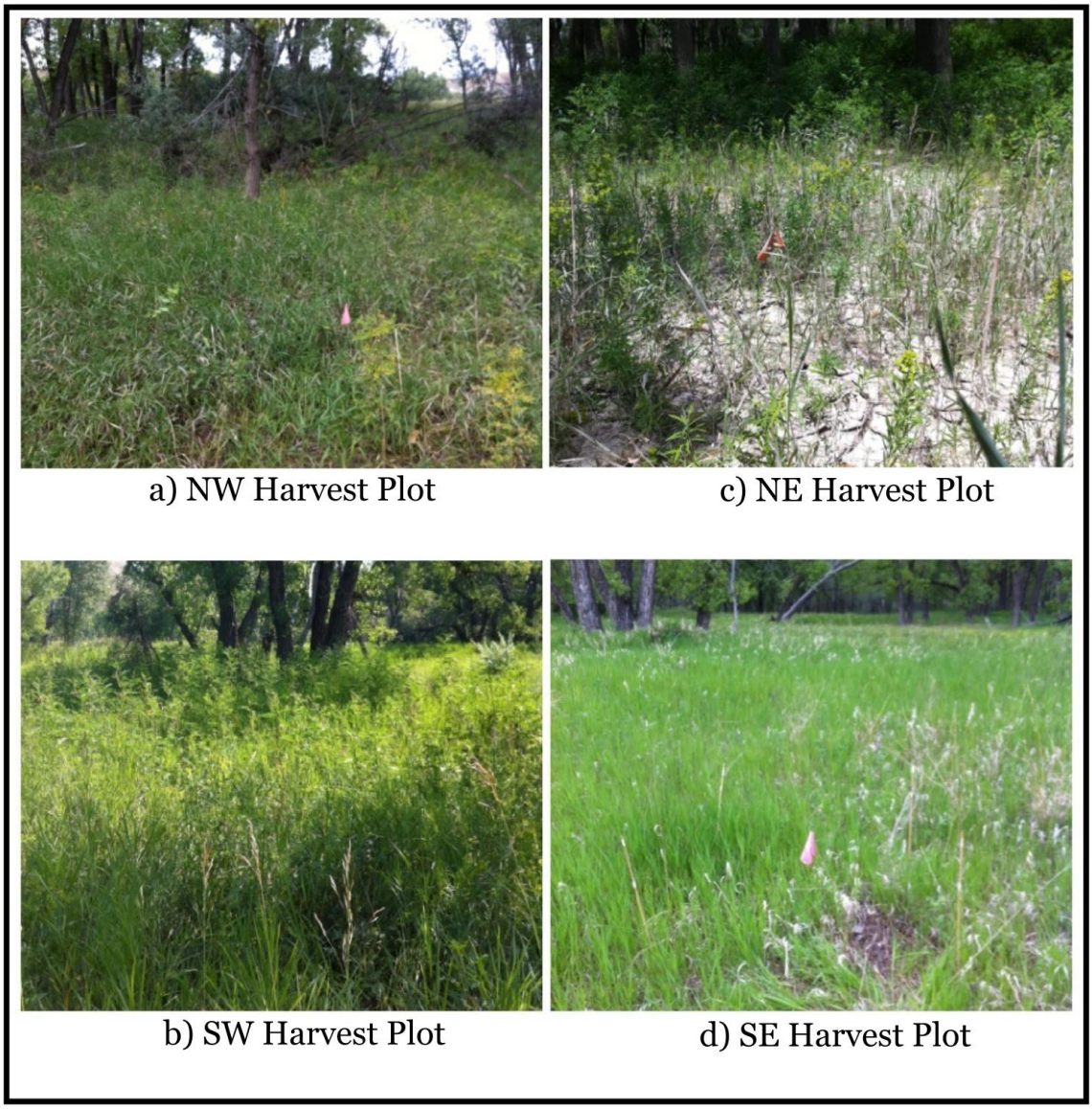

Figure 3.5: Variation among the four harvest plots at the HSNC in July during the peak of the season.

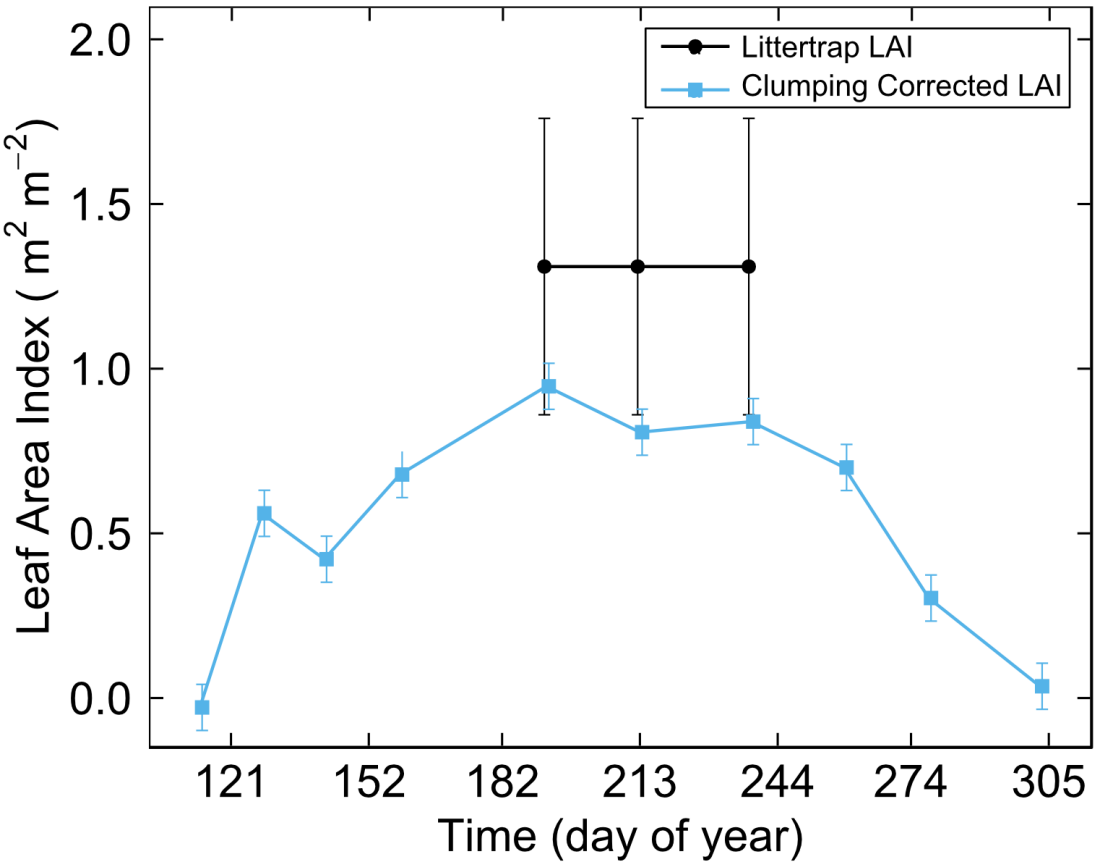

Figure 3.6: LAI of the cottonwood canopy. Corrected LAI showed the LAI corrected using the woody-to-total leaf area ratio (α) and the TRAC obtained clumping index (Ω_E) as discussed in section 2.3.2. Litter-trap LAI showed the total LAI at peak (± SD) as determined using fallen leaves collected at senescence.

3.2.2 Litter-trap cottonwood canopy LAI and functional LAI

Of the collected leaves from senescence (litter-traps), 81% were broad-leaf cottonwood (*P. deltoides, P. balsamifera*), 14% belonged to narrow-leaf cottonwood (*P. angustifolia*), and the remaining 5% belonged to miscellaneous shrubs. Hybrids were grouped in with either the broad-leaf or narrow-leaf category depending on general leaf shape. Shrub leaf area was not included in calculations of cumulative canopy leaf area due to the inclusion of understory harvest measurements of LAI. Of the three collections, the largest biomass was collected on September 26th (day 269), accounting for 72 % of collected litter (Table 3.1). Total cottonwood leaf area from litter was found to be 1.3 ± 0.4 $m^2\ m^{-2}$ compared to 0.9 ± 0.1 $m^2\ m^{-2}$ as found using optical methods (Figure 3.6).

Functional LAI, calculated for use in ET modelling, followed a similar seasonal trend as optical LAI measurements (Figure 3.6 vs Figure 3.7). However, functional LAI was seen to reach the peak earlier in the season by June 23rd (day 174) compared to July 11th (day 192) for optical LAI. The functional LAI peak corresponded to a time when optical measurements could not be performed due to the HSNC flooding. In addition to an earlier observed peak, functional LAI also began to decrease earlier showing a strong downward trend decreasing by 10 % by the start of August (day 213). Comparatively, no decreases in optical LAI were observed until after August 26th (day 238).

Table 3.1: LAI results of the three senescence litter collections. LAI was determined through multiplying dried leaf biomass by the known ratio of leaf area to dry weight for each leaf type.

Day of Year	**Broad-leaf LAI ($m^2 m^{-2}$)**	**Narrow-leaf LAI ($m^2 m^{-2}$)**	**Total LAI ($m^2 m^{-2}$)**
269	0.84	0.12	0.96
280	0.10	0.02	0.12
291	0.18	0.05	0.25
Cumulative LAI:			**1.33**

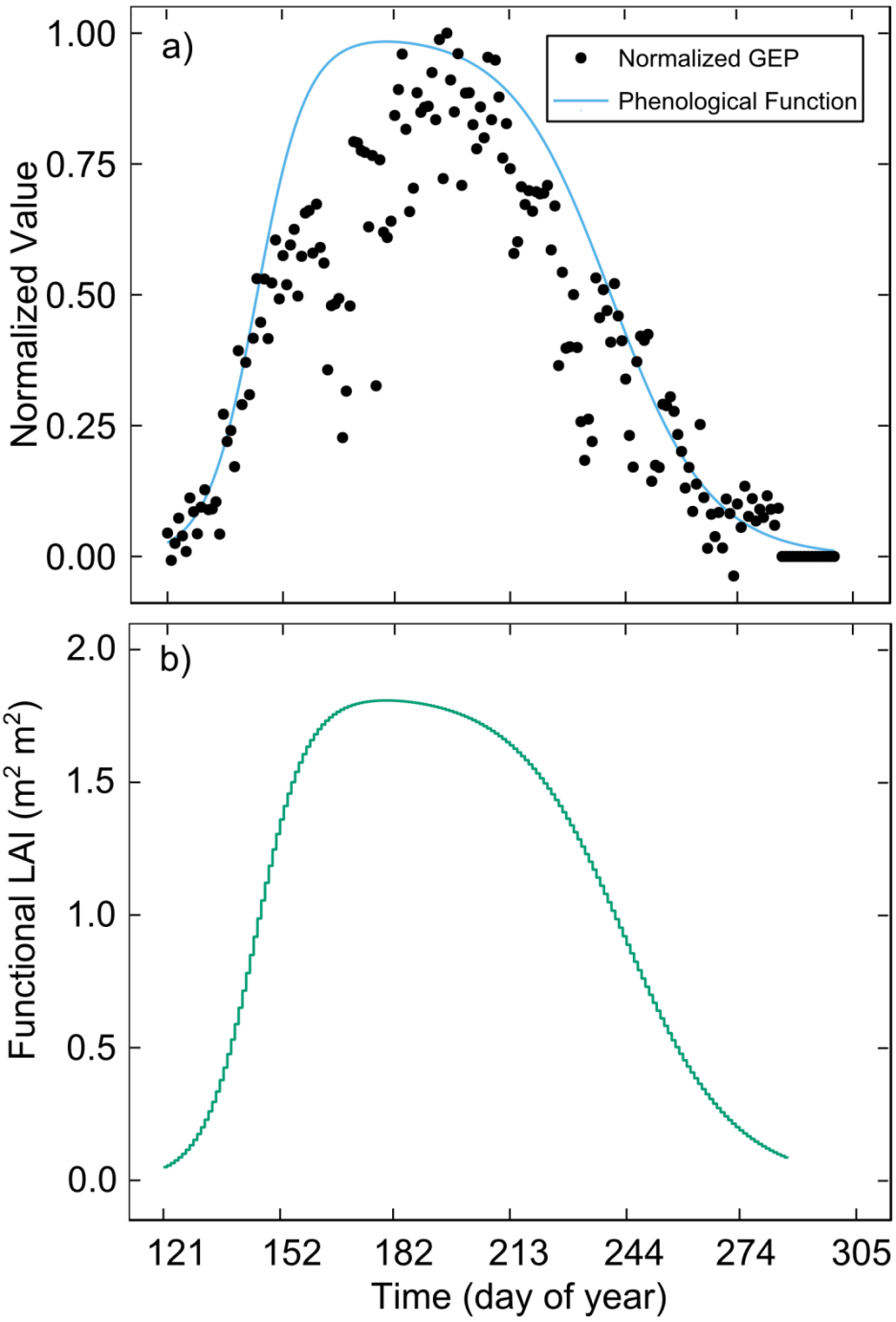

Figure 3.7: Normalized GEP values for the HSNC throughout the growing season with the result of the curve fitting, defined as the phenological function. Also shown, the phenological function after being scaled by the maximum measured HSNC LAI of 1.8 m^2 m^{-2} to get the functional LAI for the span of the growing season.

3.3 Seasonal variation in measured evapotranspiration and associated energy balance closure

3.3.1 HSNC energy balance closure

The slope of 0.87 for the geometric mean regression between available energy and sensible + latent heat flux (H + λE) gave an 87% closure, leaving 13% of the energy budget unaccounted for (Figure 3.8). When determining the energy balance closure for the HSNC a single outlying data point with a value of -367 W m^{-2} on the y-axis was removed. Of the energy balance components, net radiation was the largest in terms of W m^{-2} accounting for energy input into the site. Latent heat flux due to evaporation of water represented largest energy output, whereas sensible heat flux due to convection and soil heat flux contributed the least to energy lost from the HSNC. Sensible heat flux remained relatively constant throughout the day, reaching peak at approximately 10:00 until 14:00 and dropping slightly into the negative flux values during nighttime hours. Net radiation, soil heat flux, and latent heat flux all peaked later in the day at approximately 14:00. Soil heat flux and net radiation dropped into negative values during nighttime hours. Latent heat flux remained slightly above zero for all hours of the day.

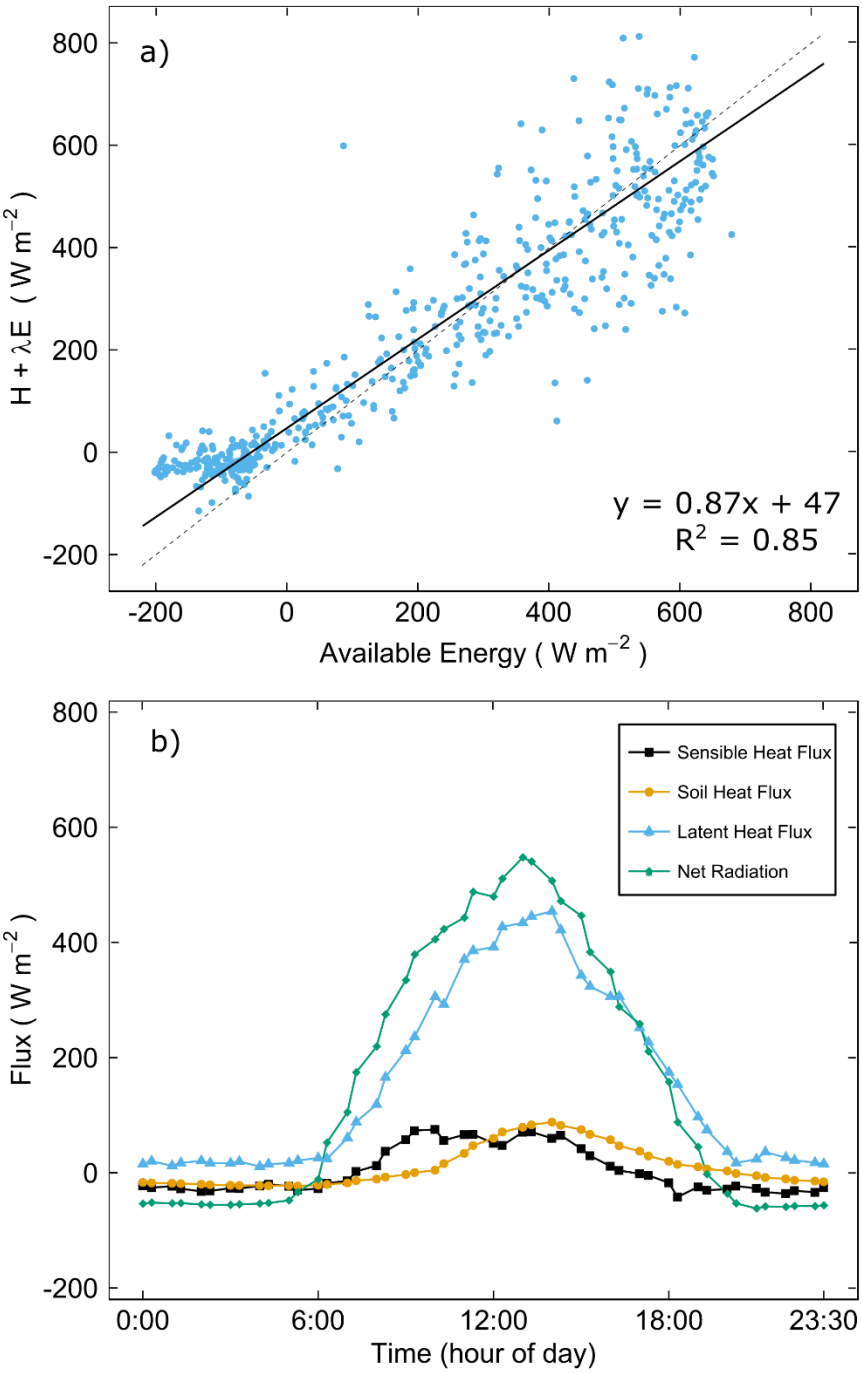

Figure 3.8: HSNC July energy balance closure and mean diurnal variation of components. Available energy is defined as net radiation – soil heat flux (NR-G). H+λE describes the sum of the sensible and latent heat fluxes respectively. The HSNC flux data accounted for 87 % of energy transfer in and out of the woodland as given by the slope of the geometric mean regression (solid line). The 1:1 ratio (y= x) is shown by the dashed line.

3.3.2 Seasonal patterns of ET

The evapotranspiration rates measured using eddy covariance at the HSNC showed a distinct seasonal pattern relating to the emergence of leaves on the cottonwood canopy and the growth of the herbaceous understory (Figure 3.9). Initial measurements of ET in May corresponded to the growth of grasses in the understory, with ET values less than 5 mmol m^{-2} s^{-1}. This was followed by the emergence of cottonwood leaves at the conclusion of May increasing the ET to daily maximums between 5 and 10 mmol m^{-2} s^{-1}. ET measurements reached their peak in July, with values between 10 and 20 mmol m^{-2} s^{-1}, when the cottonwood canopy and the understory herbaceous shrubs and grasses were at peak LAI.

Two major gaps in measured ET were present in the dataset. The first period corresponded to the removal of instrumentation in the HSNC to prevent damage by rising floodwaters from the Oldman River (days 168 to 183). The second period was the result of a gas analyzer malfunction where no water vapour densities were recorded at the site (days 209 to 234). Additional small gaps were present in the dataset as the result of screening for invalid data such as when the primary wind direction originated from the East.

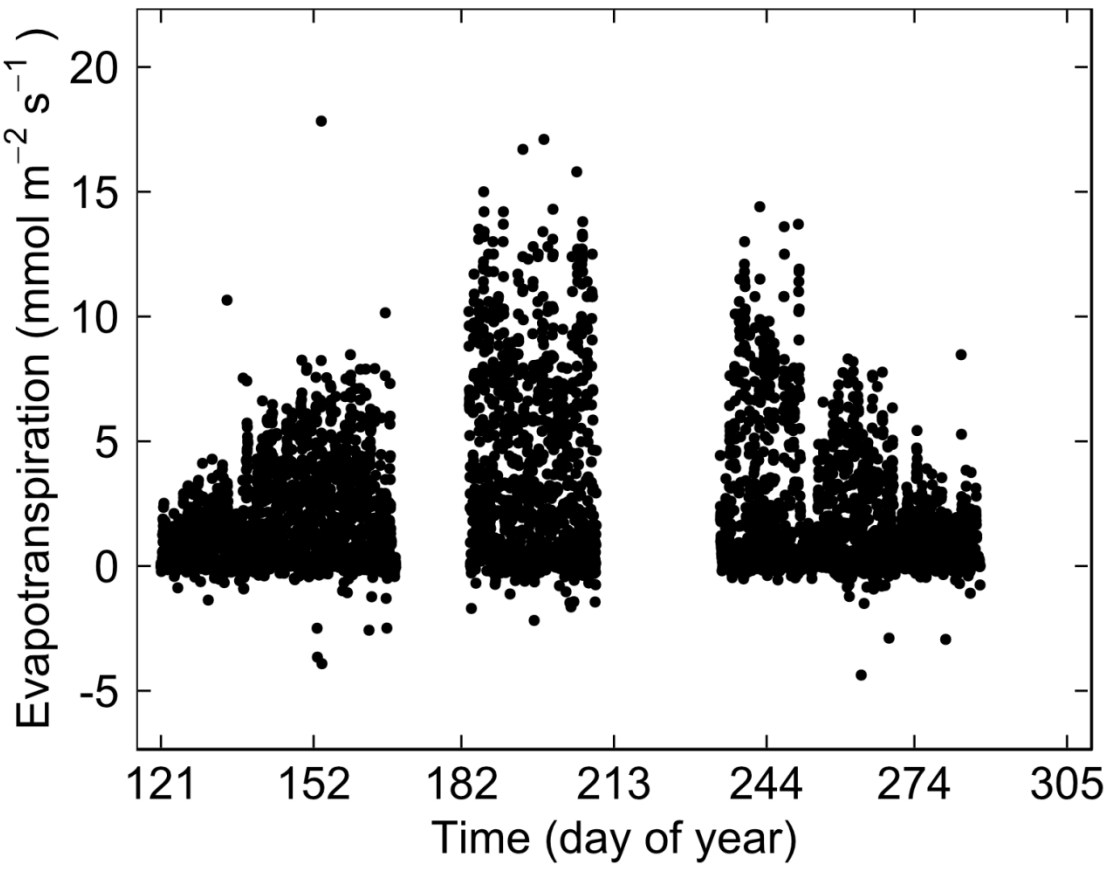

Figure 3.9: 30-minute averages of evapotranspiration rates for the entire span of the growing season, including data gaps caused by high water levels in June when instrumentation was removed and the malfunction of the gas analyzer for most of August.

3.4 Seasonal variation in canopy and stomatal conductance and evapotranspiration model fitting results

3.4.1 Calculated stomatal and canopy conductance

Canopy and stomatal conductance values were calculated using the inverted PM equation at times when ET was known. Typically canopy conductance was greatest in July (~ 550 mmol m^{-2} s^{-1}) when functional LAI was at its peak (Figure 3.10). The canopy conductance for August showed a higher peak at 619 mmol m^{-2} s^{-1}, however there was also much greater magnitude of change between neighbouring data points for August. This was likely from a lack of data for time averaging in August caused by the gas analyzer malfunction. Canopy conductance for June peaked at approximately 400 mmol m^{-2} s^{-1} and showed less diurnal variation for the daytime periods than either July or August. At the leaf-level, stomatal conductance for August was on average 40 % larger than July. Whereas, June and July were reduced by almost half compared to the corresponding canopy conductance values (Figure 3.10).

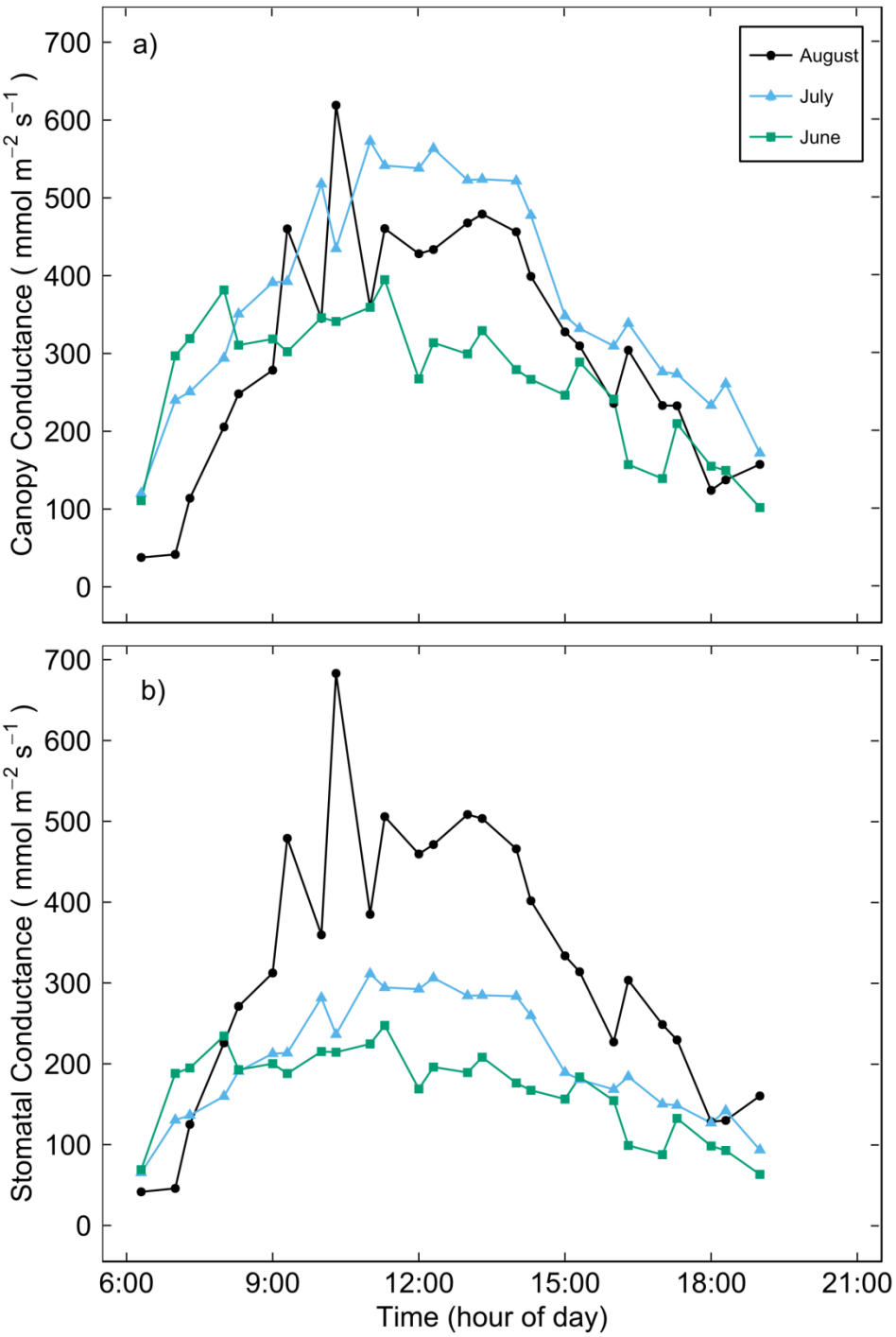

Figure 3.10: Diurnal patterns in calculated canopy and stomatal conductance at the HSNC for available data within three time periods, June, July, and August.

3.4.2 Model fitting results of ET and stomatal conductance

Linear regressions between measured and modelled ET for the 30-minute averaged ET data as well as ET data bin-averaged by time of day were used to determine which model provided the most accurate fit for each time period. The linear regression fits of 30-minute average measured to modelled ET data are summarized in Table 3.2. Whereas the linear regression fits of the bin-averaged measured to modelled ET are shown in Figures 3.11, 3.12, and 3.13.

With the 30-minute average data, the model parameterized using July data provided the best relationship between measured and modelled ET for the majority of the growing season (Table 3.2). However, following a decline in functional LAI in August at the conclusion of the season the model parameterized using the August data gave the best fit for measured to modelled data (Table 3.2). Despite the heavy seasonal flooding of the HSNC in July it was found that evaporation of flood waters did not significantly affect measured ET. No significant change was seen in measured ET per unit leaf area throughout July as the HSNC dried out (t-test of regression slope, $n=27$, t-statistic=-1.01, $p>0.05$).

The fitted model coefficient κ_D was largest for the June parameterized model and smallest for the August parameterized model, indicating that maximum conductance progressively increased throughout the season for measured values of VPD (Table 3.3). The value of the fitted model coefficient α varied between months, reaching a maximum in August which showed the largest response in conductance for measured PPFD (Table 3.3).

Table 3.2: A check of model fits using linear regression parameters for 30-mnute average modelled ET against measured ET. Models were parameterized for three separate time periods and compared measured ET data from the same three time periods in the growing season.

Time Period	**Model Parameterization Period**	**Linear regression slope**	**Linear regression intercept**	**R^2 value**
June	June	0.78	0.24	0.74
	July	1.03	0.10	0.74
	August	1.40	0.22	0.76
July	June	0.64	0.39	0.78
	July	0.86	0.20	0.81
	August	1.11	0.34	0.84
August	June	0.45	0.02	0.80
	July	0.62	0.13	0.84
	August	0.88	0.16	0.87

Table 3.3: Parameterized coefficients for the empirical stomatal conductance model for three periods throughout the 2014 growing season.

Parameterization period	**Fitted coefficient α**	**Fitted coefficient κ_D**
June	0.33	0.0013
July	0.24	0.00058
August	0.50	0.00040

With the bin-averaged July data, the model parameterized using July data consistently provided the relationship closest to a 1:1 ratio for the fit between modelled and measured ET as shown in Figure 3.12. Coefficients obtained from the June parameterized model underestimated average peak ET for July by nearly 4 mmol m^{-2} s^{-1}. Coefficients obtained from the August parameterized model overestimated peak ET for July by nearly 2 mmol m^{-2} s^{-1}. These same features were observed when looking at the regression equations from the raw 30-minute data as shown in Table 3.2.

When comparing bin-averaged ET model fits for June ET data (Figure 3.11) the coefficients created using the July parameterized model provided an accurate estimate the peak June ET. The June parameterized coefficients provided a similar fit to those created using July data, but slightly underestimated June ET when comparing the raw 30-minute averages (Table 3.2). The August based coefficients overestimated peak ET in June by nearly 4 mmol m^{-2} s^{-1}.

Lastly, when fitting to the ET measured in August, the August derived modelling coefficients provided the best fit by a significant margin (Figure 3.13). The July based coefficients underestimate peak ET in August by nearly 3 mmol m^{-2} s^{-1}. The June based coefficients underestimated peat ET in August by nearly 4 mmol m^{-2} s^{-1}.

The July and August periods were found to have observable amounts of measured ET during the nighttime periods (Figure 3.12, 3.13). For the nighttime periods where a non-negligible ET was measured it was found that sensible heat flux was significantly lower and friction velocity was significantly higher relative to

the nighttime periods where no ET was measured (H: t-test, n=308, t-statistic= -18.18, $p<0.05$; u*: t-test, n=308, t-statistic=-13.94, $p<0.05$). In the 2014 growing season, sensible heat flux was an average of 7 times lower for nights with observable measurements of ET relative to nights with negligible ET. Conversely, friction velocity was on average 3 times higher for nights with non-negligible measurements of ET relative to nights with negligible ET measurements.

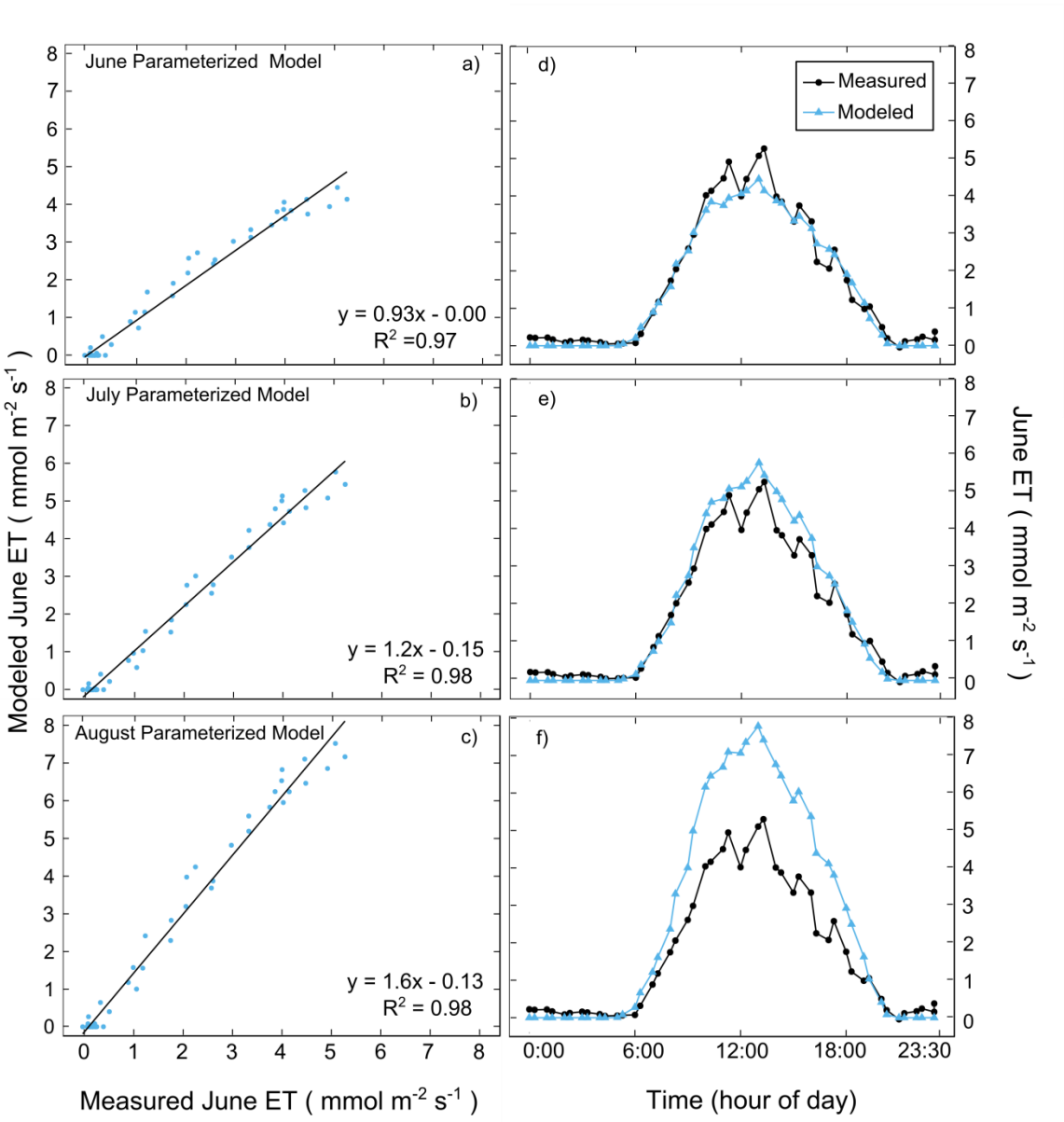

Figure 3.11: Bin-averaged (16 day) model fitting results for measured June evapotranspiration (ET) showing the comparison in fit for empirical models parameterized for three different time periods.

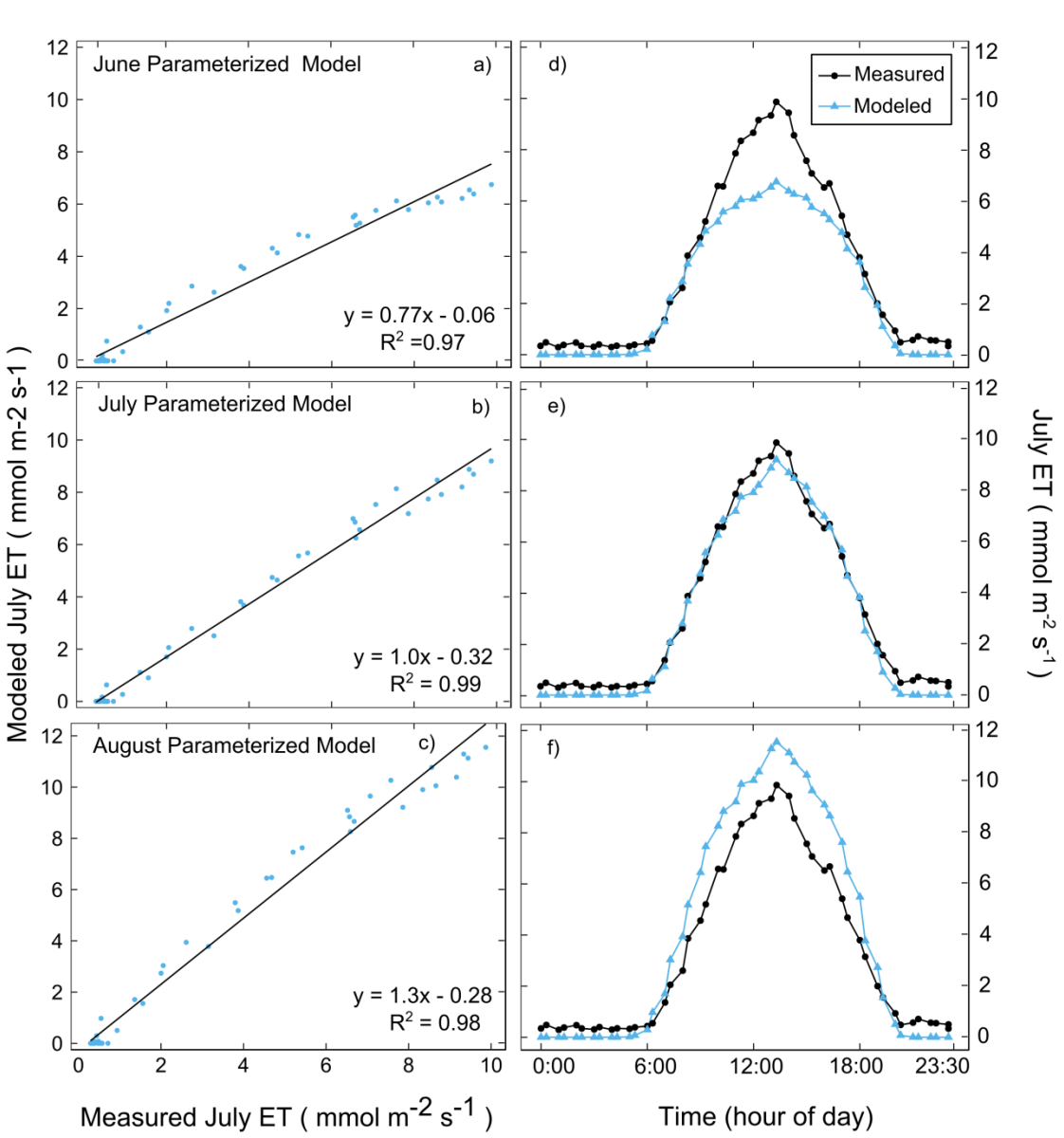

Figure 3.12: Bin-averaged (26 day) model fitting results for measured July evapotranspiration (ET) showing the comparison in fit for empirical models parameterized for three different time periods.

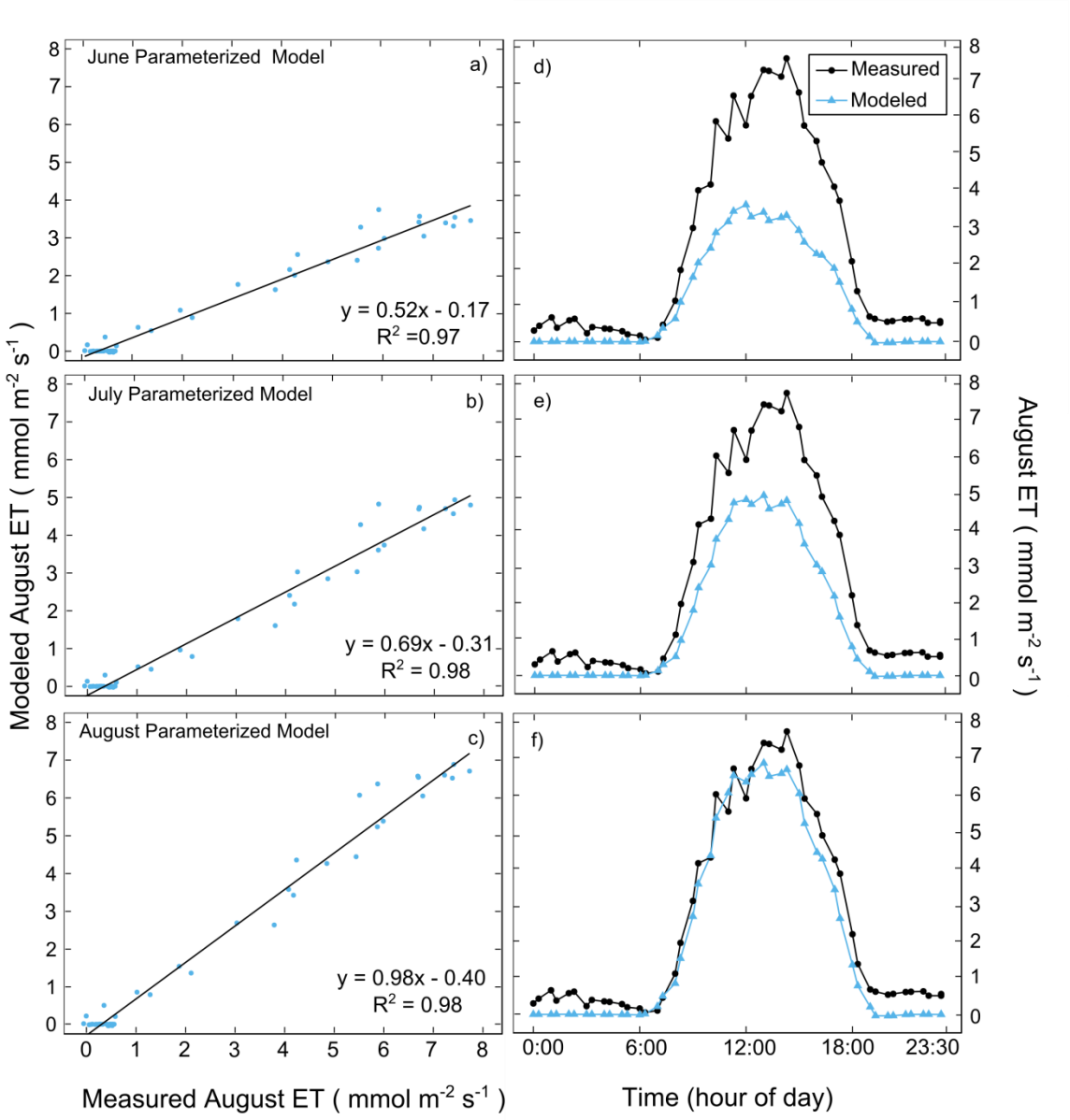

Figure 3.13: Bin-averaged (16 day) model fitting results for measured August evapotranspiration (ET) showing the comparison in fit for empirical models parameterized for three different time periods.

Based on Figures 3.11, 3.12, 3.13 and Table 3.2, the July modelling coefficients gave the best model for estimating ET up until data was lost from the gas analyzer malfunction. Functional LAI was used as a guide to determine an appropriate day to switch between parameterized ET models. Mid-August (day 228) corresponded to a 20 % decrease in functional LAI. This was a 50% decrease between the functional LAI shortly before the gas analyzer malfunctioned and the functional LAI after the gas analyzer was repaired. Following day 228 the August parameterized model was used to estimate ET for the remainder of the growing season.

This application of the two parameterized models can be viewed using canopy and stomatal conductance to water vapour (Figure 3.14). The modelled canopy and stomatal conductance for June and July were calculated using the July parameterized model. The modelled August canopy and stomatal conductance were calculated using the August parameterized model. The modelled conductance for all three periods followed a similar diurnal pattern showing the same variations in magnitude as their measured counterparts. A linear regression of the modelled to measured stomatal conductance gave a good fit with slopes of 0.81, 0.82, and 0.91 for the June, July, August time periods respectively (Table 3.4).

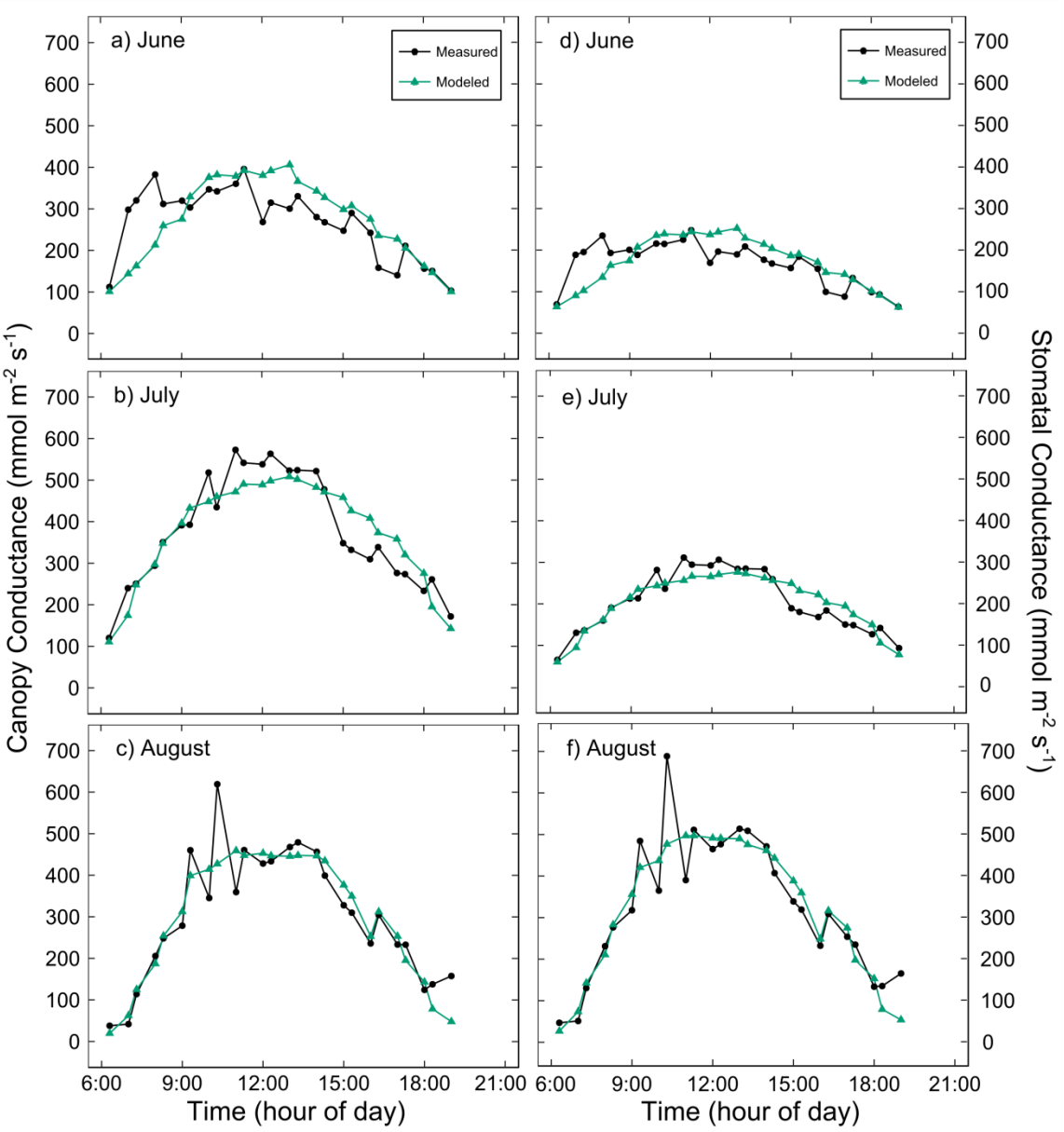

Figure 3.14: Diurnal variation in calculated stomatal and canopy conductance in comparison to the modelled canopy and stomatal conductance for three time periods. All values were bin-averaged by time of day for the recorded time period. The June and July modelled values were calculated using the July parameterized model. The August modelled values were calculated using the August parameterized model.

Table 3.4: A check of model fits using linear regression parameters for modelled stomatal and canopy conductance against measured values. The modelled June and July stomatal and canopy conductance were calculated using the July parameterized model. The August modelled values were calculated using the August parameterized model. The measured values were calculated using the inverted PM equation.

Time Period	**Conductance (mmol m^{-2} s^{-1})**	**Linear regression slope**	**Linear regression intercept**	**R^2 value**
June	Stomatal	0.81	37	0.48
	Canopy	0.78	66	0.45
July	Stomatal	0.82	36	0.82
	Canopy	0.82	66	0.82
August	Stomatal	0.91	24	0.86
	Canopy	0.92	20	0.86

3.5 Seasonal variation in evapotranspiration, water-use efficiency, and cumulative water fluxes

3.5.1 Seasonal variation in modelled and gap-filled daily ET

The PM equation and parameterized empirical model of stomatal conductance were used to model ET for the full months of June, July, and August (Figure 3.15). July showed the greatest rate of evapotranspiration, peaking at 9 mmol m^{-2} s^{-1}, June had the lowest modelled ET of 6 mmol m^{-2} s^{-1} followed by August at 7 mmol m^{-2} s^{-1}. All diurnal patterns calculated using modelled ET fell to zero in the nighttime hours. Seasonal patterns in modelled ET showed a smooth increase in daily ET from approximately 0 mm day^{-1} at the start of May to an average of 5 mm day^{-1} at the peak of the season in July. Maximum modelled ET for an individual day was 7 mm day^{-1} (Figure 3.15).

Missing data in the HSNC ET dataset were gap-filled using ET values calculated with the PM equation and the parameterized empirical model of stomatal conductance (Figure 3.16). As with the modelled ET dataset, July showed the greatest rate of evapotranspiration when using the gap-filled values. However, July gap-filled ET peaked at 10 mmol m^{-2} s^{-1}, August peaked at 8 mmol m^{-2} s^{-1}, and June was reduced to a peak of 5 mmol m^{-2} s^{-1}. Unlike the modelled ET, the diurnal patterns of the gap-filled dataset remained slightly above zero in the nighttime hours (less than 0.5 mmol m^{-2} s^{-1}). Seasonal patterns in gap-filled ET showed a smooth increase in daily ET from less than 1 mm day^{-1} at the start of May to an average of 5 mm day^{-1} at the peak of the season in July. Maximum gap-filled ET for an individual day was 8 mm day^{-1} (Figure 3.16).

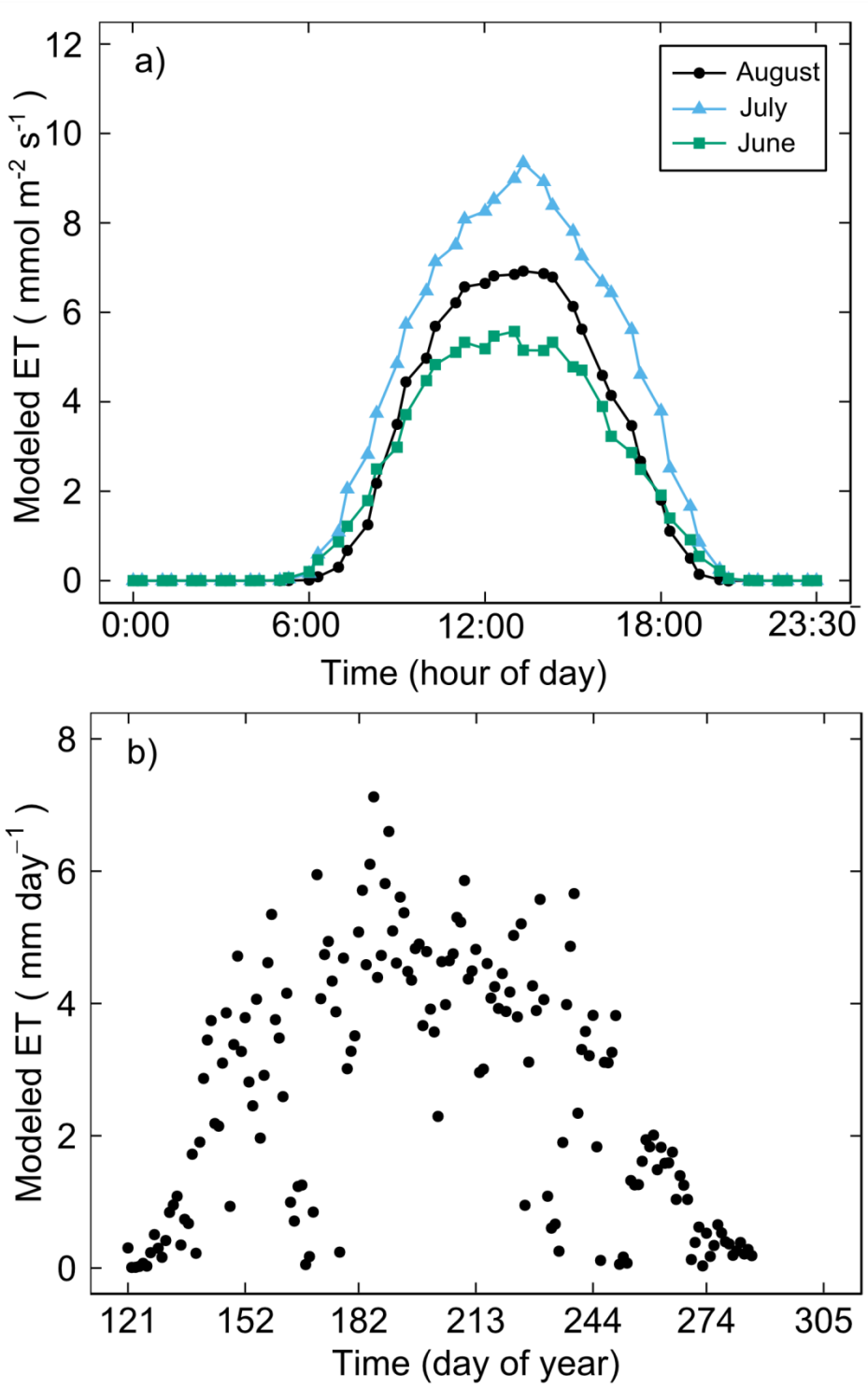

Figure 3.15: Diurnal variation in modelled ET for the full month periods of June, July, and August and full seasonal variation in modelled evapotranspiration (May to October).

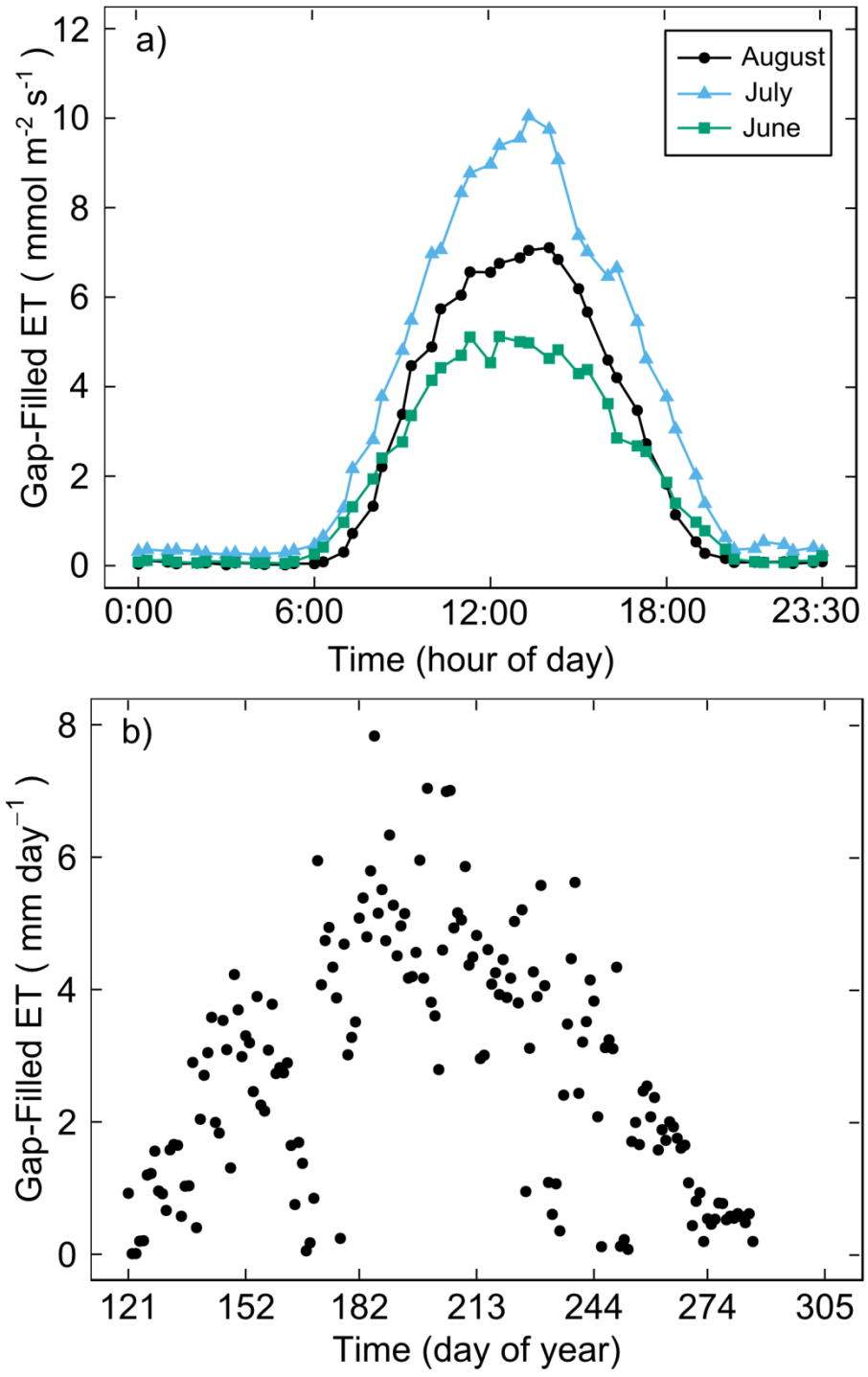

Figure 3.16: Diurnal variation in gap-filled ET for the full month periods of June, July, and August and full seasonal variation in gap-filled evapotranspiration (May to October).

Comparing the measured ET to the modelled ET for 30-minute averages over four day periods showed a slight tendency to overestimate June and underestimate peak flux in July and August (Figure 3.17). This was reflected in the diurnal variation of measured and modelled ET for all available data from June, July, and August. June and July modelled ET were calculated with the July parameterized stomatal conductance empirical model and the August period was calculated using the August parameterized model.

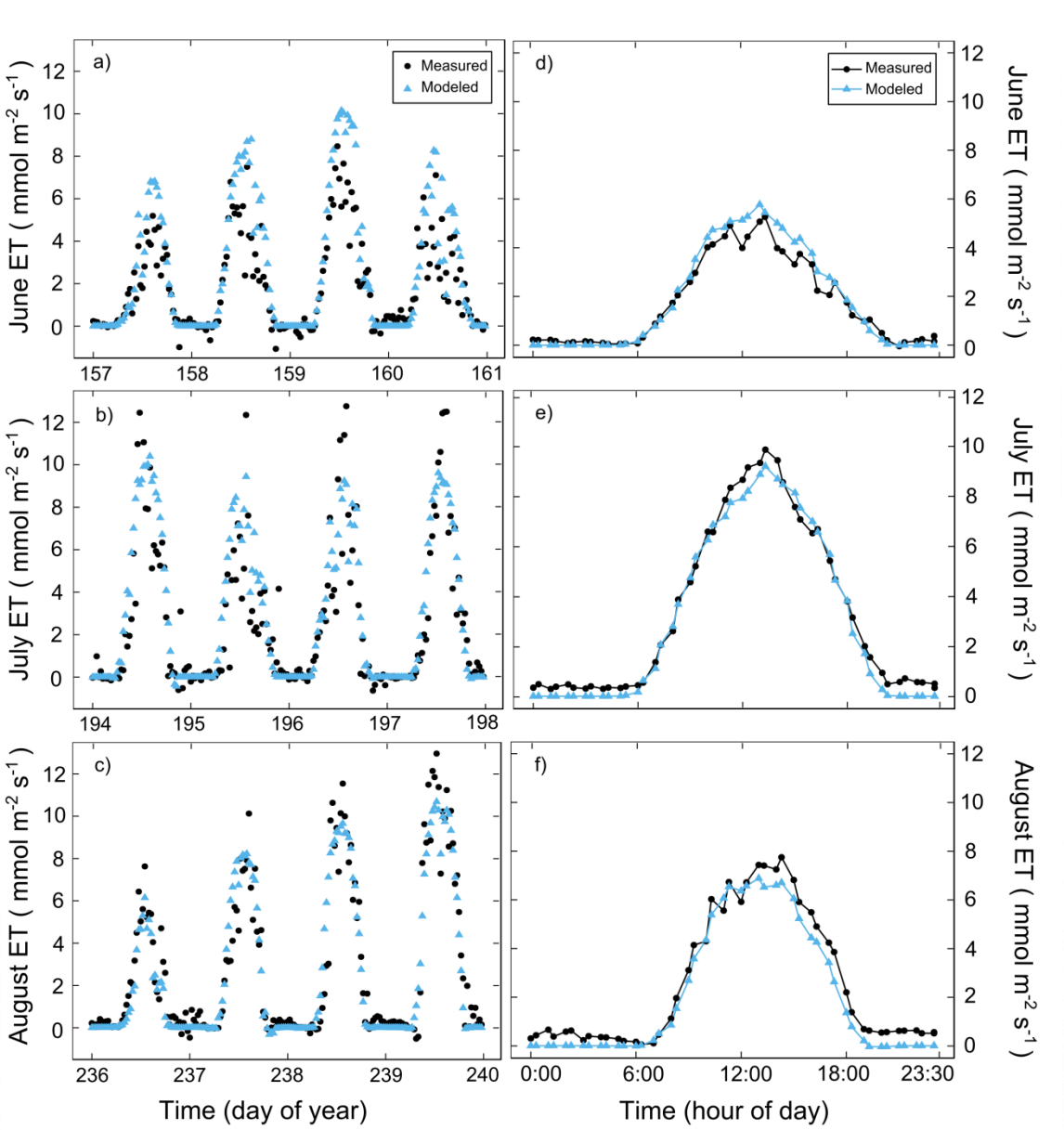

Figure 3.17: Comparison of diurnal variation in measured and modelled ET at the HSNC for all available data within June, July, and August. Also shown is the comparison of measured and modelled ET for four day subsets within each of the three time periods.

3.5.2 Seasonal water-use efficiency

In the cottonwood woodland, WUE showed a strong negative correlation to VPD (Figure 3.18) (t-test of regression slope: n=71, t-statistic=-5.2, p<0.05) and was found to significantly decrease from the start of the season when compared to the conclusion of the season (t-test of regression slope: n=71, t-statistic=-3.3, p<0.05). The WUE efficiency observed in August was only 77 % of the WUE seen in June due to a combination of losses in leaf photosynthetic capacity as the canopy aged and increased daily maximum VPD relative to June (Table 3.5). A reduced WUE was also observed for July (86 % of June WUE) which corresponded to the seasonal peak in VPD (Figure 3.3, Table 3.5) with the addendum that for much of July the HSNC was inundated with water due to seasonal flooding.

No significant difference was observed between the WUE for July and August (t-test, df=45, t-statistic=1.5, p>0.05). However, the mean WUE in July and August were both found to be significantly lower than the mean WUE in June (July: t-test, df=43, t-statistic=1.8, p<0.05; August: t-test, df=42, t-statistic=3.0, p<0.05). The mean daily maximum VPD in June was found to be significantly lower than the daily maximum VPD for both July and August (July: t-test, df=44, t-statistic=-4.5, p<0.05; August: t-test, df=42, t-statistic=-3.8, p<0.05). No significant difference was observed between mean daily maximum VPD for July and August (t-test, df=48, t-statistic=0.3, p>0.05).

Table 3.5: Monthly average water-use efficiency (WUE) and daily maximum VPD (± SD) for June, July, and August in the HSNC cottonwood woodland.

Time Period	**WUE (mmol mol^{-1})**	**VPD_{max} (kPa)**	**Days averaged**
June	4.3 ± 0.9	1.7 ± 0.5	20
July	3.8 ± 1.0	2.4 ± 0.6	26
August	3.4 ± 1.3	2.3 ± 0.7	25

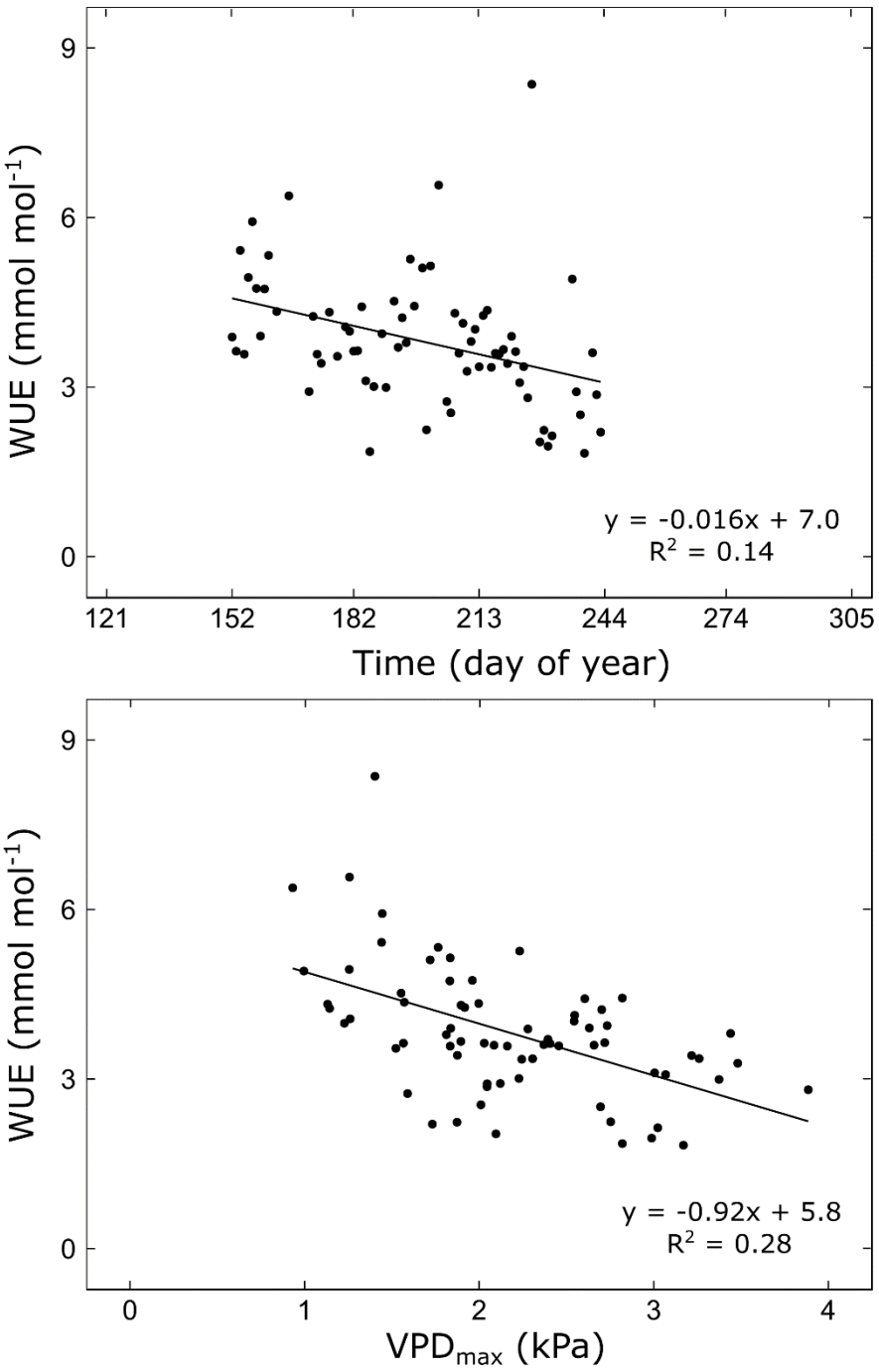

Figure 3.18: WUE in the HSNC (June through August) was calculated using the ratio of carbon assimilation (GEP) to that of water loss (ET). Negative correlation between WUE and increases in VPD was observed for the cottonwood woodland at the HSNC.

3.5.3 Cumulative ET and precipitation

Cumulative growing season ET calculated using only modelled ET resulted in a predicted value of 442 mm for total cottonwood water use. Whereas the gap-filled dataset, which consists largely of measured values, estimated cumulative water usage by the cottonwood woodland to be 465 mm (Figure 3.19). The greatest water usage occurred during July when LAI was at peak and averaged ET was approximately 5 mm day^{-1}. The HSNC woodland ET was approximately 3 mm day^{-1} in June and August and 2 mm day^{-1} in May and October. Cumulative precipitation for the growing season was 370 mm. Cumulative HSNC evapotranspiration was greater than seasonal precipitation following July 24th (day 205).

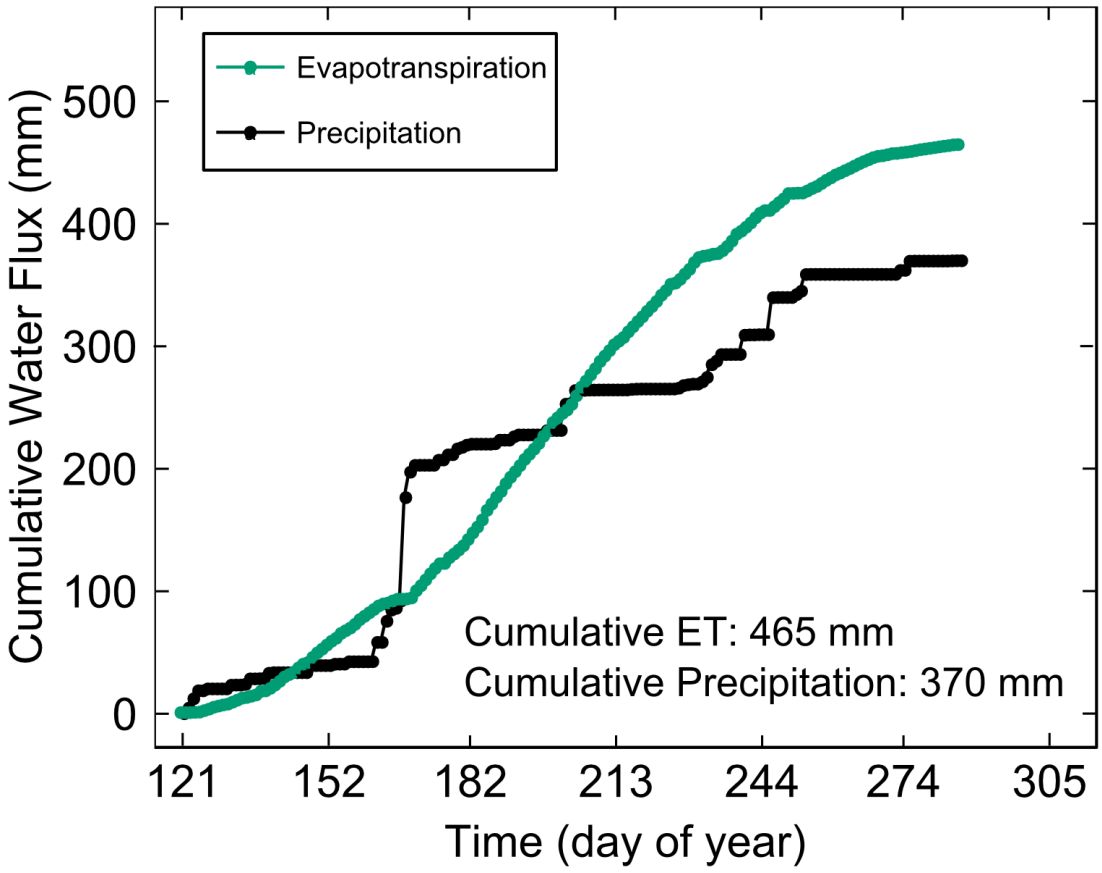

Figure 3.19: Cumulative 2014 growing season HSNC evapotranspiration and precipitation.

3.6 Isotopic analysis of cottonwood water source

3.6.1 Seasonal variation in δ^2H of HSNC water sources

Measurements of δ^2H values were completed for all collected river, ground, and stem water samples as well as collected precipitation. The resulting δ^2H values were used to determine seasonal variation and the relationship between stem water and the two possible cottonwood water sources: the Oldman River and local precipitation. The δ^2H of precipitation varied greatly among weekly collections, reaching a maximum of -53 ‰ and a minimum of -163 ‰ from May to October (Appendix, section 7.7). With a seasonal average of -123 ± 20 ‰, precipitation had much greater temporal variation in δ^2H values over the growing season when compared to the other sample types (Figure 3.20). River and groundwater showed little variation compared to the 57 ‰ change in monthly amount-weighted precipitation δ^2H values.

Over the 2014 growing season the average δ^2H values for the three HSNC groundwater wells varied by 2.6 ‰ whereas the river water varied by 8.8 ‰. The largest variation in both river and groundwater was observed at the start and conclusion of the growing season. A t-test of regression slope was performed for the river and ground water samples to check for significant temporal variability in δ^2H values (Figure 3.21). Both were found to vary significantly in δ^2H over the growing season (River water: t-test of regression slope, n=14, t-statistic=4.4, p<0.05; Groundwater: t-test of regression slope, n=14, t-statistic=3.5, p<0.05).

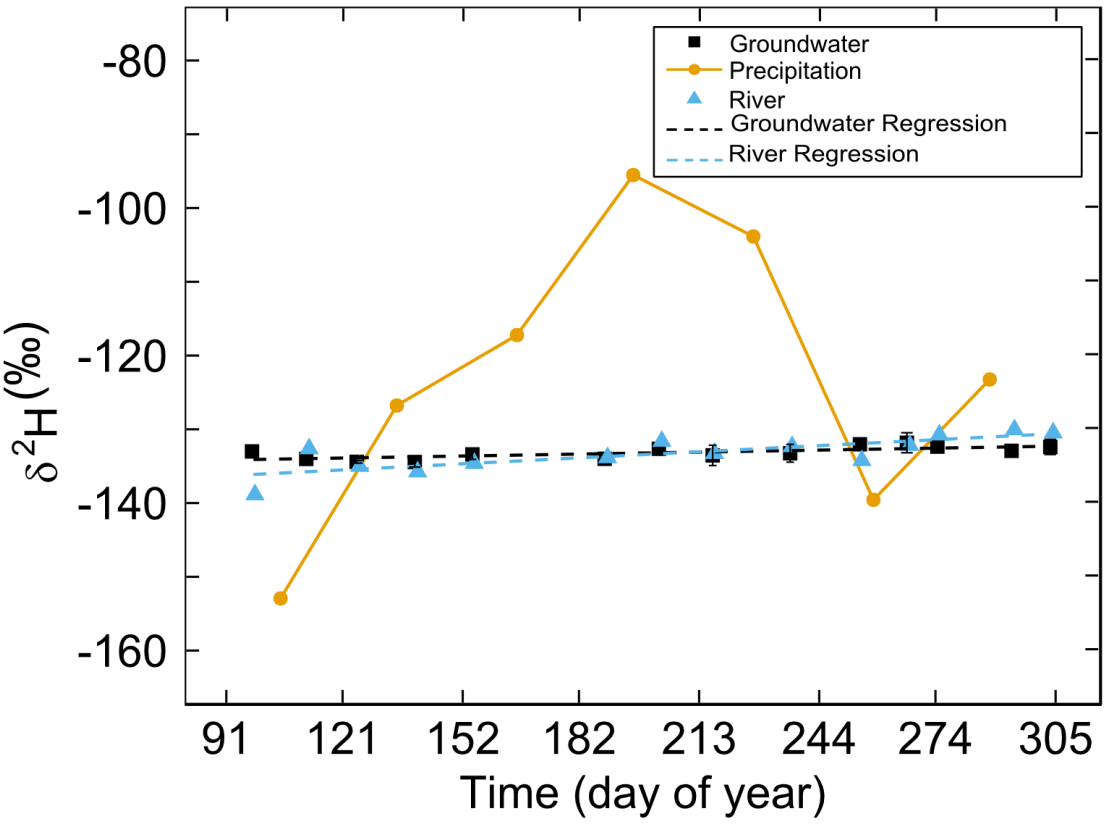

Figure 3.20: δ^2H values of HSNC water sources: Lethbridge monthly amount-weighted average precipitation, HSNC groundwater, Oldman River water. For each sample date an average of 3 replicate measurements of groundwater were made.

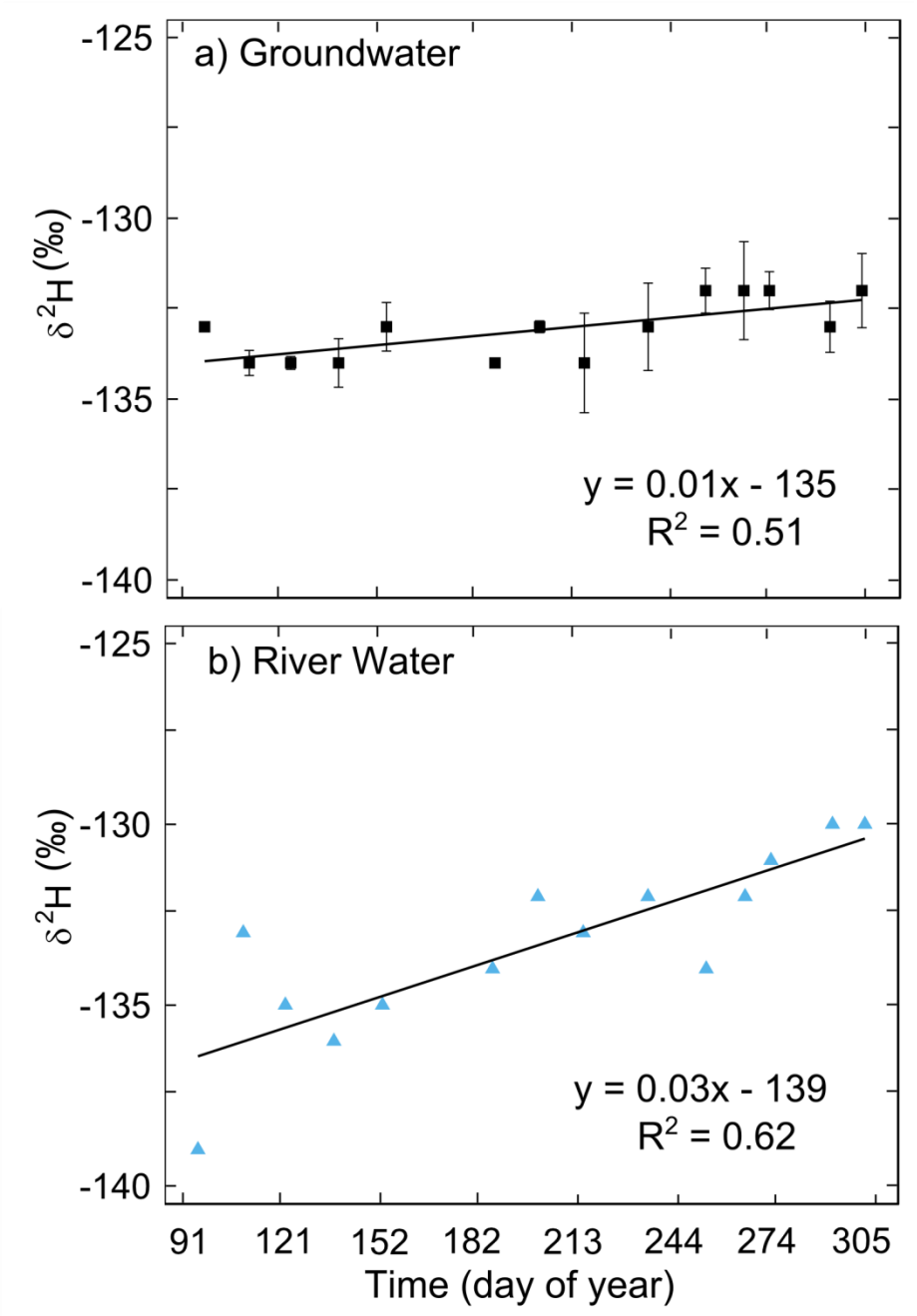

Figure 3.21: Growing season linear regressions of δ^2H (± SD) for groundwater and river water. Significant temporal variation was observed in both (River water: t-test of regression slope, n=14,t-statistic=4.4, p<0.05; Groundwater: t-test of regression slope, n=12, t-statistic=3.5, p<0.05).

3.6.2 Seasonal variation in δ^2H of cottonwood stem water

Unlike river and groundwater isotopic content, cottonwood stem water showed no significant temporal variation in δ^2H values over the span of the growing season (t-test of regression slope, $n = 7$, t-statistic=1.2, $p>0.05$). However, stem water samples were limited to times in the season when the trees were actively growing and taking up water.

When comparing the seasonal mean δ^2H of stem water to that of groundwater, no significant difference between the means was observed (t-test, $n = 14$, t-statistic=-0.15, $p>0.05$) (Table 3.6). Similarly, the seasonal mean δ^2H of stem water showed no significant difference from the seasonal mean δ^2H of Oldman River water (t-test, $n = 7$, t-statistic=-0.35, $p>0.05$) (Table 3.6). Based on these statistical tests and Figure 3.20 the cottonwood water source was identified as the Oldman River with no apparent reliance of the cottonwood trees on summer precipitation inputs.

Table 3.6: Mean δ^2H values (± SD) for collected HSNC growing season water samples and number of sampling days for each type of water.

Water Type	**Mean δ^2H (‰)**	**Sampling days**
Ground	-133.2 ± 0.9	14
River	-133.3 ± 2.4	14
Stem	-132.7 ± 1.5	7

4. DISCUSSION

4.1 Seasonal variation in ecosystem leaf area index

4.1.1 Understory herbaceous vegetation and cottonwood canopy LAI

The measured HSNC understory LAI of 0.9 ± 0.07 m^2 m^{-2} at peak was comparable to what has been measured at the Lethbridge grassland site outside of the riparian corridor. In a wet year, such as the one experienced in the 2014 growing season, grassland LAI has been observed to reach a peak of 0.97 ± 0.09 m^2 m^{-2} (Flanagan et al. 2002, Ponton et al. 2006). This changes dramatically based on available moisture inputs from precipitation. In dry years, grassland LAI may have a peak lower than 0.5 m^2 m^{-2} (Flanagan et al. 2002).

Spatial variation in understory LAI was observed for the 2014 growing season (Figure 3.4). The western harvest plots had a higher peak LAI relative to the eastern plots as a result of distance from the Oldman River. The groundwater table is higher nearest to the river allowing shallow rooting plants easier access for growth. As well, the NW harvest plot had lower peak LAI relative to the SW harvest plot and the NE lower than the SE. This variation was due to the proximity of the cottonwood canopy. Both northern plots were located directly beneath the cottonwood canopy at the southern edge of a densely wooded area, whereas the southern plots were located a minimum of 5 meters away from the cottonwood canopy.

Further studies are needed to determine the spatial and interannual variation in understory LAI at the HSNC. However, the presence of seasonal flooding and a higher groundwater table may skew the understory LAI towards

greater leaf area on a more regular basis relative to what has been seen outside of the riparian corridor.

Initial optical measurements of the tree canopy with the LAI-2000 showed an effective LAI of 1.2 ± 0.07 $m^2 m^{-2}$. In complex tree canopies the LAI-2000 instrument is known to underestimate LAI significantly compared to direct measurement methods (Leblanc et al. 2002, Bréda 2003, Nasahara et al. 2008). The LAI-2000 measures only the transmission of radiation through the canopy, this includes measurements of woody material found in the line of sight of the LAI-2000 and does not account for woody stem area or within shoot and within branch clumping of foliage elements (Gower et al. 1999). As a result, the effective LAI as measured by the LAI-2000 is known to be an inaccurate prediction of leaf area, requiring a correction in order to have a meaningful value (Gower et al. 1999).

This was in agreement with the HSNC effective LAI measurements. The corrected optical LAI of 0.9 ± 0.07 $m^2 m^{-2}$ at peak was shown to be 0.3 $m^2 m^{-2}$ lower than measured effective LAI. This was due to the removal of the woody-to-total leaf area ratio and correcting for the clumping index (Ω_E) in a single equation. The majority of the decrease in cottonwood canopy LAI after correcting for clumping index was the result of removing woody area from calculations of leaf area. When correcting effective LAI only for clumping index, the values decrease by 0.1 $m^2 m^{-2}$ relative to the 0.3 $m^2 m^{-2}$ caused by the correction for woody-to-total stem area. The removal of the woody contribution corrects the LAI to consist of only leaf surfaces. Optically measured LAI via the LAI-2000 corrected with a clumping index using the TRAC has been validated to be accurate when compared

with direct measurements of LAI (Gower et al. 1999, Bréda 2003, Nasahara et al. 2008).

The sparseness of the cottonwood canopy was reflected in the corrected value for peak cottonwood LAI, 0.9 ± 0.07 $m^2 m^{-2}$. As a comparison, average LAI for individual cottonwood trees (*Populus* spp.) measured in other studies ranges from 1 to 4 $m^2 m^{-2}$ (Schaeffer et al. 2000, Nagler et al. 2004, Murthy et al. 2005).

As a whole, based on 400+ studies, global LAI of terrestrial plant species is an average of 4.5 ± 2.5 $m^2 m^{-2}$ (Asner et al. 2003). This ranges from an average 1.3 ± 0.9 in desert type regions to 6.7 ± 6.0 for forested regions (Asner et al. 2003). Based on environment, the highest LAI was found in temperate rainforests ranging from 12 – 15 $m^2 m^{-2}$ (Asner et al. 2003). Comparing this to LAI measured for trees within the *Populus* genus, an aspen forest had a much higher canopy LAI, between 4 and 5 $m^2 m^{-2}$, which was over two times the peak LAI of the HSNC (Zha et al. 2010).

For semi-arid environments, an LAI of 1.8 ± 0.09 $m^2 m^{-2}$ was determined for a mixed-conifer forest in southern California consisting mainly of oak (*Quercus* spp.) and pine (*Pinus* spp.) (Fellows and Goulden 2013). Additionally, for a semi-arid mesquite system with a similar understory of seasonal grasses and forbs in southern Arizona, an average leaf area index of 1.6 $m^2 m^{-2}$ was determined (Scott et al. 2003). The LAI of these semi-arid systems are consistent with the total 1.8 ± 0.07 $m^2 m^{-2}$ of the HSNC despite their differences in plant species composition.

4.1.2 Litter-trap LAI and functional LAI

The measured optical LAI at peak was confirmed using litter-traps which collected fallen cottonwood leaves at the conclusion of the season. The average LAI of the litter-traps, 1.3 ± 0.45 m^2 m^{-2}, showed a peak cottonwood LAI that was 0.4 m^2 m^{-2} greater than the 0.9 m^2 m^{-2} found using the optical methods. Cottonwood canopy cover throughout the HSNC ranged from a visually full, closed canopy in the denser regions to a complete lack of trees in several large, open regions. Due to this variability in canopy cover, the amount of leaf biomass collected in each spatially separated basket was also quite variable. This variability was reflected in the standard deviation of the final litter-trap LAI estimation of 0.45 m^2 m^{-2}. Due to this large variability in the litter-trap collection it was concluded that there was no significant difference between the two results for peak LAI.

The functional LAI, used in the calculations of ET throughout the season, was scaled from normalized values of daily gross ecosystem productivity (GEP) to match the measured HSNC peak LAI of 1.8 ± 0.07 m^2 m^{-2}. However, since the functional LAI relied on measurements of GEP, the functional LAI was observed to reach peak earlier compared to the available optical LAI measurements (day 174 vs day 192). This difference in timing of measured peak LAI versus peak functional LAI was due to missing optical measurements during the flood period where no measurements could be made.

In addition to reaching peak LAI earlier, the functional LAI was observed to decrease approximately 45 days before any change was seen in total leaf area as

measured with optical instrumentation. This was due to a difference in the amount of photosynthesis occurring within the leaves versus how many leaves were physically present. As the leaves aged over the season they began to lose photosynthetic capacity before any physical changes could be observed (Field and Mooney 1983). Using functional LAI in modelling accounts for these changes in leaf properties, however the optical measurements and destructive harvest methods only measure the physical leaf area and were unable to capture these internal changes. As a result, using functional LAI in modelling ET provided a more accurate estimate of daily LAI, this was particularly apparent later in the season as leaf functionality dropped but the physical presence of green leaves had shown little to no change.

4.2 Seasonal variation in measured evapotranspiration and associated energy balance closure

4.2.1 Seasonal energy balance closure

Given a scenario where all energy flux into and out of an eddy covariance measurement site was measured, then plotting available energy (NR-G) against the sum of the sensible and latent heat fluxes (H + λE) would give a 1:1 relationship due to conservation of energy in the energy balance equation (Methods, section 2.4.3). This was not the case with the eddy covariance measurements performed at the HSNC. However, lack of energy balance closure is common with eddy covariance, although the reason for this is not known (Baldocchi 2003). Lack of

closure in the energy budget typically varies between 10 to 30% for eddy covariance measurement sites (Twine et al. 2000).

The geometric mean regression for the energy balance in the HSNC gave a closure of 87 % leaving only 13 % of the energy budget unaccounted for. Given the typical 10 to 30 % of unaccounted energy found at other locations, the energy balance closure for the HSNC is in good agreement with other similar measurement sites and as a result the HSNC data is of acceptable quality. Latent heat flux, represented by λE in the energy balance equation, accounts for heat transfer from the HSNC via evapotranspiration. Given that the total energy balance closure for the HSNC falls within the expected range it can be concluded that the evapotranspiration measured at the HSNC is also an accurate representation of the amount of evapotranspiration occurring at the HSNC by virtue of the latent heat term in the energy balance closure. A lag in the response of latent heat flux relative to net radiation was observed in the morning hours at the HSNC during which latent heat flux was slower to respond for given net radiation values (Figure 3.8). This was due to the location of the net radiation sensor in relation to the location of the cottonwood trees. The large coulees to the East shadowed the cottonwood canopy in the morning hours causing a delay in the response of evapotranspiration. Whereas, the net radiation sensor was placed at 4 meters above the mean canopy height and received more radiation in the morning hours compared to the canopy below.

The energy balance closure from eddy covariance measurements in the Lethbridge grassland has been found to be very close to the closure obtained at the

HSNC, 0.87 to 0.90 depending on the year (Flanagan et al. 2002). The mesquite riparian woodland of southern Arizona was found to have a lower seasonal energy balance closure of approximately 0.75 (Scott et al. 2004).

4.2.2 Seasonal variations in ET

In semi-arid regions, growing season productivity is tied directly to precipitation inputs (Williams et al. 2006). However, this reliance on precipitation is diminished in riparian areas within semi-arid regions due to consistent access of riparian trees to groundwater (Poff et al. 2011). The lack of reliance on precipitation inputs was seen in HSNC ET values which showed no apparent changes in the amount of transpired water in relation to precipitation input into the ecosystem (Figure 3.9).

In addition to the lack of an observable precipitation dependence, the unfiltered ET values measured at the HSNC throughout the growing season were observed to regularly fall into negative values (Figure 3.9). Negative ET values were the result of precipitation events, condensation, or damp conditions, indicating apparent water input into the system.

4.2.3 Seasonal variations in water-use efficiency

The efficiency with which plants assimilate carbon relative to water loss is known as water-use efficiency (WUE) (Chapin et al. 2011). WUE is dependent on

a number of factors including environmental conditions which affect movement of water, such as leaf temperature, incident radiation, and vapour pressure deficit (Chapin et al. 2011). WUE tends to increase with reductions in stomatal conductance due to the disproportionate reduction in water loss compared to the rate of carbon assimilation with changes in stomatal conductance (Farquhar and Sharkey 1982). However, due to a strong correlation between VPD and WUE: as VPD increases, ET increases and WUE decreases despite any change in stomatal conductance from the plant regulating the size of the stomatal openings (Ponton et al. 2006).

In addition to environmental factors, WUE can also be heavily influenced by leaf age over the length of the growing season (Field and Mooney 1983). The decline in leaf functionality, caused by a reduction in the photosynthetic capacity of the leaves as they age, is correlated with a seasonal decline in WUE (Field and Mooney 1983). The significant 23 % drop in WUE for August relative to June in the HSNC is demonstrative of the changes in photosynthetic capacity as well as influence from higher VPD in August relative to June (Table 3.4).

Also of interest was the significantly reduced WUE in July (3.8 ± 1.0 mmol mol^{-1}) compared to June (4.3 ± 0.9 mmol mol^{-1}). Peak LAI along with peak photosynthetic capacity was achieved in July, with the end of the month having showed only minor drops in functional LAI. Functionally speaking, the WUE of July should have been comparable to that of June however this was not what was observed. WUE is inversely correlated with changes in VPD (Figure 3.18) (Ponton et al. 2006). As a result, the sudden drop in WUE at the height of the

season was attributed to the increase in VPD for July relative to June. As the atmospheric vapour pressure deficit increases, drops in WUE have been observed for multiple plant functional types, including the cottonwood woodland of this study, the Lethbridge grassland as well as a temperate aspen forest (Ponton et al. 2006). Aspen trees are grouped in the *Populus* genus along with cottonwood species like those found in the HSNC.

June was taken to be a representative time period for WUE at the HSNC given that during this time period the leaves were near their peak LAI and photosynthetic capacity and other possible stressors, such as flood waters, were not present. During June, the WUE observed was greater than the WUE found in the nearby water-limited grassland (2.6 ± 2.3 mmol mol^{-1}) and approximately half of what was observed in a northern douglas-fir forest (8.1 ± 2.4 mmol mol^{-1}) (Ponton et al. 2006).

HSNC average WUE in June was found to be similar to an aspen (*Populus tremuloides*) forest which had a slightly higher seasonal average WUE of 5.4 ± 2.3 mmol mol^{-1} (Ponton et al. 2006). Lower WUE is common among riparian poplars compared to other forests types (Pearce et al. 2006). Cottonwoods tend to have little use for a highly water efficient strategy due to their establishment in riparian regions in which nearby water sources supply consistent water input to groundwater. Whereas, in non-riparian regions, such as the aspen site, water limitations can affect WUE due to drought responses in trees (Monclus et al. 2006). Additionally, the understory vegetation, with a peak LAI of 0.9 m^2 m^{-2}, in the HSNC may also contribute to the slightly lower WUE for the cottonwood

riparian woodland relative to the aspen parkland which had a thick hazelnut understory with an LAI of 2.1 m^2 m^{-2} (Ponton et al. 2006). Further investigation into the average understory WUE is required to determine the effect that the understory herbaceous vegetation has on total HSNC WUE.

4.3 Seasonal variation in canopy and stomatal conductance and evapotranspiration model fitting results

4.3.1 Calculated stomatal and canopy conductance

The calculated canopy conductance for August had a larger diurnal variation relative to that of June or July (Figure 3.10). The large isolated peak seen for August canopy and stomatal conductance was the result of the limitation in measured ET data for this period due to the gas analyzer malfunction at the end of July. With this lack of data, fewer values were available to average out half-hourly fluctuations in measured ET. In addition to the large and isolated peak conductance observed for August, this lack of available data also resulted in the large variation in neighbouring data points between 9:00 and 12:00 hours relative to the variation seen between similar neighbouring points for either June or July.

However, despite the large variation between some of the conductance data points for August, the stomatal conductance was increased relative to the canopy conductance values. Comparatively, stomatal conductance from June and July was observed to drop by nearly 50 % relative to the associated canopy conductance values. The overall reduction in August canopy conductance relative to July canopy

conductance was attributed to a loss in the photosynthetic capacity of the leaves at the conclusion of the growing season observed from the reduction in functional LAI.

4.3.2 Model fit of ET and stomatal conductance

The use of the Penman-Monteith (PM) equation with an empirical model for stomatal conductance provided an accurate fit between measured and modelled ET data from the HSNC cottonwood woodland. Parameterizing the empirical stomatal conductance model using July data gave a 1:1 ratio when comparing 30-minute measured and modelled ET data collected from June and July (Table 3.2). When comparing the bin-averaged ET data, there was minimal difference between the modelled and measured June ET for the July parameterized and the June parameterized models (Figure 3.11).

The linear regression slopes comparing raw 30-minute averaged ET with modelled ET (Table 3.2) showed that the July parameterized model values had a more accurate fit for June data than the model values generated using the June parameterized model, which slightly underestimated the measured ET. This was in contrast to the other time periods where the July parameterized model fit best with July data and likewise, the August parameterized model with the 30-minute averaged August data. However, this underestimation of the June model for June ET data was not observed in the bin-averaged modelled to measured ET comparison (Figure 3.11). It was concluded that this underestimation of the June

model with the June data was the result of precipitation events which were not filtered when comparing the 30-minute average data.

Underestimation of measured August ET was observed with both the June and July parameterized models (Figure 3.13). This underestimation was correlated with a drop in functional LAI and WUE as the canopy aged. The WUE in August is 23 % lower than the WUE found in June due to a loss in photosynthetic capacity and an increase in seasonal VPD. This underestimation in the August parameterized model was corrected using by using the two separate parameterizations of the empirical model to calculate ET throughout the season. The parameterization of the empirical model for estimating stomatal conductance relied on the measured relationship between stomatal conductance (g_s), vapour pressure deficit (VPD), and photosynthetic photon flux density (PPFD). As WUE decreased over the season the relationship between these variables changed and the parameterization of the model based on July data no longer applied causing an underestimation of ET (Figure3.13).

The Jarvis-type empirical model that was used to model ET over the growing season has been used with success in the Lethbridge grassland eddy covariance site outside of the Oldman River riparian corridor (Wever et al. 2002). However, the model used for evapotranspiration from the grassland relied on a term describing water availability in the form of volumetric soil water content. The grassland site showed a strong relationship between water availability and gross photosynthesis (Flanagan and Adkinson 2011). In initial tests of HSNC ET modelling, the volumetric water content term was included. However, due to

consistent cottonwood access to groundwater the HSNC woodland typically is not water limited. As a result, the modelled evapotranspiration showed no variation between modelling with and without the soil water content term included.

During the peak of the 2014 growing season in late June up to mid-July the HSNC cottonwood woodland was inundated with flood water from the Oldman River. Despite this abundance of water, evaporation did not contribute significantly to measured July daytime ET. Had evaporation played a significant part, the July parameterized model would have been expected to significantly overestimate June ET as a result of overestimating canopy conductance in relation to the environmental drivers of ET (Figure 3.12, Figure 3.14). While evaporation was present at the site during this period it did not significantly impact measured H_2O flux per unit leaf area over time as the HSNC dried out.

Evaporation, however, was observable in nighttime periods when photosynthesis was not occurring. This was seen through the fact that average nighttime ET does not consistently fall to zero for the July and August periods (Figure 3.12, 3.13). In EC measurements, the size of the measurement region (flux footprint) is dependent on the height of the sensor, the roughness of the canopy, wind speed, and atmospheric stability (Burba and Anderson 2010). Increases in atmospheric stability and wind speed can increase the flux footprint by several times for the same sensor height and canopy roughness (Burba and Anderson 2010). Unstable atmospheric conditions correspond to time periods when rising pockets of air from the surface are at a warmer temperature than the surrounding atmosphere, this is represented through large, positive values of sensible heat flux

(Odhiambo and Savage 2011, Samain et al. 2011). Conversely, stable atmospheric conditions correspond to time periods when rising pockets of air from the surface are at a cooler temperature than the surrounding atmosphere, represented with sensible heat flux values that are large and negative (Odhiambo and Savage 2011, Samain et al. 2011, Mahrt et al. 2012).

Nighttime periods which had both strong turbulence and large, negative values for sensible heat flux corresponded to non-negligible measurements of ET in the HSNC. For most nights, low net radiation and low stomatal conductance resulted in very little measured ET for the cottonwood woodland. This was observed in June when the average nighttime ET fell to approximately zero (Figure 3.11). June was found to have very few nights with both stable atmospheric conditions and high wind speeds. However, average nighttime ET for July and August was not negligible and both months had a much greater presence of these environmental conditions resulting in more occurrences where an extended flux footprint was possible. This suggests that under normal nighttime conditions, when the measured ET is negligible, the flux footprint is fully within the boundary of the cottonwood woodland.

In contrast, during the time periods when the flux footprint was likely extended due to large, negative sensible heat fluxes and strong turbulence, the measured ET was non-negligible indicating a source of ET that is not vegetation based. The Oldman River is an open body of water and evaporation from its surface is not restricted by stomatal conductance. As a result, boundary layer conductance is left as the primary control on conductance for the Oldman River

(Equation 2.5). As turbulence increases, boundary layer conductance increases (Equation 2.6). The increase in boundary layer conductance with higher friction velocity results in larger measurements of ET for a given flux footprint (Equation 2.5). As a result, on nights where turbulence is high the increased boundary layer conductance will result in increased evaporation from the Oldman River.

The greater presence of stable atmospheric conditions later in the growing season for July and August relative to June resulted in the extension of the flux footprint on some nights with high wind speeds. This extension of the flux footprint resulted in non-negligible measurements of nighttime ET (Figure 3.12, 3.13). During these conditions the flux footprint of the HSNC EC tower was extended beyond the western boundary of the woodland where evaporation from the Oldman River was included in ET measurements.

4.4 Seasonal variation in evapotranspiration and cumulative water fluxes

4.4.1 Seasonal variation in modelled and gap-filled daily ET

The P-M equation with the empirical model of stomatal conductance estimates less ET relative to measured values by approximately 1 mmol m^{-2} s^{-1} during peak evapotranspiration hours on a bin-averaged diurnal basis (Figures 3.15, 3.16). In the subset of four day periods from July and August, on some days the modelled ET was observed to estimate nearly 3 mmol m^{-2} s^{-1} less ET relative to measured values. This was shown to have little effect when comparing linear

regressions of modelled to measured ET however this difference in modelled values relative to measured values is present within the modelled dataset. Additional studies in the HSNC would be needed to further quantify this difference between modelled and measured values and the impact that it has on estimations of cumulative water usage.

4.4.2 Cumulative ET and precipitation

The total water usage by the HSNC cottonwood woodland over the span of the growing season (May – October) was found to be 465 mm (Figure 3.19). Total water use through ET by the HSNC woodland was greater than seasonal precipitation by July 24th (day 205). Comparing to a similar open canopy, semi-arid riparian mesquite system in Arizona, total water use was found to be only 375 mm compared to the 465 mm observed at the HSNC (Scott et al. 2000). However, the mesquite site from Scott et al. (2000) experienced significantly less precipitation of 247 mm in the 1997 growing season compared to the above average 370 mm experienced at the HSNC in the 2014 growing season. As well, the relative contribution of the understory to measured HSNC ET is unknown given that the understory contributed to 50 % of the total woodland leaf area. Additional seasonal research in the HSNC would be required to determine the exact contribution of the understory canopy to total ET flux measurements. However, the same mesquite woodland, in other years for a denser mesquite area was found to have seasonal cumulative water fluxes reaching upwards of 600 mm (Scott et al. 2003, Scott et al. 2004).

Comparatively, cumulative water flux from the Lethbridge grassland site is closely tied to the total precipitation inputs due to a lack of other water sources (Wever et al. 2002). Typically total growing season ET for the grassland is on the order of 200 - 250 mm, depending on the amount of seasonal precipitation, although in years of drought or very wet years grassland ET can be as low as 188 mm or as high as 456 mm (Wever et al. 2002, Flanagan and Adkinson 2011).

A similar seasonal evapotranspiration of 405 mm was found for a trembling aspen forest (*P. tremuloides*) in northern Saskatchewan (Zha et al. 2010). However, the HSNC cumulative seasonal evapotranspiration was markedly lower than the 1271 mm observed in a cottonwood/willow (*P. fremontii, Salix gooddingii*) forest in southern Arizona (Scott et al. 2000). The large seasonal ET observed at the cottonwood/willow measurement could have been heavily influenced by the willow presence. A site containing only willow trees was found to have a seasonal ET of 1198 mm (Scott et al. 2000). A second cottonwood woodland (*P. fremontii*) in southern Arizona was found to have a seasonal ET of 966 mm, although, this cottonwood site had higher LAI of 2.5 m^2 m^{-2} (Gazal et al. 2006). Additionally, the growing season for cottonwood trees in southern Arizona begins with tree leaf-out in April and concludes with senescence in November (Gazal et al. 2006). This is compared to HSNC cottonwood leaf-out in late-May and senescence in September. Were the growing season longer in Alberta, the cumulative seasonal HSNC ET would likely reach similar values to what is seen in the semi-arid cottonwood riparian woodlands of Arizona. Based on the values

shown above, the 465 mm total water use in the HSNC is representative of a semi-arid riparian ecosystem.

4.5 Isotopic analysis of cottonwood water source

The seasonal mean δ^2H values of cottonwood stem water, Oldman river water, and HSNC groundwater were not found to be significantly different. Thus, the cottonwoods in the HSNC cottonwood woodland do not make use of seasonal precipitation but rely on the groundwater reserves which consist entirely of Oldman River water.

The reliance on fluvial input to groundwater that was observed in the HSNC has been observed in other semi-arid riparian ecosystems. For example, isotopic analysis of stem water from mixed cottonwood and willow woodlands in Arizona showed the dominant water source for tree transpiration to be groundwater, which had been supplied via river input (Busch et al. 1992). The same result was found for semi-arid riparian vegetation near the San Pedro River in Arizona (Snyder and Williams 2000). However, at an ephemeral stream site in Arizona, shallow soil layers containing moisture from precipitation were used in addition to stream water to supplement seasonal transpiration, indicating that the water source used by semi-arid riparian vegetation can be dependent on the nature of the nearby stream type (Snyder and Williams 2000). Additionally, reliance on river input does not apply for all species of semi-arid riparian vegetation. For example, riparian eucalyptus trees in semi-arid regions of Australia are more opportunistic in their

use of available water (Mensforth et al. 1994). They were found to range in their usage of precipitation and stream water depending on distance from the associated stream (Mensforth et al. 1994).

Temporal variation was seen in river and groundwater samples over the 2014 growing season (Figure 3.21). The temporal change in the δ^2H of the Oldman River over the span of the growing season is the result of isotopic fractionation from evaporation causing a progressive increase in the δ^2H over time (Rock and Mayer 2007). This change in the δ^2H composition of the Oldman River was reflected in the adjacent groundwater. This seasonal variation did not appear to be present in stem water. Precipitation showed a strong temporal variation relative to the temporal variation seen in river or groundwater. However, the 57 ‰ seasonal variation in precipitation was controlled by seasonal temperature changes, the amount effect, and progressive changes in the isotopic content of source atmospheric vapours as the growing season progressed (Dansgaard 1964, Kendall et al. 2004, Lee and Fung 2008).

Given that stem water is not fractionated relative to the source and stem water was determined to consist exclusively of river water it would be expected that stem water would also show temporal variation. However, the slopes of the linear regression lines were small for river water and ground water, 0.03 and 0.01 respectively, indicating that the temporal change was small over the course of the 2014 growing season. The total magnitude of δ^2H change in the Oldman River was 9 ‰ for the entire season whereas the variation δ^2H of stem water for each of the sample dates which was as large as 7 ‰. This larger magnitude of variation on

individual sample days for stem water relative to the total temporal variation of river and ground water led to the conclusion that stem water likely does vary temporally over the growing season but the daily variation in stem samples from separate trees masks these small changes.

Given that the cottonwood trees were shown to rely exclusively on river water it can be concluded that much of the 465 mm of water used by the HSNC over the span of the growing season is a direct measure of water used from the Oldman River. However, the relative amount of river water used may be subject to variation based on the potential for water transpired by the understory vegetation to be sourced by precipitation. Multiplying the 465 mm of growing season water use by the physical area of the cottonwood woodland will provide the corresponding volume of water used from the river. The area of the HSNC woodland was estimated to be 1.7×10^5 m^2 (Google Earth: Digital Globe 2015). Thus, the estimated amount of Oldman River water used for ET by the HSNC cottonwood woodland over the 2014 growing season was 7.9×10^4 m^3.

5. CONCLUSION

This study determined that cottonwood trees in a southern Alberta riparian woodland relied exclusively on the Oldman River to supply water for transpiration. Based on eddy covariance measurements of seasonal evapotranspiration an estimated 465 mm of river water was used by the cottonwood woodland. Given the estimated area of the HSNC woodland to be 1.7×10^5 m^2 it was concluded that approximately 7.9×10^4 m^3 of Oldman River water was used by the woodland over the 2014 growing season.

The 2014 growing season was a wet year with 370 mm of precipitation from May to October compared to the 30-year average of 273 ± 33 mm (Government of Canada 2010). This contributed to high flows in the Oldman River with discharge in June reaching 572 m^3 s^{-1} compared to 319 m^3 s^{-1} given by the 1911 – 2012 historical average (Water Survey of Canada 2014). The LAI of the cottonwood canopy reached a peak of 0.9 ±0.1 m^2 m^{-2} in July with the understory vegetation also reaching a peak of 0.9 ±0.2 m^2 m^{-2} both contributing 50 % to the total leaf area of the HSNC.

A test of data quality was performed by checking the energy balance closure. The energy balance closure determines the amount of total energy exchange measured by the EC instrumentation relative to energy inputs measured by other meteorological instruments at the HSNC. A closure of 87 % was observed for the peak of the growing season in July. This value was found to be in agreement with similar measurements at other eddy covariance measurement sites where the

portion of unaccounted for energy typically varies between 10 and 30 % (Twine et al. 2000).

Total seasonal ET was shown to be greater than seasonal precipitation input by 95 mm. Isotopic analysis of HSNC water sources identified the Oldman River as the sole source of water for the resident cottonwood trees. No significant difference was observed between the seasonal mean δ^2H values of HSNC groundwater, Oldman River water, and cottonwood stem water.

Further research into the interannual variation of the HSNC understory vegetation LAI and the associated δ^2H isotopic composition of transpired water would provide additional resources with which to determine the precise usage of Oldman River water by the cottonwood woodland. This research could be further enhanced by using additional EC instrumentation to determine the relative contribution of the understory vegetation to cumulative woodland ET.

The information on the water requirements of the HSNC cottonwood woodland gained in this study will increase understanding of the needs of this ecosystem and provide policy makers with additional tools to use when allocating the demand for river resources. By multiplying the 465 mm of water usage with an estimated area of local riparian cottonwood woodlands, the volume of Oldman River water used by these systems on a seasonal basis can be estimated for a larger region than just the Helen Schuler Nature Centre. Lastly, the EC measurements made in the HSNC have the potential to be applied to larger, similar regions using the empirical model relationships and locally measured environmental variables. The parameterized empirical model of cottonwood stomatal conductance to water

vapour can be used with measurements of meteorological variables and the Penman-Monteith equation of evapotranspiration as a powerful tool to calculate water usage of similar riparian woodlands over longer time scales.

6. REFERENCES

Allen, R. G., L. S. Pereira, D. Raes, and M. Smith. 1998. Crop evapotranspiration-Guidelines for computing crop water requirements-FAO Irrigation and drainage paper 56. FAO, Rome **300**:D05109.

Asner, G. P., J. M. O. Scurlock, and J. A. Hicke. 2003. Global synthesis of leaf area index observations: implications for ecological and remote sensing studies. Global Ecology and Biogeography **12**:191-205.

Aubinet, M., T. Vesala, and D. Papale. 2012. Eddy covariance: a practical guide to measurement and data analysis. Springer Science & Business Media.

Ayer, G. R. 1949. A progress report on an investigation of the influence of reforestation on stream flow in State forests in central New York. 2331-1258.

Baldocchi, D. D. 2003. Assessing the eddy covariance technique for evaluating carbon dioxide exchange rates of ecosystems: past, present and future. Global Change Biology **9**:479-492.

Baumgartner, A. 1969. Meteorological approach to the exchange of CO2 between the atmosphere and vegetation, particularly forest stands. Photosynthetica.

Benjankar, R., M. Burke, E. Yager, D. Tonina, G. Egger, S. B. Rood, and N. Merz. 2014. Development of a spatially-distributed hydroecological model to simulate cottonwood seedling recruitment along rivers. Journal of Environmental Management **145**:277-288.

Braatne, J., S. Rood, L. Goater, and C. Blair. 2008. Analyzing the Impacts of Dams on Riparian Ecosystems: A Review of Research Strategies and Their Relevance to the Snake River Through Hells Canyon. Environmental Management **41**:267-281.

Bradley, C. E., and D. G. Smith. 1986. Plains cottonwood recruitment and survival on a prairie meandering river floodplain, Milk River, southern Alberta and northern Montana. Canadian Journal of Botany **64**:1433-1442.

Bréda, N. J. J. 2003. Ground-based measurements of leaf area index: a review of methods, instruments and current controversies. Journal of Experimental Botany **54**:2403-2417.

Burba, G., and D. Anderson. 2010. A brief practical guide to eddy covariance flux measurements: principles and workflow examples for scientific and industrial applications. Li-Cor Biosciences, Lincoln, Nebraska.

Busch, D. E., N. L. Ingraham, and S. D. Smith. 1992. Water Uptake in Woody Riparian Phreatophytes of the Southwestern United States: A Stable Isotope Study. Ecological Applications **2**:450-459.

Chapin, F. S., M. C. Chapin, P. A. Matson, and P. Vitousek. 2011. Principles of terrestrial ecosystem ecology. Springer.

Chen, J. M. 1996. Optically-based methods for measuring seasonal variation of leaf area index in boreal conifer stands. Agricultural and Forest Meteorology **80**:135-163.

Chen, J. M., A. Govind, O. Sonnentag, Y. Q. Zhang, A. Barr, and B. Amiro. 2006. Leaf area index measurements at Fluxnet-Canada forest sites. Agricultural and Forest Meteorology **140**:257-268.

Clipperton, G. K., C. W. Koning, A. G. Locke, J. M. Mahoney, and B. Quazi. 2003. Instream flow needs determinations for the South Saskatchewan River basin, Alberta, Canada. Alberta Environment.

Dansgaard, W. 1964. Stable isotopes in precipitation. Tellus **16**:436-468.

Dawson, T. E., and J. R. Ehleringer. 1991. Streamside trees that do not use stream water. Nature **350**:335-337.

Denmead, O. 1969. Comparative micrometeorology of a wheat field and a forest of Pinus radiata. Agricultural Meteorology **6**:357-371.

Ehleringer, J., J. Roden, and T. Dawson. 2000. Assessing Ecosystem-Level Water Relations Through Stable Isotope Ratio Analyses. Pages 181-198 *in* O. Sala, editor. Methods in Ecosystem Science. Springer New York.

Farquhar, G. D., and T. D. Sharkey. 1982. Stomatal conductance and photosynthesis. Annual review of plant physiology **33**:317-345.

Fellows, A. W., and M. L. Goulden. 2013. Controls on gross production by a semiarid forest growing near its warm and dry ecotonal limit. Agricultural and Forest Meteorology **169**:51-60.

Field, C., and H. A. Mooney. 1983. Leaf age and seasonal effects on light, water, and nitrogen use efficiency in a California shrub. Oecologia **56**:348-355.

Flanagan, L. B., and A. C. Adkinson. 2011. Interacting controls on productivity in a northern Great Plains grassland and implications for response to ENSO events. Global Change Biology **17**:3293-3311.

Flanagan, L. B., and J. R. Ehleringer. 1991. Stable Isotope Composition of Stem and Leaf Water: Applications to the Study of Plant Water Use. Functional Ecology **5**:270-277.

Flanagan, L. B., E. J. Sharp, and M. G. Letts. 2013. Response of plant biomass and soil respiration to experimental warming and precipitation manipulation in a Northern Great Plains grassland. Agricultural and Forest Meteorology **173**:40-52.

Flanagan, L. B., L. A. Wever, and P. J. Carlson. 2002. Seasonal and interannual variation in carbon dioxide exchange and carbon balance in a northern temperate grassland. Global Change Biology **8**:599-615.

Gazal, R. M., R. L. Scott, D. C. Goodrich, and D. G. Williams. 2006. Controls on transpiration in a semiarid riparian cottonwood forest. Agricultural and Forest Meteorology **137**:56-67.

Government of Canada. 2010. Canadian Climate Normals 1981-2010 Lethbridge Station Data. Retrieved January 20, 2015 from http://www.climate.weather.gc.ca/climate_normals.

Gower, S. T., C. J. Kucharik, and J. M. Norman. 1999. Direct and indirect estimation of leaf area index, f(APAR), and net primary production of terrestrial ecosystems. Remote Sensing of Environment **70**:29-51.

Haberer, C. M., M. Rolle, O. A. Cirpka, and P. Grathwohl. 2015. Impact of Heterogeneity on Oxygen Transfer in a Fluctuating Capillary Fringe. Groundwater **53**:57-70.

Harmon, C. 1961. Standard for Reporting Concentrations of Deuterium and Oxygen-18 in Natural Waters. Science **133**:1833-1834.

Heisler-White, J., A. Knapp, and E. Kelly. 2008. Increasing precipitation event size increases aboveground net primary productivity in a semi-arid grassland. Oecologia **158**:129-140.

Henderson-Sellers, B. 1984. A new formula for latent heat of vaporization of water as a function of temperature. Quarterly Journal of the Royal Meteorological Society **110**:1186-1190.

Jarvis, P. G. 1976. The Interpretation of the Variations in Leaf Water Potential and Stomatal Conductance Found in Canopies in the Field. Philosophical Transactions of the Royal Society of London. Series B, Biological Sciences **273**:593-610.

Junk, W. J., P. B. Bayley, and R. E. Sparks. 1989. The flood pulse concept in river-floodplain systems. Canadian special publication of fisheries and aquatic sciences **106**:110-127.

Kendall, C., S. D., and C. E. 2004. Resources on Isotopes. Retrieved March 29, 2015 from http://wwwrcamnl.wr.usgs.gov/ .

Lamontagne, S., P. G. Cook, A. O'Grady, and D. Eamus. 2005. Groundwater use by vegetation in a tropical savanna riparian zone (Daly River, Australia). Journal of Hydrology **310**:280-293.

Lázaro, R., F. S. Rodrigo, L. Gutiérrez, F. Domingo, and J. Puigdefábregas. 2001. Analysis of a 30-year rainfall record (1967–1997) in semi–arid SE Spain for implications on vegetation. Journal of Arid Environments **48**:373-395.

Leblanc, S., J. Chen, and M. Kwong. 2002. Tracing Radiation and Architecture of Canopies TRAC MANUAL Version 2.1. 3. Natural Resources Canada.

Lee, J.-E., and I. Fung. 2008. "Amount effect" of water isotopes and quantitative analysis of post-condensation processes. Hydrological Processes **22**:1-8.

LI-COR Biosciences. 1992. LAI-2000 Plant Canopy Analyzer: Operating Manual. LI-COR, Inc, Lincoln, Nebraska.

Lytle, D. A., and D. M. Merritt. 2004. Hydrologic Regimes and Riparian Forests: A Structured Population Model for Cottonwood. Ecology **85**:2493-2503.

Mahoney, J. M., and S. B. Rood. 1998. Streamflow requirements for cottonwood seedling recruitment - An integrative model. Wetlands **18**:634-645.

Mahrt, L., D. Vickers, E. L. Andreas, and D. Khelif. 2012. Sensible Heat Flux in Near-Neutral Conditions over the Sea. Journal of Physical Oceanography **42**:1134-1142.

Mensforth, L., P. Thorburn, S. Tyerman, and G. Walker. 1994. Sources of water used by riparian Eucalyptus camaldulensis overlying highly saline groundwater. Oecologia **100**:21-28.

Monclus, R., E. Dreyer, M. Villar, F. M. Delmotte, D. Delay, J.-M. Petit, C. Barbaroux, D. Le Thiec, C. Bréchet, and F. Brignolas. 2006. Impact of drought on productivity and water use efficiency in 29 genotypes of Populus deltoides×Populus nigra. New Phytologist **169**:765-777.

Monteith, J. 1965. Evaporation and environment. Page 4 *in* Symp. Soc. Exp. Biol.

Murthy, R., G. Barron-Gafford, P. M. Dougherty, V. C. Engel, K. Grieve, L. Handley, C. Klimas, M. J. Potosnak, S. J. Zarnoch, and J. Zhang. 2005. Increased leaf area dominates carbon flux response to elevated CO2 in stands of Populus deltoides (Bartr.). Global Change Biology **11**:716-731.

Nagler, P. L., E. P. Glenn, T. Lewis Thompson, and A. Huete. 2004. Leaf area index and normalized difference vegetation index as predictors of canopy characteristics and light interception by riparian species on the Lower Colorado River. Agricultural and Forest Meteorology **125**:1-17.

Naiman, R. J., and H. Decamps. 1997. The ecology of interfaces: Riparian zones. Annual Review of Ecology and Systematics **28**:621-658.

Nasahara, K. N., H. Muraoka, S. Nagai, and H. Mikami. 2008. Vertical integration of leaf area index in a Japanese deciduous broad-leaved forest. Agricultural and Forest Meteorology **148**:1136-1146.

O'Connor, T. G., L. M. Haines, and H. A. Snyman. 2001. Influence of precipitation and species composition on phytomass of a semi-arid African grassland. Journal of Ecology **89**:850-860.

O'Grady, A. P., D. Eamus, P. G. Cook, and S. Lamontagne. 2006. Groundwater use by riparian vegetation in the wet–dry tropics of northern Australia. Australian Journal of Botany **54**:145-154.

Odhiambo, G. O., and M. J. Savage. 2011. Comparison of Sensible Heat Flux as Measured by Surface Layer Scintillometer and Eddy Covariance Methods Under Different Atmospheric Stability Conditions. Pages 461-484 *in* S. D. Attri, L. S. Rathore, M. V. K. Sivakumar, and S. K. Dash, editors. Challenges and Opportunities in Agrometeorology. Springer Berlin Heidelberg.

Oldman Watershed Council. 2007. Oldman River Watershed Annual Report 2006/2007. Retrieved January 30th, 2015 from http://oldmanbasin.org.

Osmond, C. B., K. Winter, and H. Ziegler. 1982. Functional Significance of Different Pathways of CO2 Fixation in Photosynthesis. Pages 479-547 *in* O. L. Lange, P. S. Nobel, C. B. Osmond, and H. Ziegler, editors. Physiological Plant Ecology II. Springer Berlin Heidelberg.

Pearce, D. W., S. Millard, D. F. Bray, and S. B. Rood. 2006. Stomatal characteristics of riparian poplar species in a semi-arid environment. Tree Physiology **26**:211-218.

Penman, H. L. 1948. Natural evaporation from open water, bare soil and grass. Pages 120-145 *in* Proceedings of the Royal Society of London A: Mathematical, Physical and Engineering Sciences. The Royal Society.

Poff, B., K. A. Koestner, D. G. Neary, and V. Henderson. 2011. Threats to Riparian Ecosystems in Western North America: An Analysis of Existing Literature1. JAWRA Journal of the American Water Resources Association **47**:1241-1254.

Ponton, S., L. B. Flanagan, K. P. Alstad, B. G. Johnson, K. Morgenstern, N. Kljun, T. A. Black, and A. G. Barr. 2006. Comparison of ecosystem water-use efficiency among Douglas-fir forest, aspen forest and grassland using eddy covariance and carbon isotope techniques. Global Change Biology **12**:294-310.

Rock, L., and B. Mayer. 2007. Isotope hydrology of the Oldman River basin, southern Alberta, Canada. Hydrological Processes **21**:3301-3315.

Rood, S., A. Kalischuk, and J. Mahoney. 1998. Initial cottonwood seedling recruitment following the flood of the century of the Oldman River, Alberta, Canada. Wetlands **18**:557-570.

Rood, S. B., D. J. Ball, K. M. Gill, S. Kaluthota, M. G. Letts, and D. W. Pearce. 2013. Hydrologic linkages between a climate oscillation, river flows, growth, and wood Δ13C of male and female cottonwood trees. Plant, Cell & Environment **36**:984-993.

Rood, S. B., S. G. Bigelow, and A. A. Hall. 2011. Root architecture of riparian trees: river cut-banks provide natural hydraulic excavation, revealing that cottonwoods are facultative phreatophytes. Trees-Structure and Function **25**:907-917.

Rood, S. B., J. H. Braatne, and F. M. R. Hughes. 2003a. Ecophysiology of riparian cottonwoods: stream flow dependency, water relations and restoration. Tree Physiology **23**:1113-1124.

Rood, S. B., C. R. Gourley, E. M. Ammon, L. G. Heki, J. R. Klotz, M. L. Morrison, D. A. N. Mosley, G. G. Scoppettone, S. Swanson, and P. L. Wagner. 2003b. Flows for Floodplain Forests: A Successful Riparian Restoration. BioScience **53**:647-656.

Rood, S. B., J. M. Mahoney, D. E. Reid, and L. Zilm. 1995. Instream flows and the decline of riparian cottonwoods along the St. Mary River, Alberta. Canadian Journal of Botany **73**:1250-1260.

Rood, S. B., G. M. Samuelson, J. H. Braatne, C. R. Gourley, F. M. R. Hughes, and J. M. Mahoney. 2005. Managing River Flows to Restore Floodplain Forests. Frontiers in Ecology and the Environment **3**:193-201.

Samain, B., W. Defloor, and V. R. N. Pauwels. 2011. Continuous Time Series of Catchment-Averaged Sensible Heat Flux from a Large Aperture Scintillometer: Efficient Estimation of Stability Conditions and Importance of Fluxes under Stable Conditions. Journal of Hydrometeorology **13**:423-442.

Samuelson, G. M., and S. B. Rood. 2004. Differing influences of natural and artificial disturbances on riparian cottonwoods from prairie to mountain ecoregions in Alberta, Canada. Journal of Biogeography **31**:435-450.

Schaeffer, S. M., D. G. Williams, and D. C. Goodrich. 2000. Transpiration of cottonwood/willow forest estimated from sap flux. Agricultural and Forest Meteorology **105**:257-270.

Scott, R. L., E. A. Edwards, W. J. Shuttleworth, T. E. Huxman, C. Watts, and D. C. Goodrich. 2004. Interannual and seasonal variation in fluxes of water and carbon dioxide from a riparian woodland ecosystem. Agricultural and Forest Meteorology **122**:65-84.

Scott, R. L., W. James Shuttleworth, D. C. Goodrich, and T. Maddock Iii. 2000. The water use of two dominant vegetation communities in a semiarid riparian ecosystem. Agricultural and Forest Meteorology **105**:241-256.

Scott, R. L., C. Watts, J. G. Payan, E. Edwards, D. C. Goodrich, D. Williams, and W. James Shuttleworth. 2003. The understory and overstory partitioning of energy and water fluxes in an open canopy, semiarid woodland. Agricultural and Forest Meteorology **114**:127-139.

Serbin, S. P., D. E. Ahl, and S. T. Gower. 2013. Spatial and temporal validation of the MODIS LAI and FPAR products across a boreal forest wildfire chronosequence. Remote Sensing of Environment **133**:71-84.

Snyder, K. A., and D. G. Williams. 2000. Water sources used by riparian trees varies among stream types on the San Pedro River, Arizona. Agricultural and Forest Meteorology **105**:227-240.

Stromberg, J. C., R. Tiller, and B. Richter. 1996. Effects of Groundwater Decline on Riparian Vegetation of Semiarid Regions: The San Pedro, Arizona. Ecological Applications **6**:113-131.

Swinbank, W. 1951. The measurement of vertical transfer of heat and water vapor by eddies in the lower atmosphere. Journal of Meteorology **8**:135-145.

Tabari, H. a. T., P. 2011. Local Calibration of the Hargreaves and Priestley-Taylor Equations for Estimating Reference Evapotranspiration in Arid and Cold Climates of Iran Based on the Penman-Monteith Model. Journal of Hydrologic Engineering **16**:837-845.

Teuling, A. J., M. Hirschi, A. Ohmura, M. Wild, M. Reichstein, P. Ciais, N. Buchmann, C. Ammann, L. Montagnani, A. D. Richardson, G. Wohlfahrt, and S. I. Seneviratne. 2009. A regional perspective on trends in continental evaporation. Geophysical Research Letters **36**.

Twine, T. E., W. P. Kustas, J. M. Norman, D. R. Cook, P. R. Houser, T. P. Meyers, J. H. Prueger, P. J. Starks, and M. L. Wesely. 2000. Correcting eddy-covariance flux underestimates over a grassland. Agricultural and Forest Meteorology **103**:279-300.

Ventura, F., D. Spano, P. Duce, and R. L. Snyder. 1999. An evaluation of common evapotranspiration equations. Irrigation Science **18**:163-170.

Wang, K., and R. E. Dickinson. 2012. A review of global terrestrial evapotranspiration: Observation, modeling, climatology, and climatic variability. Reviews of Geophysics **50**:1-54.

Water Matters Society of Alberta. 2012. Oldman River Sub-basin. Retrieved January 30, 2015 from http://www.water-matters.org/watershed/oldman-river-sub-basin.

Water Survey of Canada. 2014. Historical Oldman river discharge data 1911 - 2012. Station no. 05AD007. Retrieved April 6, 2015 from http://www.ec.gc.ca/rhc-wsc/.

West, A. G., S. J. Patrickson, and J. R. Ehleringer. 2006. Water extraction times for plant and soil materials used in stable isotope analysis. Rapid Communications in Mass Spectrometry **20**:1317-1321.

Wever, L. A., L. B. Flanagan, and P. J. Carlson. 2002. Seasonal and interannual variation in evapotranspiration, energy balance and surface conductance in a northern temperate grassland. Agricultural and Forest Meteorology **112**:31-49.

Williams, D. G., R. L. Scott, T. E. Huxman, D. C. Goodrich, and G. Lin. 2006. Sensitivity of riparian ecosystems in arid and semiarid environments to moisture pulses. Hydrological Processes **20**:3191-3205.

Wilson, K. B., P. J. Hanson, P. J. Mulholland, D. D. Baldocchi, and S. D. Wullschleger. 2001. A comparison of methods for determining forest evapotranspiration and its components: sap-flow, soil water budget, eddy covariance and catchment water balance. Agricultural and Forest Meteorology **106**:153-168.

Wofsy, S. C., M. L. Goulden, J. W. Munger, S. M. Fan, P. S. Bakwin, B. C. Daube, S. L. Bassow, and F. A. Bazzaz. 1993. Net Exchange of CO2 in a Mid-Latitude Forest. Science.

Woodwell, G. M., and R. H. Whittaker. 1968. Primary Production in Terrestrial Ecosystems. American Zoologist **8**:19-30.

Yu, G., X. Song, Q. Wang, Y. Liu, D. Guan, J. Yan, X. Sun, L. Zhang, and X. Wen. 2008. Water-use efficiency of forest ecosystems in eastern China and its relations to climatic variables. New Phytologist **177**:927-937.

Zha, T. S., A. G. Barr, G. van der Kamp, T. A. Black, J. H. McCaughey, and L. B. Flanagan. 2010. Interannual variation of evapotranspiration from forest and grassland ecosystems in western canada in relation to drought. Agricultural and Forest Meteorology **150**:1476-1484.

7. APPENDIX

The following appendix contains analyses which supplement the primary data analysis discussed within the body of the thesis. These include information on the gap-filling procedure for meteorological variables, the turbulence threshold analysis, and analysis of the primary wind direction at the HSNC. Also included are the modelled to measured ET linear regressions for different levels of data screening and the HSNC specific soil calibration for the volumetric water content in the shallow surface layers. Lastly, information is included on the accuracy and precision of the isotope analyzer in the University of Calgary Stable Isotope Lab as well as the variation observed in Lethbridge 2014 precipitation.

Table of Contents **pg.**

7.1 Gap filling of missing data

ET data was unavailable at the HSNC for two extended periods where tower instrumentation was not fully functioning. The first period of data loss was from June 17th (day 168) to July 2nd (day 183) due to flooding at the HSNC during which much of the instrumentation was removed to prevent water damage. A second extended period of data loss was due to a malfunction of the gas analyzer from July 28th (day 209) to August 22nd (day 234) where no water vapour densities were being measured.

In lieu of missing meteorological data at the Lethbridge HSNC measurement site, direct substitution with the same type of data measured at the Lethbridge grassland eddy covariance measurement site was used. This was done for air pressure (kPa), air temperature (°C), relative humidity (%), vapour pressure deficit (kPa), net radiation (W m^{-2}), photosynthetically active radiation (μmol m^{-2} s^{-1}), friction velocity (m s^{-1}), and wind speed (m s^{-1}). The Lethbridge grassland measurement site is located roughly 2 km west of the Lethbridge city limits, Alberta, Canada (49° 28' 15.31" N, 112° 56' 24.90" W) (Flanagan et al. 2013). Linear regressions showed a 1:1 relationship between measured grassland and HSNC meteorological data (Lawrence B. Flanagan, personal communication, 2014).

In addition to the meteorological variables listed above, soil heat flux was also required to use in the evapotranspiration modelling process. However, the soil heat flux data were unique for the HSNC so direct substitution from the grassland site did not apply. During the flooding in late June (day 168) until early July (day 183) no data was collected from the soil heat flux plates. To correct for this, available soil heat flux data was bin-averaged by time of day for each month of the growing season (May to October), shown in Figure 7.1. In times when soil heat flux data were missing, the bin-averaged data for the corresponding time of day and month of the year were substituted in.

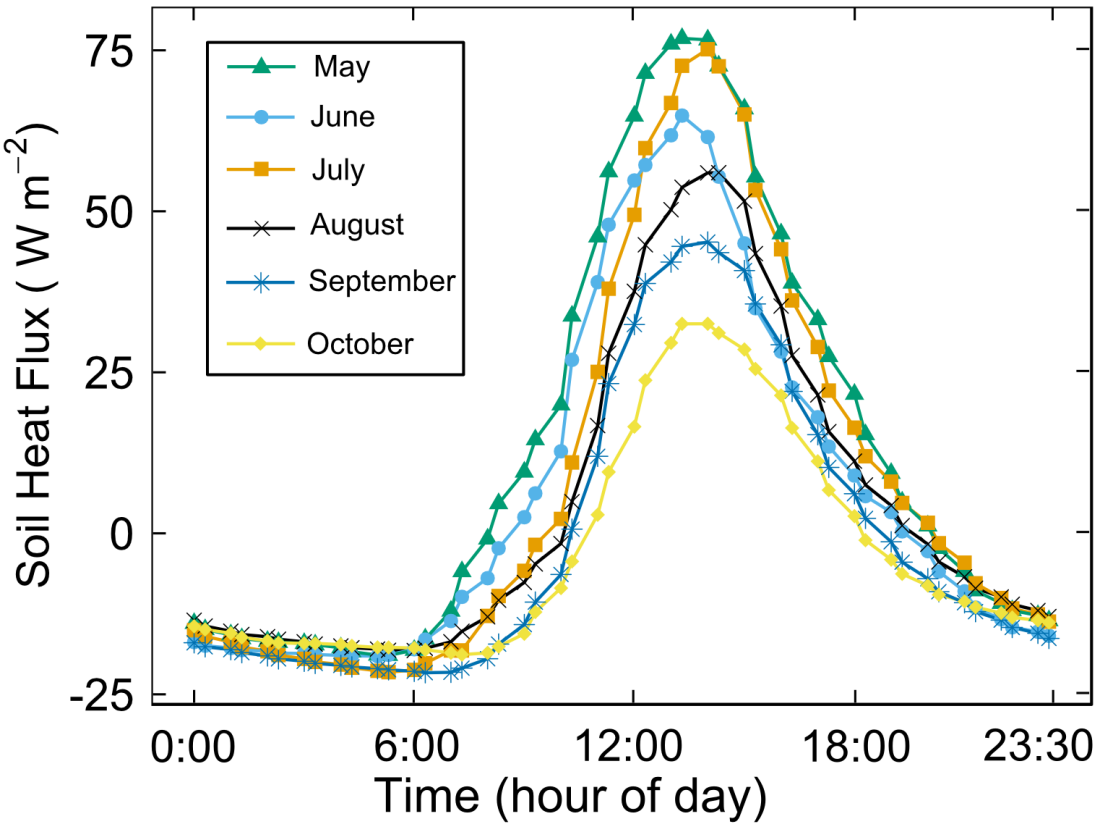

Figure 7.1: Monthly bin-averaged HSNC soil heat flux. Missing soil heat flux values were gap-filled according to month and time of day.

7.2 Turbulence threshold analysis

The relationship between nighttime net ecosystem exchange (NEE) and friction velocity (u^*) was used to determine the amount of turbulence required for eddy covariance flux measurements at the HSNC. If boundary layer turbulence, represented using friction velocity (u^*, m s^{-1}), is too low then no flux will be observed. This is due to lack of transport for gases to reach to instrumentation above the woodland (Baldocchi 2003). However, as turbulence increases then increases in nighttime NEE (ecosystem respiration) will be observed. NEE will increase up to a maximum value which would be representative of the amount of respiration occurring in the woodland. After which, a plateau region will be observed which shows no further increases in NEE with increases in u^*.

Measured u^* values from the HSNC were sorted from their lowest to highest values using data from July when the canopy was at its maximum LAI and photosynthetic capacity. These values were averaged into 0.03 m s^{-1} bins ranging from 0.0 m s^{-1} to 1.0 m s^{-1}. The same process was performed for the corresponding NEE data which were grouped according to the u^* values. No distinct plateau in the NEE data was observed when plotting against u^* (Figure 7.2). To determine the turbulence threshold, a range of possible thresholds were tested (Figure 7.3). For each possible turbulence threshold, data were plotted in two groups: u^* values that fall below the possible threshold and those that fall above. For each set of data above the chosen threshold, a linear regression was done to test if the regression line created the expected plateau. This was confirmed with a t-test of regression slope to determine if the slope differed significantly from zero (Table 7.1).

Five out of six possible u^* thresholds showed upper regression slopes that did not significantly differ from zero (Table 7.1). This corresponded to a horizontal line such as that which would be seen in the plateau region of a turbulence threshold plot. Of these possible thresholds, the one with the best regression line for data below the threshold was determined to be the most rigorous u^* threshold. The criteria for determining the best fit regression line was the one with the highest slope and R^2 value and the intercept that was closest to zero indicating a direct increase of NEE with increasing u^*. Based on the analysis shown in Figure 7.3, the u^* threshold was determined to be 0.33 m s^{-1}.

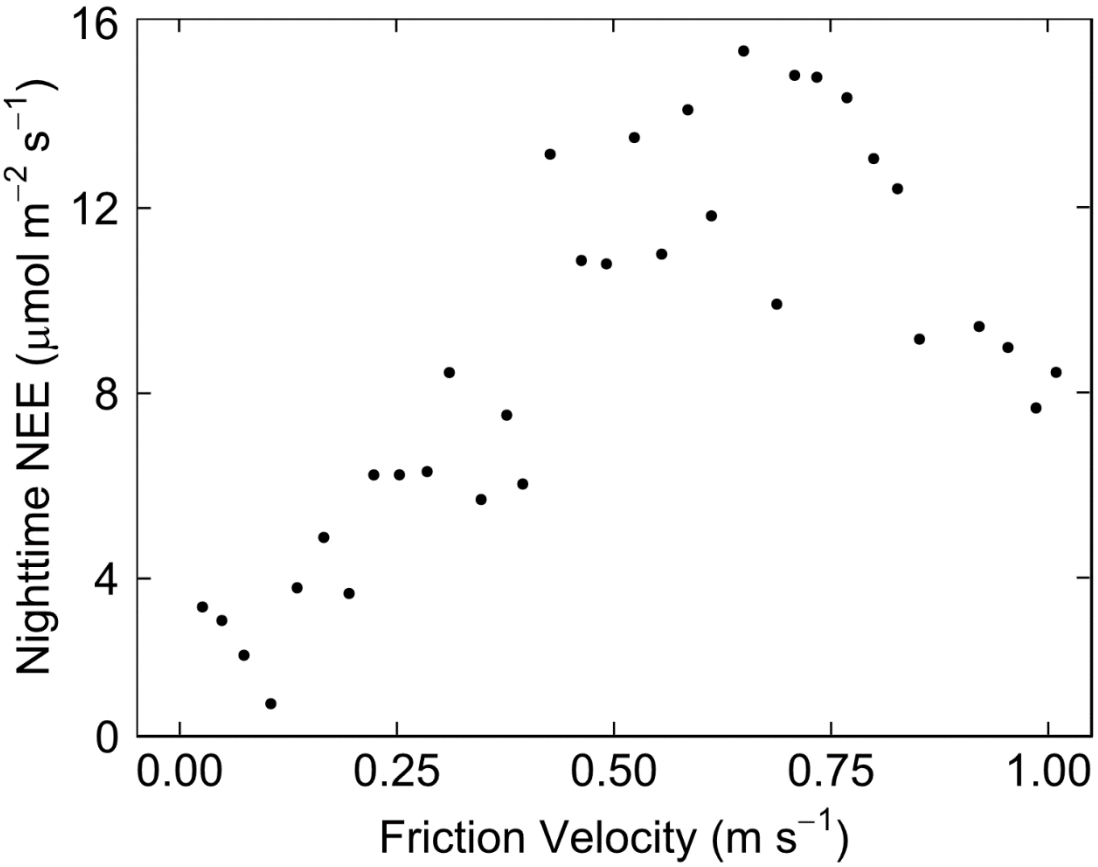

Figure 7.2: Initial turbulence threshold plot using data averaged according to friction velocity in 0.03 m s^{-1} bins. No clear relationship between nighttime NEE and friction velocity was observed.

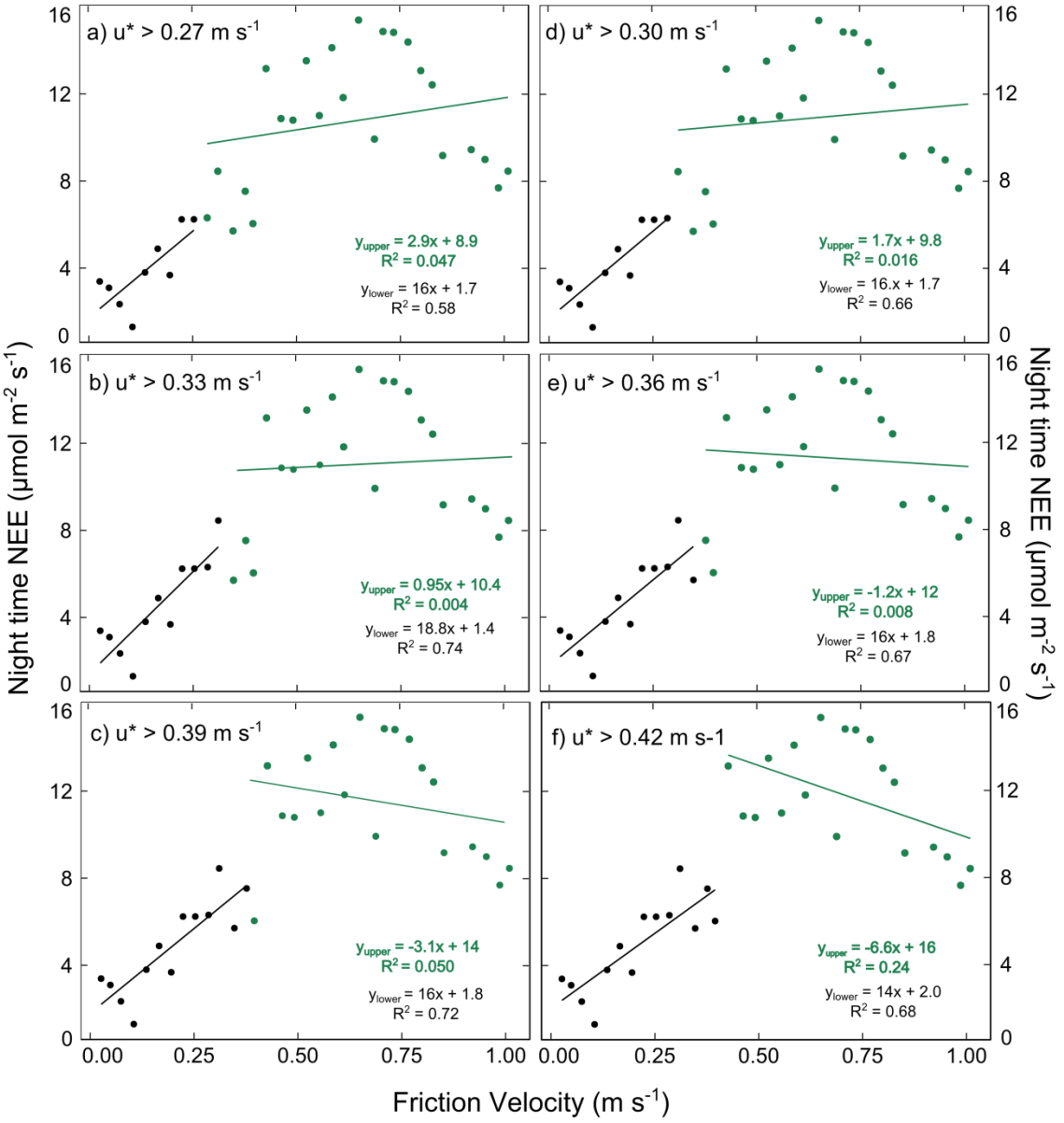

Figure 7.3: Tests of possible u^* thresholds. The threshold of $u^* > 0.33$ m s^{-1} has the best fit for both the upper and lower regressions. For the upper regression it has the lowest slope corresponding to a horizontal line such as that which would be seen in the plateau region of a turbulence threshold plot. The lower regression has the highest slope and the intercept that lies closest to zero indicating a direct increase of NEE with increasing u^*.

Table 7.1: t-test of regression slope results for various possible u^* thresholds. The upper regression slopes were not found to be significantly different from zero with the exception of a u^* threshold of 0.42 m s^{-1}.

u Threshold (m s⁻¹)*	***df***	***t*-statistic**	**Critical Value**	***p* Value**
0.27	22	1.05	2.07	>0.05
0.30	21	0.580	2.08	>0.05
0.33	20	0.298	2.09	>0.05
0.36	19	-0.379	-2.09	>0.05
0.39	18	-0.970	-2.11	>0.05
0.42	17	-2.34	-2.11	<0.05

7.3 Wind direction analysis

Eddy covariance data recorded at times when the primary wind direction was originating in the east had to be removed. This was due to the presence of the raised grassland coulees lying immediately outside of the riparian corridor. An analysis was performed to determine the dominant wind direction in the HSNC and what proportion of growing season winds originated in the east. Two histograms were used to group wind direction data into 45° and 90° bins. All bins were centered on the primary directions North, East, South, and West.

To test if a predominate wind direction existed over the growing season, a chi-squared test was performed on both bin sizes (45°, 90°), with the null-hypothesis being that winds were distributed equally in all directions. For both bin sizes it was found that there was no significant difference between the measured data and the null-hypothesis (45°: Chi-squared, df =7, t-statistic=11.8, p=0.11; 90°: Chi-squared, df=3, t-statistic=5.6, p=0.13).

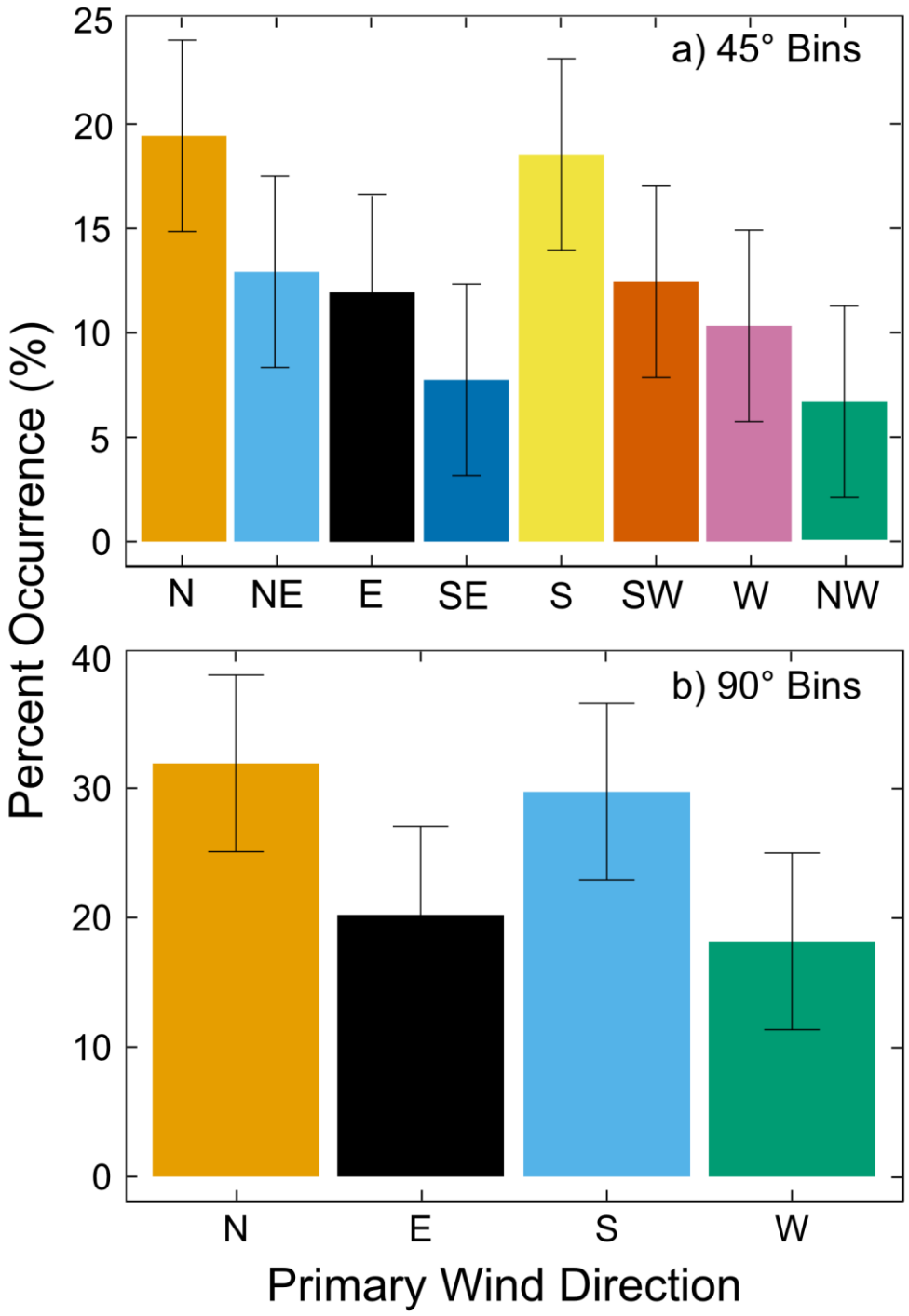

Figure 7.4: Percentage of occurrence for primary wind directions (± SD) throughout the growing season at the HSNC.

7.4 Eddy Covariance data screening

ET values calculated with the PM equation and the conductance model parameterized using July data (α=0.24, κ_D=0.00058) were found to be the most effective for predicting ET over the majority of the growing season (Results, section 3.4.2). The conductance modelling procedure was repeated using July data for four levels of data screening to determine the best balance between removal of data that was not representative of cottonwood woodland transpiration and retaining the bulk of ET data for accurate modelling. (Table 2.2). Linear regressions were used to determine which level of filtering provided the best fit between measured and modelled ET (Figure 7.5).

Regression slopes ranged from 0.83 to 0.86. The slope of 0.83 corresponded to the modelling procedure performed with no data screening. The highest slope of 0.86 corresponded to the reduced filtering method which removed data collected during precipitation events greater than 1 mm (and two hours after) and data collected during times with eastern winds (45° < wind direction < 135°).

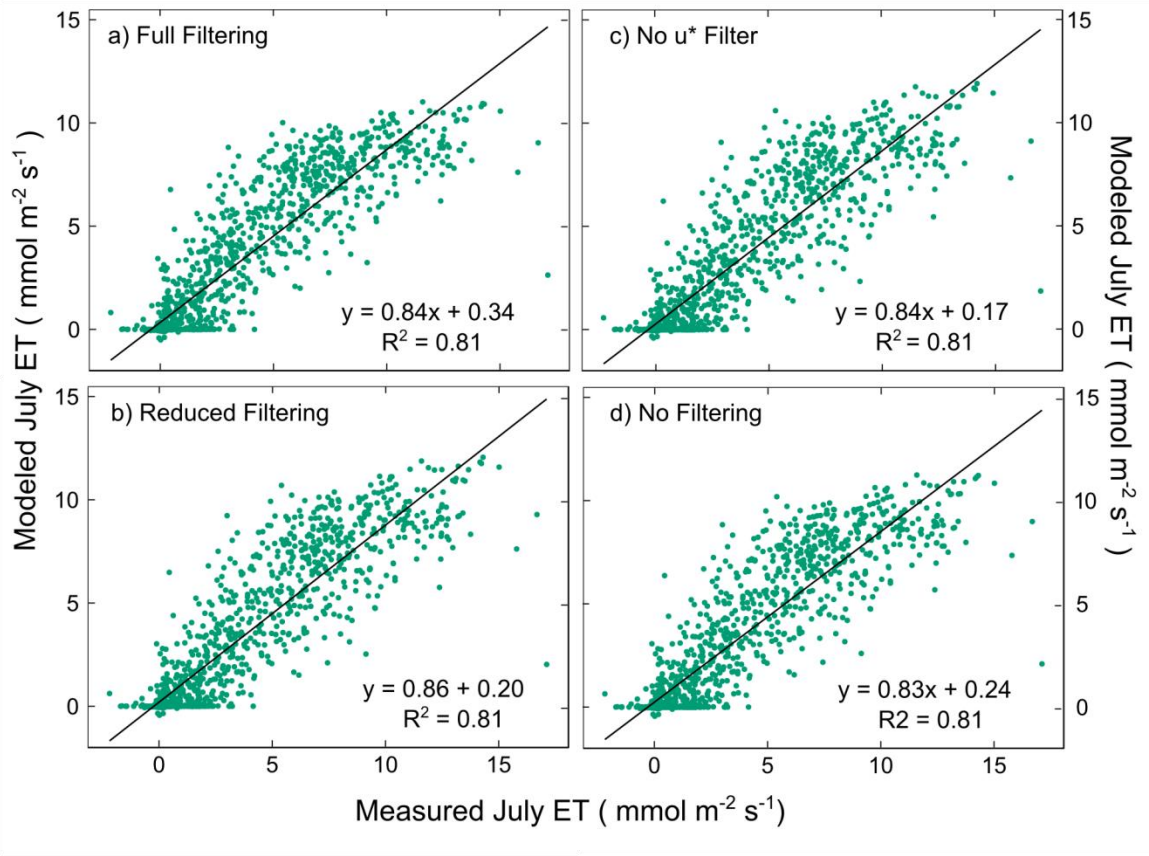

Figure 7.5: Modelled to measured ET comparisons for varying levels of initial data filtering. Full filtering removes data collected during time periods with eastern winds, any data where u^* was below the 0.33 m s^{-1} threshold as well as, any precipitation events greater than 1 mm (and 24 hours afterwards). No u^* filter removes data collected during time periods with eastern winds and precipitation events (and 24 hours afterwards). Reduced filtering removes only data collected during time periods with eastern winds and precipitation events greater than 1 mm (and 2 hours afterwards). No filtering leaves all data intact for model creation.

7.5 Soil volumetric soil water content calibration

Measurements made in the shallow soil layers (0 – 15 cm depth) were corrected for the conductivity of the soil at the HSNC during the driest and wettest times of the season using the linear calibration method described in the CS616 Water Content Reflectometer manual (Campbell Scientific Inc., Logan UT, USA).

The calibration equation found is given below (n=4, R^2=0.996) (Lawrence B. Flanagan, personal communication, May 2015):

$$\theta_v(\tau) = 0.0132\tau - 0.2019 \qquad (7.1)$$

Where $\theta_v(\tau)$ is the volumetric water content (g cm^{-3}) and τ is the temperature corrected pulse period (μs). Calculated daily average soil water content was averaged over the full 24 hours of each day (Figure 3.3).

7.6 Accuracy and precision of isotopic data

The laser isotope analyzer (DLT-100 v.2, LosGatosResearch Inc., Mountain View CA, USA) was found to have a mean precision of 0.6 ‰ and an accuracy of 1 ‰ based on repeated analysis with four laboratory standards of known δ^2H isotopic composition (Table 7.2). The precision was determined as the average standard deviation of the sample mean for each set of standard measurements (n=5). The accuracy of 1 ‰ was determined by taking the average difference between the known δ^2H value of the standards and the measured mean value.

Table 7.2: Four water standards of known δ^2H composition were analyzed using the University of Calgary Isotope Science Lab laser isotope analyzer (DLT-100 v.2, LosGatosResearch Inc., Mountain View CA, USA). The difference in means of the measured values from the UofC and the known standard values were used to determine the accuracy of the instrument. Precision was determined using the average standard deviation for replicate measurements (n=5) of each of the four lab standards.

Standard ID	**Standard δ^2H (‰)**	**Measured δ^2H (‰)**	**SD (‰)**	**Accuracy (‰)**
LMX	-105.57	-103.59	0.45	1.98
RMSW	-147.68	-148.99	0.60	1.31
BCGW	-131.78	-131.93	0.89	0.15
VIC	-76.55	-75.57	0.55	0.99
Average δ^2H Accuracy:				**1.11**
Average δ^2H Precision:			**0.62**	

7.7 δ^2H isotopic composition of Lethbridge precipitation

Precipitation was collected on a weekly basis and the δ^2H value of precipitation was found to vary strongly among weekly samples (Table 7.3). The large range of 110 ‰ observed for the δ^2H values included samples where only a few mm or less were collected. A monthly amount-weighted average was calculated for April through October of the 2014 to illustrate the pattern of seasonal variation in precipitation. The amount-weighted average had a total seasonal variation of 57 ‰ with a seasonal minimum of -153 ‰ in April and a maximum of -96 ‰ in July (Table 7.4).

Table 7.3: δ^2H of weekly precipitation collection for the 2014 growing season as well as the amount of collected precipitation for each week. Large precipitation events were collected on an as-needed basis.

Time (day of year)	Amount (mm)	δ^2H (‰)
104	13.24	-145
112	15.82	-163
116	1.50	-111
125	25.75	-126
132	6.94	-153
140	5.54	-97
146	0.13	-77
154	10.82	-65
160	1.97	-113
167	31.48	-122
168	31.07	-122
170	31.23	-124
181	28.07	-119
188	2.67	-120
197	1.50	-87
202	0.83	-85
205	31.45	-94
217	0.38	-62
230	3.95	-53
237	22.20	-114
245	11.01	-107
255	31.51	-152
267	0.51	-62
276	11.46	-116
289	1.56	-159
304	3.60	-123

Table 7.4: Monthly amount-weighted average precipitation in Lethbridge, AB over the 2014 growing season.

Time (month)	**Amount-weighted average δ^2H (‰)**
April	-153
May	-127
June	-117
July	-96
August	-104
September	-140
October	-123